Transcription factor Zbtb20 controls regional specification of mammalian archicortex

Von der Fakultät für Lebenswissenschaften

der Technischen Universität Carolo-Wilhelmina

zu Braunschweig

zur Erlangung des Grades einer

Doktorin der Naturwissenschaften

(Dr. rer. nat.)

genehmigte

D i s s e r t a t i o n

von Eva Helga Rosenthal
aus Kassel

1. Referent: Prof. Dr. Hans-Henning Arnold
2. Referent: Prof. Dr. Martin Korte
eingereicht am: 24.02.2010
mündliche Prüfung (Disputation) am: 02.06.2010

Druckjahr 2010

Diese Arbeit wurde am Max-Planck-Institut für biophysikalische Chemie,
-Karl-Friedrich-Bonhoeffer-Institut-
in Göttingen
in der Abteilung für Molekulare Zellbiologie (Direktor Prof. Dr. Peter Gruss)
Arbeitsgruppe Molekulare Neuroentwicklungsbiologie
durchgeführt.

Table of contents

I. Introduction

The brain is the most complex structure, which has evolved during biological evolution. Unique to the mammalian brain is the cerebral cortex. The phylogenetically most recently evolved part of the cerebral cortex is the neocortex (isocortex), a thin sheet of cells covering the dorsolateral surface of the cerebrum. The neocortex consists of hundreds different neuronal and a range of glial cell types that are distributed in six radial layers and numerous functional domains, each serving specific function. During evolution, the cortical surface has dramatically increased, which was accompanied by the addition and elaboration of functional subdivisions, numbering more that 52 areas in the human brain (Brodmann, 1909). The medial surface of the cerebrum, the allocortex, is an evolutionary ancient subdivision, whose cell constituents are not firmly ordered into defined layers. Interconnected in distinct functional pathways, the cortical cells represent the neural basis of human sensory perception, motor, cognitive functions, and consciousness.

Although the modern molecular, anatomical and physiological methods are constantly expanding the knowledge about regionalization, neurogenesis, neuronal pathfinding, and synapse formation in the developing brain, these processes are far from being understood completely. Understanding the cellular, molecular and genetic mechanisms underlying cortical arealization remains one of the most challenging problems of modern biology. As genetic perturbations of these mechanisms are known to result in brain disorders, their understanding is crucial for therapeutical applications in the clinical neurosciences.

Since the completion of the Human Genome Project in 2003, tremendous progress has been made in ascribing functions to distinct genes, which remains an important task of modern biology in general, and neuroscience in particular. For this purpose, the mouse model has become the key tool to facilitate insight into gene function. Since the common ancestral line that gives rise to mice and men has ramified relatively recent in biological evolution, their development, body plan, metabolism and pathology follow comparable principles. About 99% of murine and human genes are orthologs (Tecott, 2003). Therefore, each discovery in mouse genomics is of high value and contributes to the understanding the contents of the human genome.

1.1. Organization of mammalian forebrain with a focus on the cerebral cortex

In vertebrates, the formation of the central nervous system (CNS) starts with the process of neural induction during late gastrulation, when the three germinal layers, endoderm,

mesoderm and ectoderm are already formed. Morphogens and signaling factors, emanated from the notochord, a stick-like structure underlying the ectoderm, induce the formation of the neural plate. Initially seen as a thickening of the ectodermal layer, the neural plate starts folding and after closure at its dorsal edges, the early neural tube is formed, which occurs in mouse at embryonic stage (E) 8.5. At the caudal part of the neural tube the spinal cord is generated, while anteriorly, three primary vesicles are formed: prosencephalon, mesencephalon and rhombencephalon (fore-, mid- and hindbrain). The prosencephalon becomes subdivided into two parts, diencephalon (posteriorly) and telencephalon (anteriorly) (Fig. 1; Table 1, Kandel et al., 2000). The diencephalon later gives rise to two main structures, the thalamus and hypothalamus. The telencephalon is further regionalized into two domains, (dorsal) pallium and (ventral) subpallium that represent the anlagen of the cortex and basal ganglia, respectively, while rhombencephalon forms three other brain structures, pons, cerebellum and medulla oblongata.

Table 1. Organization of the CNS.

Spinal cord			
Brain	Brain stem	Rhombencephalon (Hindbrain)	Pons, Cerebellum, Medulla oblongata
		Mesencephalon (Midbrain)	Tectum, Cerebral peduncle, Pretectum, Mesencephalic duct
	Prosencephalon (Forebrain)	Diencephalon	Epithalamus, Thalamus, Hypothalamus, Subthalamus, Pituitary gland, Pineal gland, Third ventricle
		Telencephalon	Basal ganglia, Amygdala, Olfactory bulb, Hippocampus, Neocortex, Lateral ventricles

Adapted from Kandel et al., 2000

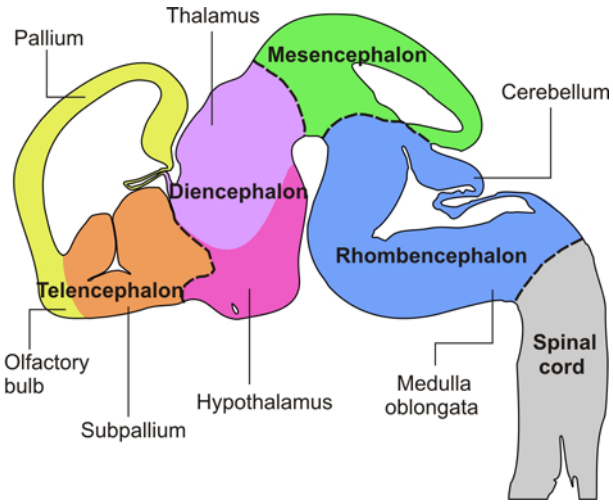

Fig. 1. General organization of the mammalian brain. The schema represents the major subdivisions of an embryonic (E) 13.5 mouse brain in sagittal view. The borders between telencephalon, diencephalon, mesencephalon, rhombencephalon and spinal cord (bold) are indicated by a dashed line. Rostral is to the left.

1.1.1. Regionalization of telencephalon

At embryonic (E) stage E8.5 in mice, the telencephalic primordium represents a sheet of neuroepithelium with single cell thickness. Already at this early stage, the restricted expression of transcription factors (TFs) Pax6 and Gsh2 in the dorsal and ventral telencephalon outlines the anlagen of pallium (cortex) and subpallium (basal ganglia), respectively. As illustrated in Fig. 2, the pallium becomes subdivided into medial pallium (MP), which generates the archicortex (including hippocampus), dorsal pallium (DP), which forms the neocortex, lateral pallium (LP), which gives rise to the olfactory cortex, and ventral pallium (VP), which later forms the claustroamygdaloid complex. In the subpallium, the progenitors of the lateral (LGE) and medial (MGE) ganglionic eminences generate the striatum and pallidum, respectively. The initial specification of all these domains occurs through a differential expression of transcription factors in their germinative zones. Subsequently, the germinal zone of the telencephalon becomes subdivided into distinct territories expressing their special set of molecular markers and displaying different ratios of cell proliferation (Hébert and Fishell, 2008; Mallamaci and Stoykova, 2006). For instance, the pallial progenitors express high levels of the basic helix-loop-helix (bHLH) TFs *Ngn1* and *Ngn2,* homeodomain TFs *Emx1*, *Emx2*, *Lhx2* and *Pax6,* or *Tbr2* (Eomes). While *Emx1*, *Emx2* and *Lhx2* show most abundant expression in the medial pallium, *Pax6* and *Tbr2* are most highly expressed in the VZ of the ventral and lateral pallium (Campbell, 2003). Another set of genes expressed in the germinative zones of LGE (*Gsh2*, *Dlx1*, *Dlx2*, *Dlx5* and *Dlx6*) and MGE (e.g. *Nkx2.1*) specify their territories. Notably, some small compartments of telencephalon could be demarcated only by the restricted expression of some markers, such as TF Dbx, outlining the germinative zone of the ventral pallium, TF Er81, which marks a small progenitor zone of the dorsal LGE, thus specifying progenitors and cells populating the olfactory bulb or the LIM homeobox protein Islet-1, labeling the SVZ of ventral LGE.

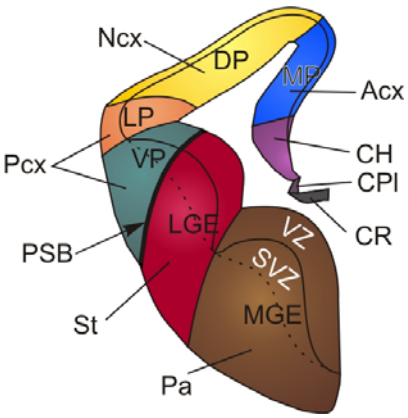

Fig. 2. Dorsoventral organization of the mammalian telencephalon. This schema depicts a coronal hemisection of the mouse telencephalon at E12.5. The major morphologically defined structures and the progenitor subdomains identified by restricted expression of TF genes: Medial (MP), dorsal (DP), lateral (LP), and ventral (VP) pallium contribute to the pallium, while medial, lateral and caudal ganglionic eminences (MGE, LGE, and CGE, respectively) are parts of the subpallium. CGE is not visible in this plane. Further subdivisions or derivates of the

mentioned major subdivisions are choroidal roof (CR), choroid plexus (CPl), cortical hem (CH), archicortex (Acx including hippocampus), neocortex (Ncx), paleocortex (Pcx), striatum (St), pallidum (Pa). PSB, Pallio-subpallial boundary, SVZ, subventricular zone; VZ, ventricular zone. After Stoykova et al., 2000 and Molyneaux et al., 2007 .

1.1.2. Cortical regionalization: inductive centers

According to a current view, the establishment of the initial AP and ML axes of cortical primordium is initiated by ligands, secreted by forebrain inductive centers, that induce graded expression of sets of TFs (Mallamaci and Stoykova, 2006; O'Leary et al., 2007; O'Leary and Nakagawa, 2002; Sur and Rubenstein, 2005). The secreted ligands, acting as signaling molecules or morphogens (or both), are released from four structures at the border of the cortical field. From E10 onwards, Wnts (Wnt2b, 3a, 5a, 7b, 8b) and bone morphogenetic proteins (Bmps; Bmp2, 4, 5, 6, 7) are secreted from the cortical **hem** in the dorsal midline (see Fig. 3). The hem later becomes the embryonal fimbria and is located at the medial edge of the cortex next to the hippocampus. In mice lacking functional Wnt3a or the Wnt signaling factor Lef1, the formation of the hippocampus is severely disrupted (Galceran et al., 2000; Lee et al., 2000). From E10 to approx. E12.5, Fgf3, 8, 17 and 18 (fibroblast growth factors) are secreted from the anterior patterning center, the **anterior neural ridge** (ANR), which later forms the commissural plate (CoP). Fgfs are believed to promote a rostral vs. caudal fate of cortical primordium. Sonic hedgehog (Shh) is released from the **ventral telencephalon** and hypothalamus (Sur and Rubenstein, 2005). Another lateral putative signaling center, called the **antihem,** is located in the lateral edge of the cortex adjacent to the boundary between dorsal and ventral telencephalon. Beginning at E12.5, the antihem secretes five types of molecules, namely Tgf-α, Nrg1, Nrg3, Fgf7, and the Wnt antagonist Sfrp2 (Assimacopoulos et al., 2003).

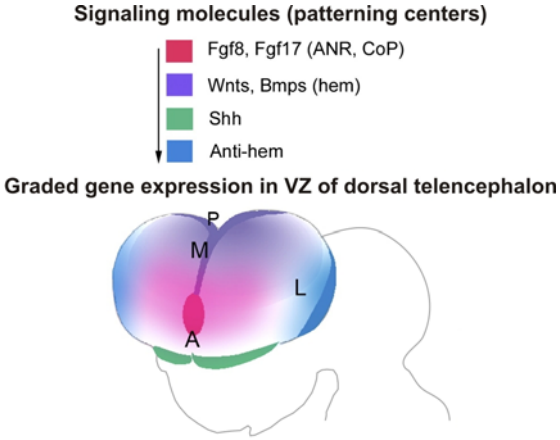

Fig. 3. Signaling centers of the cortical VZ. At early developmental stages, secreted ligands (signaling molecules) are crucial to set up the initial, tangential gradients of TFs in the VZ (such as Emx2, Pax6, Coup-TF1 and Sp8), which thus help to establish neocortical areas. The signaling molecules are secreted from putative inductive centers: Fgf8, from the anterior neural ridge (ANR), which later becomes the CoP (commissural plate); Wnts and Bmps from the cortical hem, Shh from the

medial ganglionic eminence (MGE), and other molecules from a putative patterning center, the antihem. Because most CP neurons migrate radially, the positional information stored in such gradients is likely to be inherited. Adapted from O'Leary et al., 2007 .

1.1.3. Neurogenesis in developing cortex: germinative layers, asymmetric/symmetric divisions

After positioning of cortical progenitors along AP and ML axes of the cortical primordium, at E10.0 the neurogenesis starts. In mouse, all cortical neurons are generated for nine days (E10-E18) by progenitors that undergo 8 mitotic cycles (Mallamaci and Stoykova, 2006).The majority of neocortical neurons, including all projection neurons, originate from the progenitors located in the layer immediately adjacent to the ventricle ventricular zone (VZ) of the dorsal telencephalon. Later, an additional proliferative layer, termed the subventricular zone (SVZ) is generated above the VZ. In the nascent neocortex, there are at least three different types of neuronal progenitors: neuroepithelial (NE) or stem cells, radial glial (RGP) and basal progenitor cells (BP, also termed intermediate progenitors, IP). At the onset of neurogenesis (E9-E10) NE, initially arrayed in a single pseudostratified sheet in the VZ, undergo symmetric cell divisions to expand the pool of multipotent progenitors, while a smaller portion of asymmetric NE divisions give rise to the earliest born neurons (Molyneaux et al., 2007), the Cajal-Retzius cells. After stage E10.5, the predominant cortical progenitors are the pluripotent RGPs, generated by NE, but expressing some glial characteristics (Götz and Huttner, 2005). Cortical neurons are generated by two proliferative modes. During the period of direct neurogenesis (mostly E10.5-E12.5), RGPs divide asymmetrically in VZ to produce one RGP (self-renewing) and one neuron. After stage E12.5 however, RGPs divide predominantly asymmetrically and produce two progenitors, one RGP and one IP, the last one dividing further in SVZ symmetrically to generate two neurons (indirect neurogenesis) (Götz and Huttner, 2005; Huttner and Kosodo, 2005). The expression of TF Pax6 plays a role of an intrinsic determinant of RGPs (Götz et al., 1998), while Tbr2 expression specifies the IPs (Sessa et al., 2008). Recent evidence indicates that during the period of direct and indirect neurogenesis, distinct partially overlapping and timely specific sets of TFs are expressed in VZ or SVZ progenitors (Hevner, 2006).

1.1.4. Cortical layering

The excitatory pyramidal projection neuron is the predominant type of cortical neuron, which makes up to 75 to 85% of the neurons of mammalian cortex (Hevner, 2006). Pyramidal cells are born by progenitors of the pallium, typically have a pyramidal-shaped cell body, and use glutamate as neurotransmitter. The remaining 15 to 25% of cortical neurons are interneurons, which are inhibitory, use γ-aminobutyric acid (GABA) as neurotransmitter and are characterized by a non-pyramidal morphology. These neurons are born by subpallial progenitors and reach, by a tangential migration, their specific layer location into the cortex.

The earliest born neurons by the pallial progenitors (around E10.5) form initially the so-called preplate (PP). After that, the generated neurons of the cortical plate (CP) intercalate into the PP, splitting into the outermost marginal zone (MZ) and the deeply located subplate (SP). The cortical neurons are generated following an inside-first-outside-last order. Thus, the low-layer neurons (layer 6, 5, L6, L5) are born at early stages (E11.5-E13.5) and are located in the low CP. The upper layer neurons (L4-L2) are born after E13.5 and when arriving into CP they migrate past earlier born neurons and occupy progressively upper positions (Fig. 4). Each layer is build up by neurons that show specific morphology, connectivity, and function.

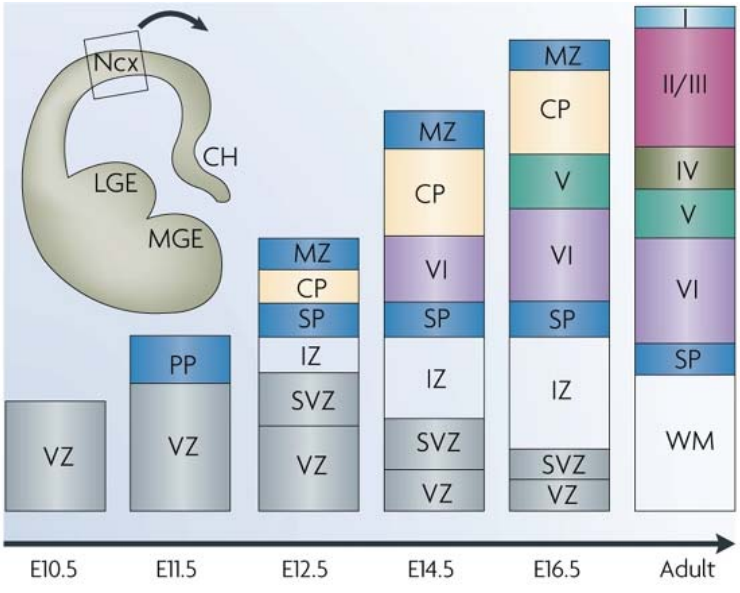

Fig. 4. Generation of the neocortical layers during development. The preplate (PP) is formed by the earliest born neurons. The PP is later split into the more superficial marginal zone (MZ) and the deeply located subplate (SP). The cortical plate (CP), which will generate the multilayered neocortex, develops in between these two layers. I-VI, layer 1-6; CH, cortical hem; E, embryonic day; Ncx, neocortex; IZ, intermediate zone; LGE, lateral ganglionic eminence; MGE, medial ganglionic eminence; SVZ, subventricular zone; VZ, ventricular zone; WM, white matter. Adapted from Molyneaux et al., 2007.

While widely accepted that the laminar fate of the neurons is determined by environmental cues acting during the S phase of the last mitotic cycle of the progenitors (McConnell, 1990), recent evidence indicate that laminar fate is also specified by the

expression of specific layer-specific TFs (Arlotta et al., 2005; Britanova et al., 2005; Joshi et al., 2008). For instance, by repressing the generation of CR cells, the initiation of expression of TF Foxg1 at E10.5 is essential for promoting the neocortical lamination, imparting NE to switch from preplate neurogenesis to cortical plate neurogenesis (Hanashima et al., 2004). Furthermore, recent evidence strongly suggests that TF Satb2, expressed abundantly in the upper layer neurons, promotes even the projection neuron identity, supporting the extension of interhemispheric connectivity through corpus callosum (Alcamo et al., 2008; Britanova et al., 2008).

1.1.5. Functional arealization of mammalian cortex

While radially ordered into six layers, the cortical neurons are also tangentially arrayed into functionally specialized areas. In mouse, four primary functional domains are distinguishable: motor, sensory, visual and auditory cortex (O'Leary et al., 2007; Ragsdale and Grove, 2001).

Two main theories have been proposed to explain the cellular and molecular mechanisms leading to the diversity of cortical regions. In the protomap model (Rakic, 1988), cerebral cortical areas are assumed to be primarily specified by the control through molecular determinants intrinsic to the proliferative zone of the neocortex. The second theory, the protocortex (or *tabula rasa*) model (O'Leary, 1989) postulates that neocortical arealization is largely regulated by extrinsic factors, e.g. thalamocortical axons (TCA), which make strict connections between distinct thalamic sensory nuclei and corresponding functional domains (Jones, 2007). Robust experimental data exist in support of each model. It is therefore assumed that depending on the phase of cortical development a different mechanism of arealization is prevailing, bringing both proposed theories into line (Mallamaci and Stoykova, 2006).

During the early phase of cortical patterning (before arrival of TCA into CP at stage E16.5), molecular regionalization of the cortical primordium is triggered by intrinsic information, which corresponds to the protomap model. During the later phase, thalamocortical fibers help to refine cortical arealization, which takes account of the protocortex model.

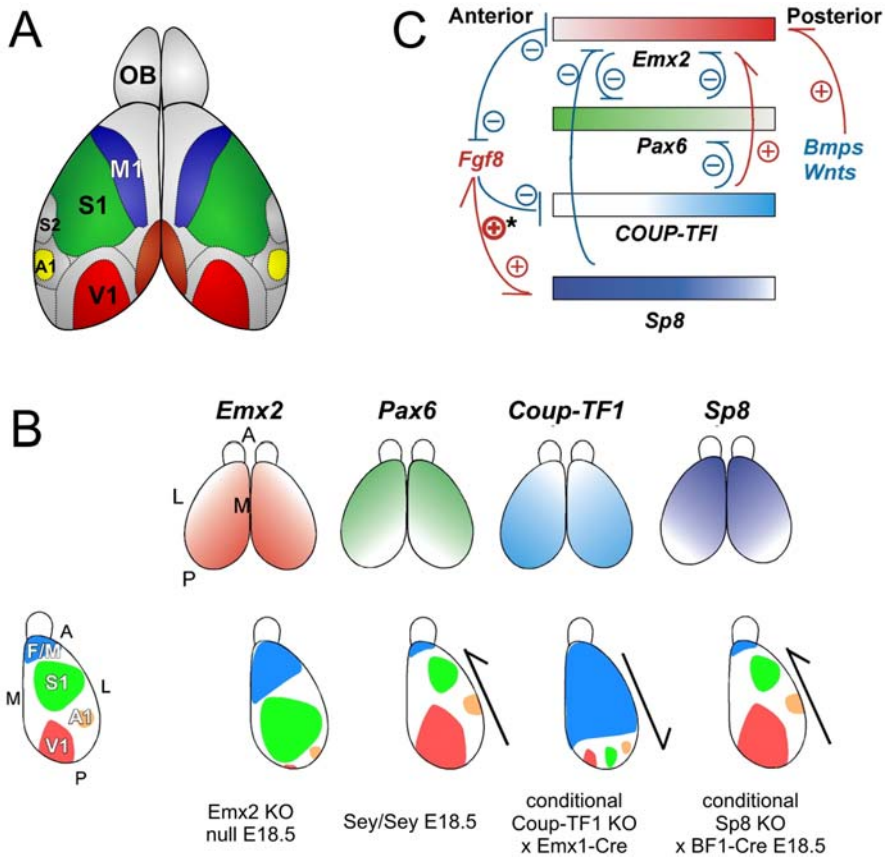

Fig. 5. Areal patterning of the mammalian cortex, mutant phenotypes and intrinsic genetic mechanisms. (**A**) Area map of an adult mouse cerebral cortex in dorsal view of the cerebral hemispheres. Rostral (anterior) is to the top: Major cortical areas are outlined in different colors; the neocortex comprises M1, primary motor cortex (blue); S1 and S2, primary (green) and secondary somatosensory cortex; V1, primary visual cortex (red); A1, primary auditory cortex (yellow). The archicortex including hippocampus is depicted in brown. (**B**) First row: Expression gradients of *Emx2*, *Pax6*, *Coup-TF1*, and *Sp8* along anterior-posterior (A/P) and lateral-medial (L/M) axes. *Emx2* is expressed from P/M high to A/L low, while the *Pax6* is expressed opposite to *Emx2*, with a high A/L to low P/M gradient. *Coup-TF1* exerts a high P/L to low A/M gradient, while *Sp8* expression is from A/M high to P/L low. Second row: Summary of reports of loss-of-function mice mutants for TFs that regulate areal patterning. Loss of *Emx2* results in posterior shifts of areas including shrinkage of V1, while the small eye mutant with non-functional *Pax6* displays anterior area shifts. Ablation of *COUP-TF1* In cortical progenitors causes transformation of primary sensory areas into frontal/motor areas. In *Sp8* conditional knockout mice areas are shifted anteriorly, a similar phenotype like that observed in *Fgf8* hypomorphic mice. (**C**) Interplay of TFs and signaling molecules in the mechanism of cortical patterning. *Fgf8*, expressed from the anterior neural ridge (ANR) establishes expression gradients of *Emx2* and *Coup-TF1*, by repression. *Sp8* expression, on the other hand, is promoted by *Fgf8*. *Emx2* in turn indirectly represses *Fgf8*. *Emx2* and *Pax6* mutually inhibit each others expression. *Coup-TF1* negatively regulates *Pax6* expression, while promoting *Emx2* expression. *Bmps* and *Wnts*, expressed from the cortical hem, support the high caudal gradient of *Emx2* expression. +, positive interaction; -, negative interaction. A, anterior; F/M, frontal/motor areas; L, lateral; M, medial; P, posterior. Adapted from Ragsdale and Grove, 2001 and from O' Leary et al., 2007.

Accumulating recent data clearly demonstrate the central role of intrinsic mechanisms in the control of cortical regional specification and differentiation. As noticed above, signaling molecules and morphogens are released from the forebrain inductive centers, establishing the graded expression patterns of TFs in the proliferative zone lining the lateral ventricles as illustrated in Fig. 5. Disruption of the normal graded expression of these factors leads to severe defects in cortical arealization. The homeobox TF Emx2 (a vertebrate homolog of the *Drosophila*, empty spiracles) and the paired domain containing TF Pax6 (*Drosophila* ortholog *eyeless***)** are expressed in opposing gradients along the A/P axis of the cortical anlage: *Emx2* is expressed in a caudomedial-high to rostrolateral-low gradient (Gulisano et al., 1996; Mallamaci et al., 1998; Simeone et al., 1992), whereas *Pax6* displays opposite gradient, rostrolateral-high to caudomedial-low (Stoykova et al., 1996; Walther and Gruss, 1991). In *Emx2* and *Pax6* mutants, cortical areas are disproportioned in opposite manner as demonstrated by molecular marker analysis (Bishop et al., 2000) confirming the original assumption that *Emx2* and *Pax6* are promotors of caudomedial or rostrolateral fate to neural progenitors, respectively. Indeed, in *Emx2* deficient brains, caudomedial areas are shrunken, while rostrolateral ones are augmented. Similarly to *Emx2*, the orphan nuclear receptor gene *COUP-TF1* shows highest expression in the caudolateral cortex. Ablation of *COUP-TF1* results in dramatic enlargement of the size of the rostral, motor cortex in expense of all other cortical domains displaced in the caudalmost edge (Fig. 5). Moreover, area-specific connections between the thalamus and the cortex were found to be miswired (Zhou et al., 2001). In the *Pax6*$^{Sey/Sey}$ mutant, the complementary effect was observed – shrinkage of rostral motor cortex area and enlargement of the posterior (visual) area. Similar to Pax6 graded expression in germinative zone shows TF Sp8 (homolog of *Drosophila buttonhead*), and similar defects in arealization were found after targeted disruption of this gene (Zembrzycki et al., 2007). Thus both, *Pax6* and *Sp6* appear to promote anterior (frontal/motor) cortical identities.

Along the ML axis, two other TFs, Foxg1 and Lhx2, exert a regionalized expression in the progenitors. The winged helix TF gene *Foxg1* shows a caudomedial-low to rostrolateral-high gradient in the early telencephalon. As the loss of functional *Foxg1* leads to an abnormally small or absent paleo- and neocortex at the expense of an enlarged caudomedial domain, it is assumed that Foxg1 normally suppresses the caudomedial (hippocampal) cortical fate (Muzio and Mallamaci, 2005). In opposite, expressed in a caudomedial-high to rostrolateral-low gradient, *Lhx2* represses the spread of the fimbria and the choroid plexus

(Bulchand et al., 2001; Monuki et al., 2001). Transcripts of the LIM-box-homeobox gene *Lhx2* are distributed in the entire telencephalic neuroepithelium, forming a caudomedial-high to rostrolateral-low gradient, but omitting the cortical hem. *Lhx2* represses the spread of the fimbria and the choroid plexus (Bulchand et al., 2001; Monuki et al., 2001), which are derivates of the medial edge of the dorsal midline.

Collectively, the available evidence demonstrate that encoded positional information by secreted ligands and differentially expressed TFs along AP and ML axis of VZ/SVZ plays a crucial role in cortical regionalization. One still unanswered question is how the graded expression of such molecular determinants in the germinative zones of the embryonic cortex is translated into sharply bordered functional domains of the adult brain. How the genetic information is used to master the final morphological and functional integrity of the cortex is a challenging question of the neurobiology today.

In the present study, evidence is shown indicating that regionalized expression of TF Zbtb20 in progenitors and postmitotic neurons of the medial pallium may enable the proper regional specification of archicortex, including hippocampus. Therefore, the short description below outlines the most important features of the structural components of the archicortex and TF Zbtb20.

1.2. Hippocampal formation and retrosplenial cortex

The hippocampal region (Paxinos, 2004), whose basic layout of cells and fiber tracts is mainly the same in all mammmals, includes two sets of cortical structures, the hippocampal formation and the parahippocampal region, distinguishable from one another mainly by the arrangement of the neurons into layers and the overall principles of connectivity.

Buried deep by the cortical hemispheres, the hippocampal formation consists of hippocampus proper or Ammon's horn, subiculum, and dentate gyrus (Fig. 6). Hippocampus proper together with the dentate gyrus are often termed hippocampus, because this remarkable, curved brain structure protruding into the lateral ventricles resembles the correspondent tropical fish (hippocampus, the Greek word for seahorse (Andersen, 2007). The three regions of the hippocampal formation share, more or less, the characteristic three-layered archicortical appearance. The hippocampal formation has a crucial function in learning and memory as well in anxiety-related behaviors (Bannerman et al., 2004). The bilateral removal of the hippocampus in people (treatment of severe epilepsy) leads to total loss of memory. While memories from the past can be recalled, new facts are retained only

for seconds (Kahle and Frotscher, 2002). Interestingly, the hippocampal formation is one of the first brain regions affected in Alzheimer's disease (Braak and Braak, 1998). Many neurologic and psychiatric disorders, including epilepsy (Haas et al., 2002; Houser et al., 1990; Lurton et al., 1997), lissencephaly (Ross et al., 2001; Sato et al., 2001), Down's syndrome (Raz et al., 1995), schizophrenia (Weinberger, 1999), depression (Frodl et al., 2002), autism (Cook, 1990) and attention-deficit/hyperactivity disorder (ADHD) (Plessen et al., 2006) are strongly associated with histological abnormalities within abnormal hippocampal formation, which seem to result from disrupted neuronal migration during development.

The parahippocampal region comprises entorhinal, perirhinal and postrhinal cortices, pre- and parasubiculum. It is involved in memory processing and is implicated in brain disorders such as Alzheimer's disease, schizophrenia and epilepsy (Witter and Wouterlood, 2002).

The retrosplenial cortex (Rsp) is a transitory (neocortical) region intercalated between archicortex and neocortex involved in memory and navigation (see below).

1.2.1. Hippocampus proper

From medial to lateral direction, the hippocampus proper is divided into three fields, CA3, CA2, and CA1 (Lorente de Nó, 1934), comprising two major regions, a proximal region (CA3 and CA2) and a distal region (CA1), which contain large or small pyramidal cells, respectively. CA2 shares some features with the other two fields (see Fig. 6B-D).

Radially, listed from the inside (closest to ventricle) to the outside (surface), the following distinct layers can be distinguished in the hippocampus: (1.) the fiber-containing alveus; (2.) the *stratum oriens*, which is a relatively cell-free layer; (3.) the *stratum pyramidale* or pyramidal cell layer, (pcl) which is the principal cell layer; (4.) the *stratum lucidum*, a narrow acellular zone, only found in CA3 (5.) the *stratum radiatum* (6.) the *stratum lacunosum-moleculare*.

The principal neuronal type of the hippocampus is the pyramidal cell, which outnumbers by far other neuron types. The dense-appearing pyramidal cell layer (plc) harbors the soma of these pyramidal cells, whose basal and apical dendritic trees protrude into the *stratum oriens* and the strati above the plc, respectively.

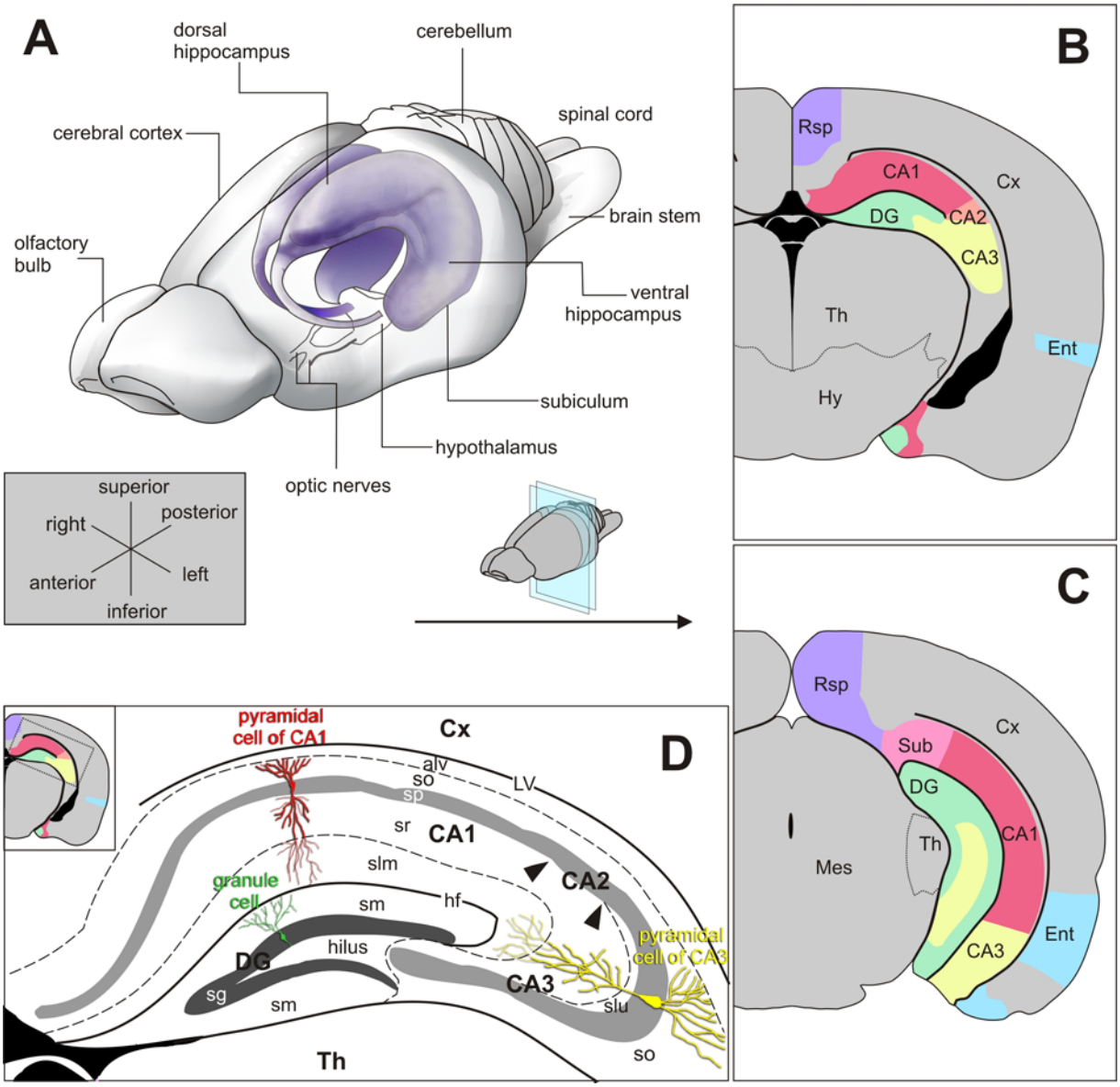

Fig. 6. Morphology and organization of the rodent hippocampal region. (**A**) Three-dimensional overview murine adult mouse brain showing main structures. The translucently drawn forebrain allows view of hippocampus and associated areas, shaded in violet. (**B, C**) Coronal hemisections through the forebrain at rostral (**B**) and caudal (**C**) level are shown as schema. Components of the hippocampal formation are colored. See text. (**D**) Stratification of the hippocampus. Location of the principal cells (pyramidal and granule cell of Ammon's horn and DG, respectively) within the different strati is illustrated. (**D**) is a close up of (**B**). Alv, alveus; CA1, CA2, CA3, cornu ammonis fields 1–3; Cx, cortex; DG, dentate gyrus; Ent, entorhinal cortex; hf, hippocampal fissure; Hy, hypothalamus; Mes, mesencephalon; Rsp, retrosplenial cortex; sg, *stratum granulosum*; slm, *stratum lacunosum-moleculare*; slu, *stratum lucidum*; sm, *stratum moleculare*; so, *stratum oriens*; sp, *stratum pyramidale*; sr, *stratum radiatum*; Sub, subiculum; Th, thalamus. After Danglot et al., 2006; Paxinos, 2004 .

1.2.2. Dentate gyrus

The dentate gyrus and the olfactory bulb are the two brain regions with robustly ongoing neurogenesis during adulthood (Gould, 2007). The three layers of DG from outside in are (1.) the *stratum moleculare* (sm), which is relative cell free, (2.) the granule cell layer (gcl or *stratum granulosum*, sg), consisting mainly of densely packed columnar stacks of granule cells, and (3.) the polymorphic cell layer, the hilus (Fig. 6D). At the border between the hilus and the gcl the subgranular layer (sgl) is located, which contains progenitors dividing slowly even in the mature brain. The gcl is the principal cell layer of the DG. The portion of the gcl that is adjacent to CA1 is called the enclosed blade (synonyms: suprapyramidal blade or limb) while the remaining portion of the gcl is called the free blade (synonyms: infrapyramidal blade or limb). Depending on the cut plane the gcl has a “V” or “U” shape, called the crest.

1.2.3. Subiculum

The subicular complex consisting of presubiculum, parasubiculum and subiculum (S) is positioned between area CA1 of the hippocampus proper and the entorhinal cortex (EC) ventrally, and CA1 and the retrosplenial cortex, dorsally (O'Mara et al., 2001), (Fig. 6B-D). The pre- and parasubiculum both have deeper layers of principal neurons continuous with the EC. As these areas are multilaminate, they are more similar to the adjacent EC that is composed of six-layers. The subiculum however, resembles in its cytoachitectonic more the adjacent hippocampus proper. Both structures comprise three principal layers, thus having the characteristic cytoarchitectonic of the allocortex (archicortex and paleocortex). The three-layered subiculum is composed of: (a) a molecular layer, which is continuous with *stratum lacunosum-moleculare* (sl-m) and *stratum radiatum* (sr) of the CA1 field; (b) a pyramidal cell layer (pcl) containing the soma of principal neurons, and (c) a polymorphic layer. The neurons in pcl of subiculum are much less tightly packed as compared with those of CA1 of hippocampus. Thus, the S appears cell sparse compared to CA1 region as well as to adjacent Rsp and Ncx with their densely packed upper layer neurons. As a functional unit, the subiculum plays a role in certain forms of spatial memory and in mnemonic processing (O'Mara et al., 2001).

1.2.4. Retrosplenial cortex

The retrosplenial cortex (Rsp) in the human brain is delineated to Brodmann's areas 29 and 30 within the posterior cingulate region, covering the mediocaudal surface of each hemisphere, between the visual cortex and hippocampal formation (Fig. 6B, C).

Rsp as a neocortical structure is viewed as an "intermediate" or "transitory" cortex because its lamination is transitional between neo- and archicortex (Vann et al., 2009). Tangentially, the Rsp can be subdivided into a granular retrosplenial area (RSG) and an agranular retrosplenial area (RSA). RSG and RSA are located at the medial surface and the dorsomedial surface, respectively. Cytoarchitectonically, the RSG is characterized by a conspicuous layer II but a poorly differentiated layer IV and splitting of layer V into Va and Vb. Being reciprocally connected with other brain regions (e.g. subiculum, presubiculum, parasubiculum, entorhinal cortex, cingulate cortex, prefrontal cortex and thalamus), the Rsp is likely to be involved in hippocampus-dependent functions. Thus, the Rsp plays a crucial role in episodic memory and spatial navigation while it shows pathological changes in most neurological disorders implicating memory loss (Vann et al., 2009).

1.2.5. Principal cell of hippocampus proper and dentate and their generation

The prospective pyramidal cells (**pc**) in the nascent hippocampus proper are born in the Ammonic neuroepithelium. Neurogenesis in the murine hippocampus takes place from E10 till birth (Angevine, 1965), while most pyramidal cells are generated around E14.5 (Nakahira and Yuasa, 2005). The peak of CA3 **pc** production is followed by that of CA1 **pc** with a delay of 3 days. The migrational path of **pc** has been extensively studied in mouse and rat (Altman and Bayer, 1990c; Nakahira and Yuasa, 2005). Upon labeling at E14.5 in mouse, these cells can be registered in intermediate zone of the hippocampus one day later, where they rest for 2 days before becoming progressively settled in the dominant *stratum pyramidale* (**pcl**) in an "inside-out" sequence, which is the same mode as for other cortical regions except dentate gyrus. On day 4 the **pcl** of CA1 region will be penetrated while in CA3 the cells still pass through in the intermediate zone, because CA3 is the region located farthest from the hippocampal neuroepithelium.

In the dentate gyrus, neurons are generated from E10 and P20 onwards in the mouse (Angevine, 1965). Their production continues into adulthood. The generation of the dentate granule cells (**gc**) forms an exception within the cortex. In contrast to the **pc** of hippocampus proper, the dentate **gc** are born in the primary dentate neuroepithelium (**dgp**), a region

adjacent to the Ammonic neuroepithelium. These neuroblasts leave the **dgp** and form the secondary proliferative zone (**dgs**). Migrating, the dentate progenitors become progressively displaced, forming a secondary and tertiary matrix until they finally form the dentate granule cell layer, capping the proximal tip of CA3 **pcl**. The bulk of dentate **gc** are formed within the first postnatal weeks (Altman and Bayer, 1990a), while in the tertiary matrix, **gc** are produced throughout adulthood.

1.3. Transcription factor Zbtb20

1.3.1. Conserved function of Zbtb20

The BTB zinc finger gene *Zbtb20*, also named DPZF (Zhang et al., 2001), HOF (Mitchelmore et al., 2002), and ZNF288 encodes a transcription factor belonging to the POK (Poxviruses and Zinc-finger (POZ) and *Krüppel*) family of transcriptional repressors. They encompass a N-terminal POZ/broad Complex, tramtrack, and bric à brac (BTB) domain and several C-terminal C_2H_2 *Krüppel*-type zinc finger motifs. The POZ/BTB domain enables homo- and heterodimerization as well as protein-protein interactions, necessary for the recruitment of corepressor complexes. Recognition and binding of DNA sequences is mediated by the specific zinc fingers. In both mouse and human, more than 40 genes are associated with the combination of these two evolutionary conserved domains. POK transcription factors regulate the transcription of their target genes via the interaction with a range of co-factors including SIN3A, SMRT, and NCOR1 corepressors, which in turn recruit HDACs (Histone deacetylases). HDACs mediate deacetylation of chromatin what leads to transcriptional repression. In vertebrates, all known BTB/POZ-ZFs act as transcriptional repressors, while some function additionally as activators (reviewed by Kelly and Daniel, 2006). POK TFs are implicated in processes such as development, cancer and stem cell biology (Costoya, 2007).

1.3.2. Molecular properties of the Zbtb20 protein

Zbtb20 was first cloned from human and later from mouse (Mitchelmore et al., 2002; Zhang et al., 2001). The human *ZBTB20* gene is located on chromosome 3 whereas the murine homolog is located on chromosome 16. In mouse, the *Zbtb20* gene encodes two protein isoforms, Zbtb20L and Zbtb20S, which are of 741 and 668 amino acids, respectively (Mitchelmore, 2002 and Ensembl, Fig. 15). The two isoforms are identical except that Zbtb20S lacks the N-terminal 73 amino acids present in Zbtb20L. Both isoforms were shown to be engaged in homo- and heterotypic protein interactions via the BTB/POZ domain while

the C-terminal zinc finger domain specifically binds to the binding site for PLZF (Mitchelmore et al., 2002).

1.3.3. Zbtb20 expression in the mammalian brain

In the developing mouse brain, Zbtb20 protein is expressed in the cerebral cortex during late embryonic and postnatal stages (Mitchelmore et al., 2002). During late embryonic and postnatal development of the cerebral cortex Zbtb20 is predominantly expressed in early differentiating CA (cornu ammonis) pyramidal and dentate gyrus (DG) granule neurons of the hippocampal subdivision. Zbtb20 is transiently up-regulated in immature post-mitotic neurons derived from the hippocampal neuroepithelium as well as in migrating granule cell precursors of DG. Moreover, *Zbtb20* transcript is found in the indusium griseum, in scattered cells in the ventricular and subventricular zone of the hippocampal neuroepithelium (E18.5), archicortical neuroepithelium lining the lateral ventricle, the hippocampal intermediate zone, the expanding hippocampal plate, the dentate gyrus and the fornix.

Postnatally, *Zbtb20* message was found in the hippocampal intermediate zone, pyramidal cells of CA1 and CA3, granule cells of dentate gyrus, external and internal granule layer, molecular cell layer and white matter of the cerebellum. Furthermore, Zbtb20 is expressed in early astrocytes in the SVZ of the lateral ventricle and rostral migratory stream as well as in oligodendrocytic cells.

1.3.4. *Zbtb20* in the regional patterning of the forebrain

Recent evidence support *Zbtb20* to be involved in more than one physiological/ developmental process. Analyses of ectopic *Zbtb20* expression in transgenic brains revealed that *Zbtb20* is capable to induce a kind of ectopic corticogenesis into the neocortex, typical for the hippocampus (Nielsen et al., 2007). The authors assume a potential role for *Zbtb20* in regulation of invariant cortical neurogenesis.

1.3.5. *Zbtb20* expression and function outside central nervous system

In human, Zbtb20 protein is widely expressed in hematopoietic tissues (Harboe et al., 2000; Zhang et al., 2001). In mouse, it was found to be up-regulated postnatally in liver where Zbtb20 was demonstrated to be a transcriptional repressor of the Alpha-fetoprotein (AFP) gene by directly binding to its promoter, as revealed by studies in liver-specific *Zbtb20* conditional knockout mice (Xie et al., 2008). AFP itself is necessary for protecting the

developing fetal brain from prenatal exposure to estrogen, thus crucial for female fertility (Bakker et al., 2006; Gabant et al., 2002). Recently, *Zbtb20* was found to be essential for glucose homeostasis (Sutherland et al., 2009).

1.4. Aims of this study

Which genes and pathways lead to the complexity of the human brain? The mechanisms underlying the genesis and the patterning of the mammalian cerebral cortex are only in the beginning to be understood. As a result of microarray screen performed previously by the group, multiple genes had been identified to show stage specific enriched expression in distinct areas of the mouse E16.5 cortex (Mühlfriedel et al., 2007). To gain further knowledge on functional significance of such genes, the aim of my project included the identification and functional characterization of selected candidates, possibly involved in *Emx2*-dependent regionalization of the developing cortex.

In the first part of this work, selected genes with a predominant expression in the caudal cortex were subjected to detailed RNA-in situ hybridization analysis on sections from wild type and *Emx2*-deficient brains. This analysis helped to gain detailed new information about the expression characteristic of six TFs and regulatory molecules.

The second part of this study presents results from the performed expression and functional analysis of TF Zbtb20. In order to elucidate *Zbtb20*'s biological function, *Zbtb20* deficient mice were created. The analysis of these animals was focused on two obvious phenotypes observed in (1) the cerebral cortex and (2) the skeleton.

II. Results

2.1. Screen for identification of genes expressed in Emx2-dependent manner in developing mouse cortex

Despite the role of Emx2 in cortical arealization is widely documented, little is known about determinants acting downstream of this transcription factor. Aiming to identify such candidate genes for further functional analysis, genes were selected from the previously performed microarray/in situ hybridization screen in the laboratory (Mühlfriedel et al., 2007). This screen was carried out with tissue samples of distinct cortical areas at embryonic stage E16.5. At this stage, the cortical neurogenesis is in an advanced stage. Although the thalamocortical axons have already reached the subplate, they are still not invading the CP in a region specific manner. It is assumed therefore that the registered differential gene expression patterns are likely to be intrinsic to the late germinative neuroepithelium and may be involved in the development of area specific feature. On the other hand, regionalized gene expression in postmitotic neurons of CP is indicative for involvement in mediation of the encoded in VZ/SVZ positional information.

Eight known, *Odz3*, *Nef3*, *Zbtb20*, *Flrt3*, *Ebf3*, *Nrp2*, *Grp*, *Nr4a3,* and two unannotated genes with a similar to Emx2 graded expression were selected and their expression was studied in both wild type and *Emx2-/-* genetic background. The applied criteria for such a selection were the following: a) the gene should exert an expression gradient similar to that of *Emx2*, either in the germinal zones or in CP; b) the encoded factor should have molecular characteristics, implicating important function (e.g. TF, receptor, adhesive molecule); c) the function of such gene in mammalian corticogenesis should be still not clear.

As a result of the performed detailed expression analysis, six potential candidates, possibly acting in *Emx2*-dependent manner, were identified as described below.

Two genes, *Odz3* and *Nef3* showed a nice graded caudal-high to rostral-low expression in CP of the neocortex (Ncx). ***Odz3*** is a vertebrate homolog of the *Drosophila odd Oz* (*Odz*) (Baumgartner et al., 1994; Ben-Zur et al., 2000; Levine et al., 1994; Oohashi et al., 1999). It encodes a transmembrane protein involved in segmental patterning (Baumgartner et al., 1994; Levine et al., 1994). The most robust *Odz3* expression was detected in the occipital (visual) and retrosplenial cortex (Rsp) (Fig. 7A, D). The expression progressively decreased rostrally, so that the motor cortex was almost completely free of *Odz3* mRNA transcripts (Fig. 7A, B). Postmitotic cells in the striatum (Str, also named basal ganglia) moderately expressed *Odz3* (Fig. 7B, C). In addition, many differentiating nuclei in diencephalon (Fig. 7C, D) and

midbrain (Fig. 7E) showed strong *Odz3* expression signal. Strikingly, the expression of *Odz3* in CP was clearly decreased in *Emx2-/-* cortex, detected on sagittal (Fig. 7A/A') and coronal sections (Fig. 7B/B', C/C', D/D'). Because areal topology in *Emx2-/-* mutant cortex is generally preserved (Mallamaci et al., 2000b), the profound decrease of *Odz3* expression in the *Emx2* mutant brain strongly suggests that *Odz3* appears to act downstream of TF Emx2.

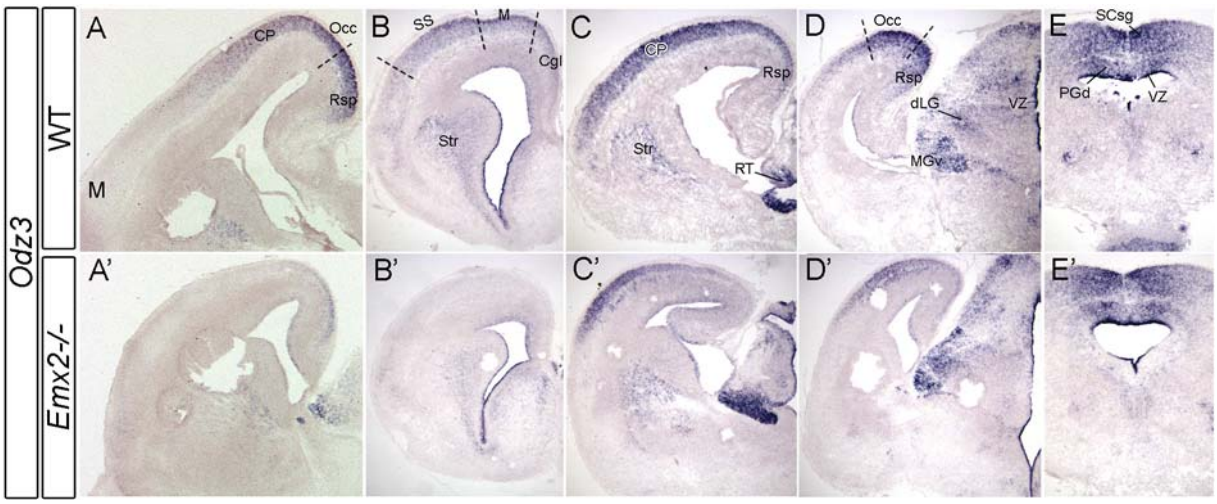

Fig. 7. *Odz3* appears to act downstream of *Emx2* in cortical patterning. (**A/A'**) Sagittal sections of E16.5 control (**A**) and *Emx2-/-* (**A'**) mutant brains. In (**A**/**A'**) note the almost full abrogation of the caudal-high to rostral-low *Odz3* expression gradient in the *Emx2-/-* background. (**B-E'**) are coronal sections displayed from rostral (left) to caudal (right) level of the control (**B-E**) and *Emx2-/-* brain (**B'-E'**). Note the robust expression of *Odz3* in CP at most caudal level (**D**), in retrosplenial (Rsp) and occipital (Occ) cortex, as compared to the rostral domain, motor and somatosensory cortex (SS) (**B, C).** In the *Emx2* mutant, *Odz3* expression was severely inhibited (compare **B/B'**, **C/C'**, **D/D'**), with a small residual expression kept in the parietal cortex. (**C, D**) In the control brain at E16.5, *Odz3* expression was detected in distinct differentiating nuclei of diencephalon: reticular nucleus of thalamus (RT), dorsal lateral geniculate nucleus (dLG), ventral subdivision of medial geniculate nucleus (MGv). (**E)** In midbrain: dorsal periaqueductal gray (PGd), superficial layer of superior colliculus (SCsg). CP, cortical plate; Cgl, cingulate cortex; M, motor cortex; Str, striatum; VZ, ventricular zone.

Similarly, the expression of ***Nef3*** (*Nefm*, neurofilament, medium polypeptide, (Julien et al., 1986) was confined to the superficial layers of the caudal CP. Strong expression in patches was detected in the anlage of the caudalmost occipital (visual) cortex (Fig. 8C) and in the parietal (temporal) cortex (Fig. 8B), while only a very faint signal was seen in the rostral (motor) CP (Fig. 8A). Remarkably, in the *Emx2-/-* mutant, *Nef3* signal was abolished in the caudalmost CP (Fig. 8C/C'), in the motor (M) and somatosensory (SS) area (Fig. 8A/A'), however, the patchy signal in the temporal cortex was significantly reduced (Fig. 8B/B'). Together these findings suggest that *Emx2* might modulate the *Nef3* expression. To test

further this idea, *Nef3* expression was compared in control and *Emx2* mutant cortex at a later stage, E18.5. At this stage, the graded expression caudomedial-high to rostrolateral-low of *Nef3* in CP becomes even more pronounced. As illustrated in Fig. 8, the strongest *Nef3* signal at this stage was confined to the caudal Rsp (Fig. 8G, H). In the *Emx2-/-* mutant, the expression gradient of *Nef3* in CP was clearly down regulated (Fig. 8E'-G'). In accordance with the observations at stage E16.5, the *Nef3* expression in the temporal cortex was not fully abolished (Fig. 8G/G'). Together, these findings suggest that although *Nef3* may be not a direct *Emx2* target, the expression of *Nef3* in CP depends on TF Emx2.

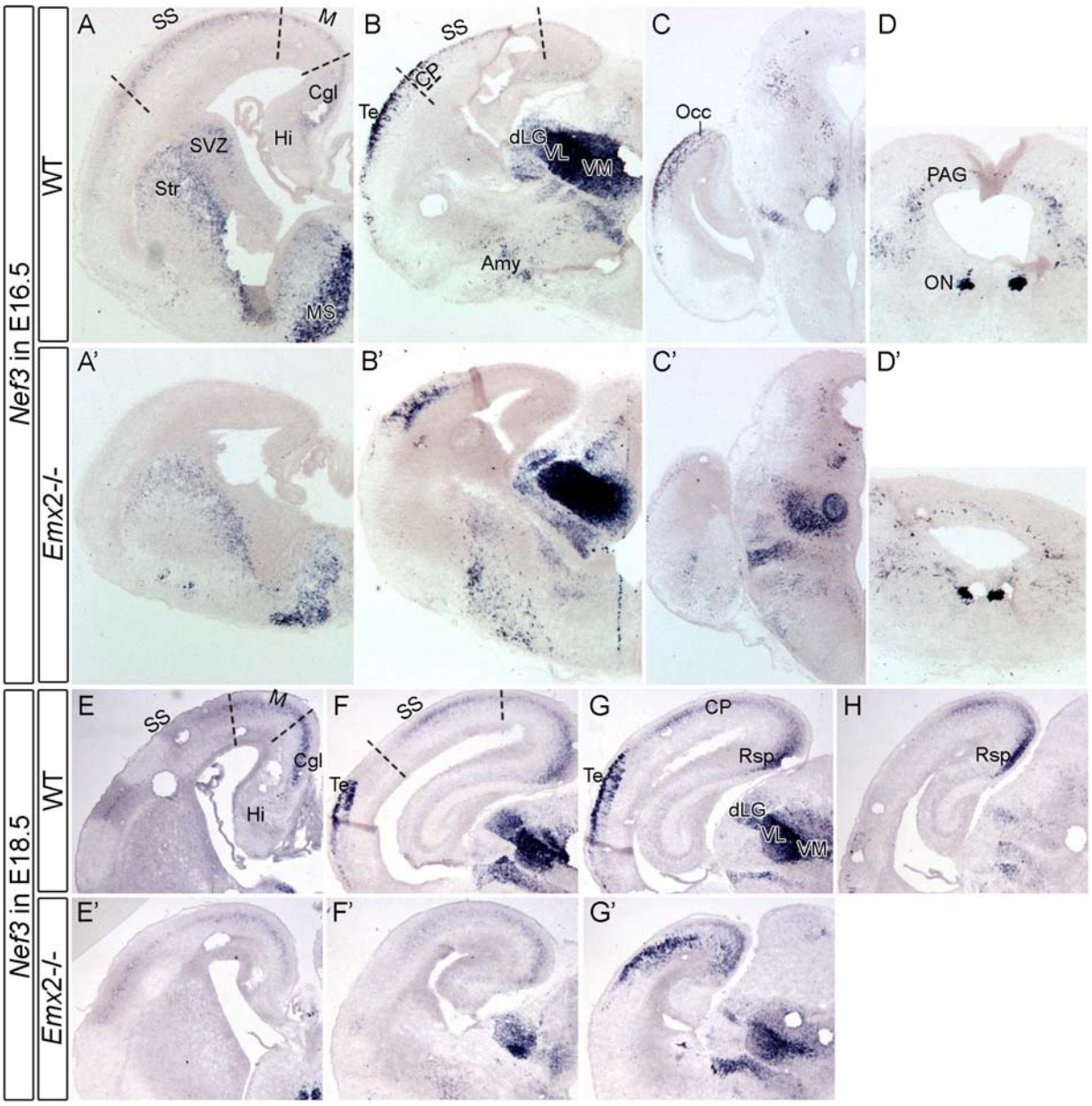

Fig. 8. The graded expression of *Nef3* in developing cortex is strongly diminished in *Emx2-/-* background. Coronal sections from E16.5 (**A-D'**) and E18.5 (**E-H'**) wild type and *Emx2*-/- brains were hybridized with *Nef3* in situ probe. Rostral sections are presented on the left, caudal sections on the right. In both stages, the graded expression of *Nef3* was almost fully abolished in the *Emx2-/-* mutant cortex, except for the patchy expression in

the temporal (Te) cortex (**B/B'** and **G/G'**). (**A**) In basal ganglia, *Nef3* signal labeled the striatum (Str) and outlined the striatal subventricular zone (SVZ). Additional strong expression was seen in the medial septum (MS), while amygdala (Amy) showed only a faint grainy signal. (**B**) In the diencephalon, *Nef3* showed a strikingly restricted expression pattern. The homogeneously stained domain in the dorsal thalamus included the ventrolateral (VL) and ventromedial (VM) nuclear complex and the dorsal lateral geniculate nucleus (dLG). (**D**) Diverse structures in the mesencephalon displayed restricted *Nef3* expression including the oculomotor nucleus (ON), and dorsal periaqueductal gray (PAG). Cgl, cingulate cortex; CP, cortical plate; Hi, hippocampus proper; M, motor cortex; Occ, occipital cortex; Rsp, retrosplenial cortex; SS, somatosensory cortex.

A second group of genes, *Zbtb20, Flrt3* and *Ebf3*, demonstrated similar to *Emx2* caudomedial-high to rostrolateral-low expression gradients either in VZ and/or differentiated CP.

The ***Zbtb20*** gene (zinc finger and BTB containing 20) encodes a TF (Mitchelmore et al., 2002). In telencephalon, the expression of *Zbtb20* was confined to the germinal zones (VZ, SVZ) of the cortex, and basal ganglia (Fig. 9A, B). In fact, reminiscent to *Emx2*, *Zbtb20* exhibited a graded medial-high to lateral-low expression in VZ/SVZ of the cortex (Fig. 9A-C). The highest registered expression was, however, in differentiating neurons in hippocampal IZ and pyramidal cell layer (pcl) of hippocampus proper and in DG (Fig. 3 F). At this stage, only few neurons at uppermost position in CP and in MZ showed faint *Zbtb20* hybridization signal (Fig. 9E, F). In addition, *Zbtb20* expression was observed all along the rostral migratory stream (RMS) that contains migrating progenitors and differentiating interneurons (INs) towards the olfactory bulb (OB), as well as in VZ of diencephalon (Fig. 9C) and hindbrain (not shown).

Based on these expression characteristics, it was expected that activity of *Zbtb20* might be directly dependent on *Emx2* function. The performed analysis in *Emx2*-/- background however, did not confirm this expectation. Indeed, analysis of the *Zbtb20* expression on brain sections of *Emx2*-/- mutant at matched levels revealed only a slight reduction of the in situ hybridization signal in the germinative zones of the telencephalon, olfactory bulb (not shown), MZ (Fig. 9E/E') and IZ. The expression of *Zbtb20* in developing DG and Hi was more strongly diminished (Fig. 9B/B', C/C', D/D'), possibly reflecting the malformation of DG in the *Emx2*-/- mutant (Pellegrini et al., 1996).

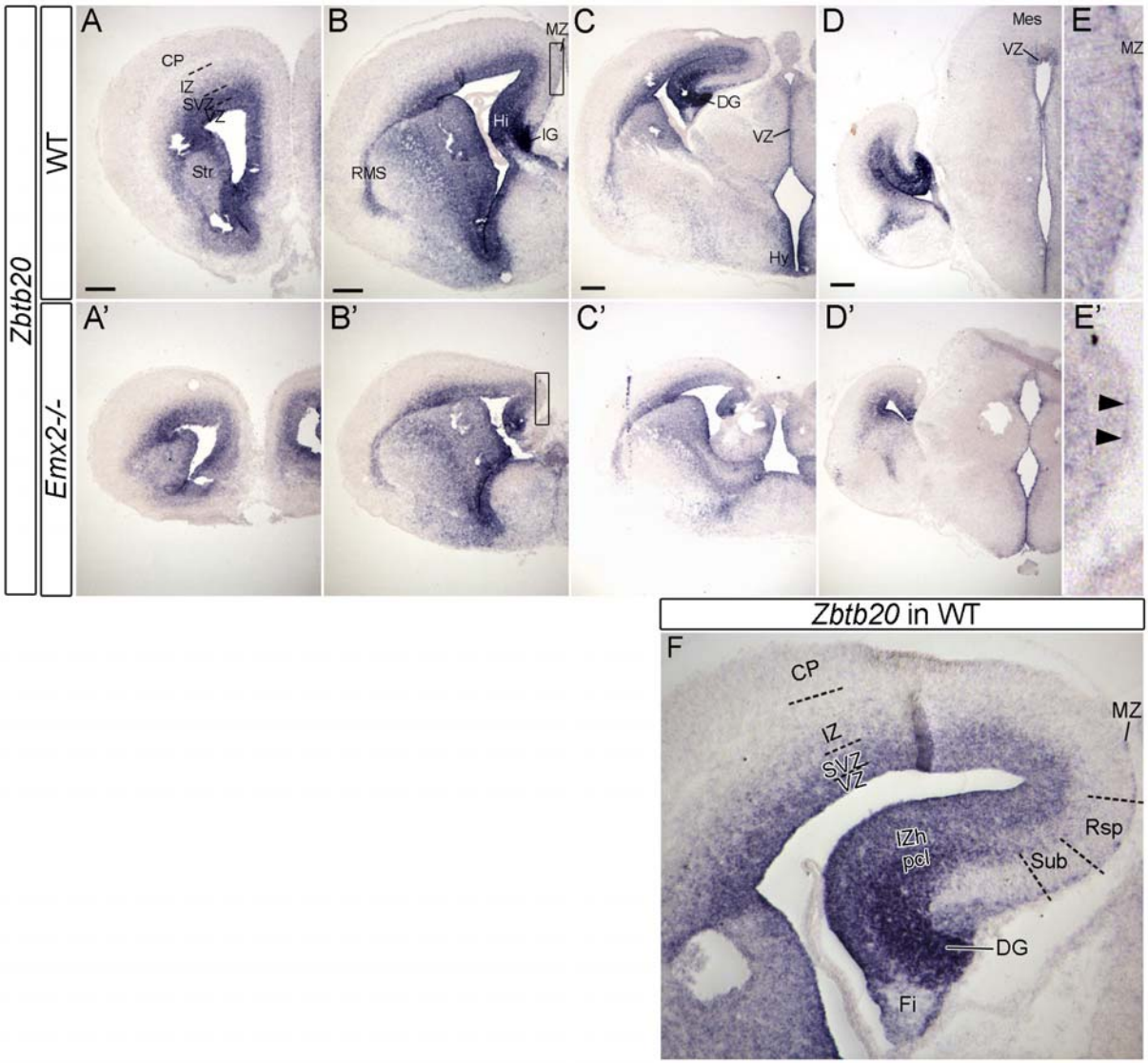

Fig. 9. Reduced expression of TF gene *Zbtb20* in the cortex of *Emx2*-/- mutant. Coronal sections from E16.5 control (**A**-**E**) and *Emx2*-/- mutant (**A'**-**F'**) brains were hybridized with *Zbtb20* specific in situ probe. Sections in (**A**, **A'**) are at rostralmost and sections in (**D**, **D'**) at caudalmost cortical level. (**A**-**F**) *Zbtb20* expression was confined to VZ/SVZ/IZ/MZ of developing cortex, basal ganglia, and rostral migratory stream (RMS). The most robust expression was detected in germinal zone of the medial telencephalon, in the differentiating hippocampus proper (Hi) and dentate gyrus (DG), with a decline at the subicular border. (**A**'-**D**') In absence of *Emx2*, the *Zbtb20* expression was reduced in all these domains. *Zbtb20* signal was also detected in the olfactory bulbs, where it was restricted to the VZ/SVZ (not shown). (**E**/**E**') are close ups of **B**/**B**'. (**E**/**E**') Arrowheads in (**E**') indicate remaining faint *Zbtb20* signal in *Emx2*-/- MZ. (**C**) The hypothalamus (Hy) showed high levels of *Zbtb20* expression. The VZ of diencephalon (**C**), mesencephalon (Mes) (**D**) and hindbrain (not shown) expressed *Zbtb20*. (**F**) A higher magnification of the hippocampal formation demonstrates *Zbtb20* expression in the germinal layers, hippocampal IZ (IZh) and the pyramidal cell layer (pcl) of Hi**.** The IZh contains differentiating cells, destined to become pyramidal neurons, on their migratory route from the neuroepithelium to their final destination, the pcl. CP, cortical plate; IG, indusium griseum; IZ, intermediate zone; MZ, marginal zone; Str, striatum; SVZ, subventricular zone; VZ, ventricular zone. Scale bar: 200 μm.

The Fibronectin leucine-rich transmembrane protein 3 gene (***Flrt3***) (Lacy et al., 1999) exhibited a caudomedial-high to rostrolateral-low expression gradient in postmitotic cells in both IZ and upper CP, as well as in MZ of E16.5 cortex (Fig. 10A-D). In the *Emx2-/-* cortex, the *Flrt3* hybridization signal was not detectable in the MZ, and the expression in outer layers of CP was almost completely abrogated (Fig. 10A'-C'). Noteworthy, a strongly enhanced *Flrt3* in situ signal was observed in IZ of the *Emx2-/-* mutant (Fig. 10A/A', B/B', C/C'), suggesting that in absence of *Emx2*, the patterning of the caudomedial cortex is affected, possibly due to migrational defect of neurons out of the IZ.

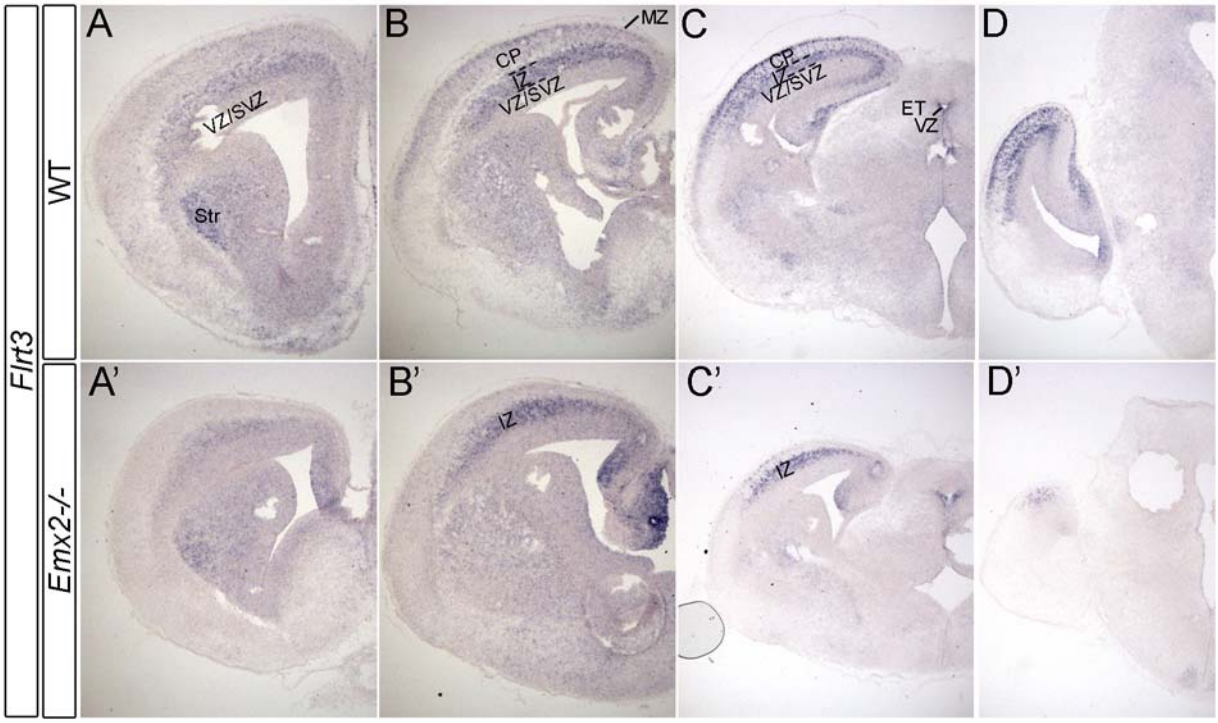

Fig. 10. Pattern abnormalities of *Flrt3* expression in *Emx2*-/- mutant cortex. Brain coronal sections are shown at rostral (left) to caudal (right) levels from control (**A**-**D**) and *Emx2*-/- (**A'**-**D'**) mutant brains. In (**B**/**B'**) note that *Flrt3* expression in cortical plate (CP) and marginal zone (MZ) was down regulated in the *Emx2* mutant, while on the contrary, the *Flrt3* expression in intermediate zone (IZ) appeared elevated. *Flrt3* mRNA transcripts were detected in ventricular zone (VZ) of epithalamus (ET) and periaqueductal gray (PAG) of mesencephalon (not shown). Str, striatum; SVZ, subventricular zone.

In E16.5 cortex, the expression of ***Ebf3*** demarcated exclusively cells in MZ of the caudalmost cortex, the occipital cortex (Fig. 11A-D). Ebf3 belongs to the family of basic helix-loop-helix (bHLH) transcription factors with a crucial role in neuronal differentiation (Travis et al., 1993). Interestingly, the *Ebf3* expression was highest in the MZ of the

caudomedial cortex, including occipital cortex (Occ, Fig. 11C, D). In addition, *Ebf3* exhibited restricted and strong expression in several diencephalic nuclei as indicated in Fig. 11B-D and midbrain structures (not shown). In *Emx2*-/- background, *Ebf3* signal in MZ was abolished except in the hippocampal fissure (Fig. 11C') and adjacent medial cortical regions.

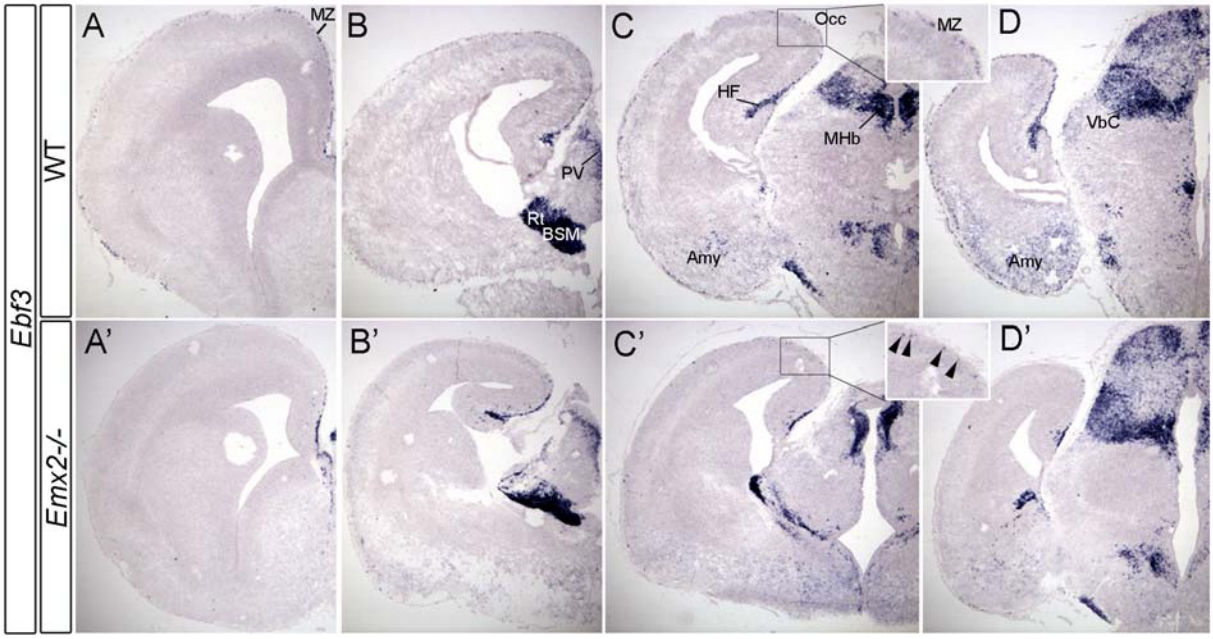

Fig. 11. *Ebf3* expression is abolished in MZ of *Emx2*-/- mutant. Coronal sections are shown from rostral to caudal. Note the graded layer-specific expression of *Ebf3* in the cortex, confined only to the marginal zone (MZ) of cortex and the hippocampal fissure (HF). (**A'-D'**) In the *Emx2* deficient cortex, *Ebf3* signal vanished from the neocortical MZ. Expression was only maintained in the hippocampal fissure and neighboring regions. Close up in (**C'**) shows only few remaining *Ebf3*$^{+}$-cells in the mutant MZ (arrowheads). (**B-C**) In wild type, the *Ebf3* probe labeled also the amygdala (Amy) (**C, D**), as well as several nuclei in diencephalon: the paraventricular thalamic nucleus (PV) in dorsal thalamus, the bed nucleus stria medullaris (BSM) in eminentia thalami, the reticular thalamic nucleus (Rt) in ventral thalamus (**B**), the medial habenular nucleus (MHb) of the epithalamus (**C**), and the ventrobasal nuclear complex (VbC) of dorsal thalamus (**D**). In mesencephalon, the superficial layers of superior colliculus, the periaqueductal gray and the midbrain reticular formation were strongly labeled (not shown). Occ, occipital cortex.

Strikingly regionalized expression in MP was detected for *Neuropilin 2* (***Nrp2***). The *Nrp2* hybridization signal was exclusively confined to the hippocampus proper (CA1-CA3) (Fig. 12B, C) and indusium griseum (IG) (Fig. 12A), while DG was only faintly labeled (Fig. 12B, C). *Nrp2* signal was seen exclusively in the CP of caudal and caudolateral parts, while in CP of rostral cortex the signal was neglectable (Fig. 12A-C). A number of structures located in the basolateral cortex and basal telencephalon showed faint but restricted *Nrp2* expression

as indicated in Fig. 12. In the *Emx2-/-* background, the restricted expression of *Nrp2* to in hippocampus and DG was reduced possibly reflecting the dysgenesis of this structure in the mutant (Fig. 12B', C').

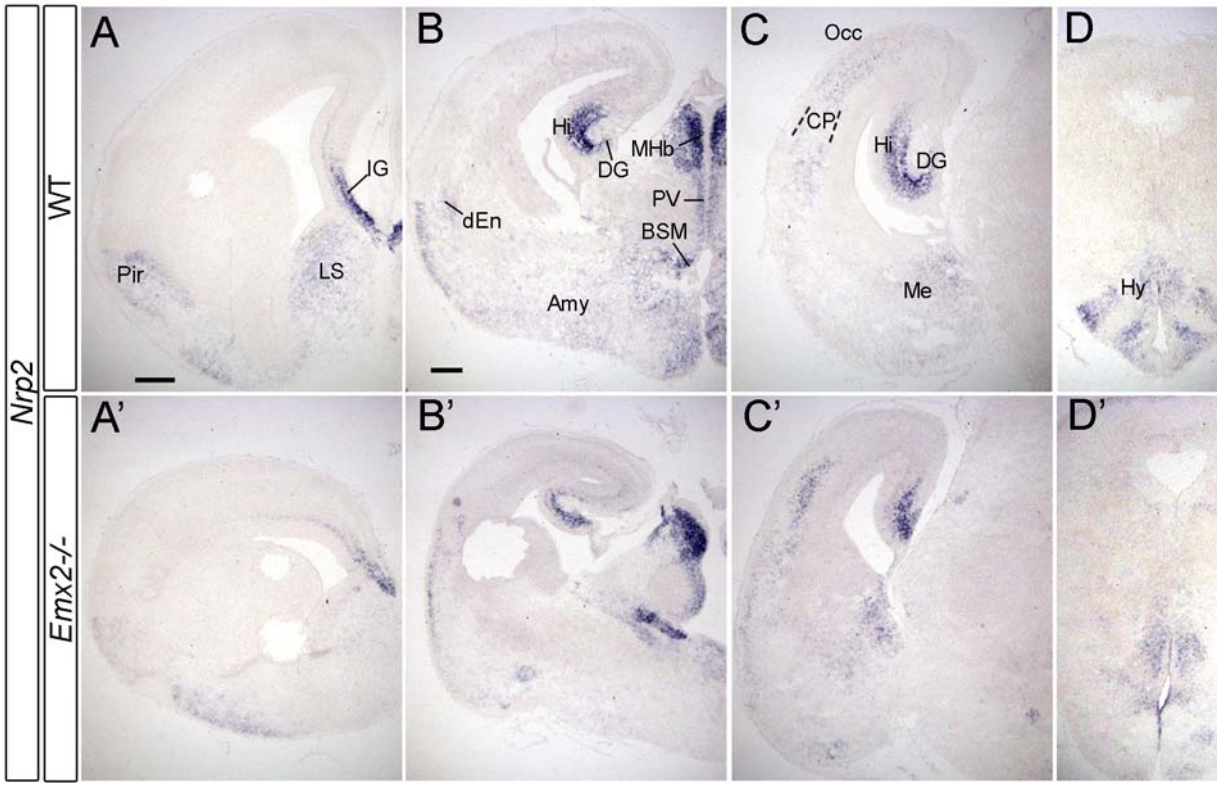

Fig. 12. *Nrp2* expression patterns in control and *Emx2-/-* E16.5 cortex. (**B-D**) *Nrp2* showed a restricted expression in the caudomedial cortical plate (CP), confined to the region of differentiating hippocampus proper (Hi) and dentate gyrus (DG) (**B**, **C**). Furthermore, lower *Nrp2* expression was seen in CP of caudal/caudolateral Ncx, which is corresponding mostly to occipital cortex (Occ) (**C**), ventral temporal association areas and auditory areas (not shown). Expression was also seen in several structures, that is in the basal ganglia: the lateral septal nucleus (LS) (**A**); in the basolateral telencephalon: dorsal endopiriform nucleus (dEN), piriform cortex (Pir) (**A**, **B**), medial amygdalar nucleus (Me) (**C**), in diencephalon: medial habenular nucleus (MHb) (**B**), paraventricular thalamic nucleus (PV) (**B**), the bed nucleus stria medullaris (BSM) (**B**) and hypothalamus (Hy) (**D**). In *Emx2-/-* background, the *Nrp2* expression was clearly down regulated in Hi and uppermost layers of Ncx (compare **B/B', C/C'**). Scale bar 200 μm.

To sum up, the performed expression analysis helped to identify candidate genes (*Odz3*, *Nef3*, *Zbtb20*, *Flrt3*, *Ebf3* and *Nrp2*) that might act in *Emx2*-dependent pathway in molecular patterning of the caudal cortex. The most attractive candidate was *Odz3,* however, during the progress of this work, the knockout of this gene was reported (Leamey et al., 2007). This was also the case for *Flrt3*, another interesting candidate (personal communication). Finally, *Zbtb20* was selected for functional characterization, because of its intriguing graded expression pattern in E16.5 brain and the fact that *Zbtb20* function was poorly characterized

at the start of the current study. Moreover, no mice with a targeted disruption for *Zbtb20* had been reported by this time. Therefore, by using targeted deletion mutagenesis, in this study it was investigated whether and how this gene is involved in mammalian corticogenesis.

2.2. Analysis of the function of *Zbtb20*

2.2.1. Expression pattern of *Zbtb20* in the developing embryo

Although some data on the expression of Zbtb20 protein have been published (Mitchelmore et al., 2002), the expression pattern of *Zbtb20* at transcriptional level was still unknown. In order to study whether the expression of *Zbtb20* is brain specific, sagittal sections from E16.5 embryos were examined by in situ hybridization. As shown in (Fig. 13), the highest expression of *Zbtb20* was detected exclusively in developing forebrain and olfactory bulb and several cranial (e.g. 5th, trigeminal ganglion, (Fig. 13B, C) and dorsal root ganglia (DRG) (Fig. 13A). Less dense signal was detected in hypothalamus (Fig. 13A), neural retina (Fig. 13C), nasal epithelium (Fig. 13B), and ventral part of the spinal cord (Fig. 13A). *Zbtb20* mRNA at an extremely low abundance was present in different organs as summarized in Table 2.

Table 2. Distribution of *Zbtb20* mRNA expression in the E16.5 embryo, determined by in situ hybridization.

Spinal cord	++	Trigeminal ganglion	+
Cerebral cortex (VZ)	++	Neural retina	++
Hippocampus/DG	++++	Olfactory neuroepithelium	++
Rostral migratory stream	+	Ear	++
Basal ganglia	++	Intestine	++
Diencephalon	++	Lung	+
Optic stalk	++	Kidney	++
Mesencephalon	++	Thyroid gland	++
Cerebellum	++	Pituitary gland	+
Dorsal root ganglia	++	Heart	+

Relative density of in situ hybridization indicated as follows: +, low; ++, moderate; +++, high; ++++, very high

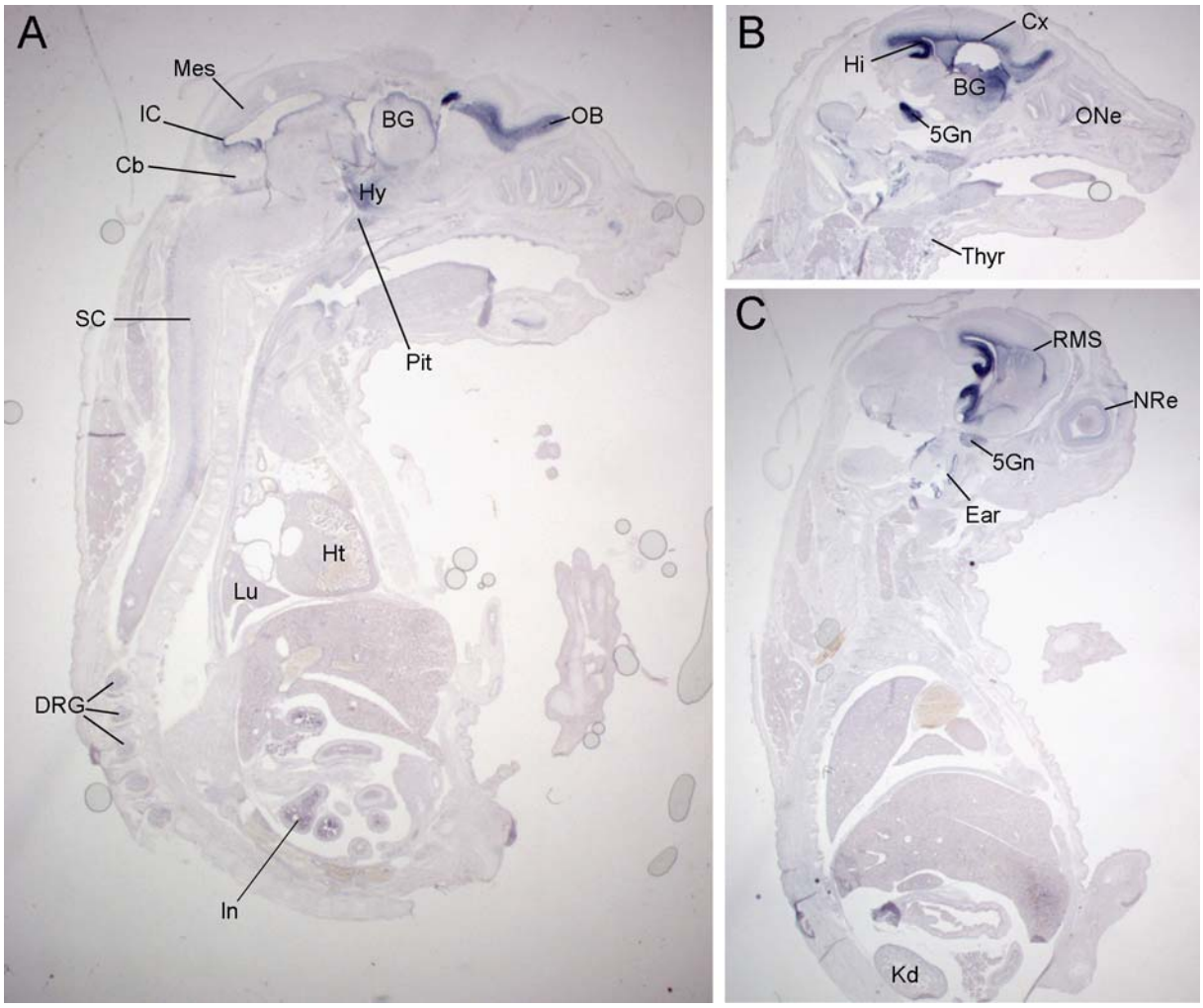

Fig. 13. In situ hybridization analysis of *Zbtb20* expression in the E16.5 embryo. *Zbtb20* transcripts were mainly restricted to germinative neuroepithelium of CNS, including that of the olfactory bulb (OB), the rostral migratory stream (RMS), cortex (Cx), hippocampus (Hi), basal ganglia (BG) (**A, B**) and the cranial ganglia (e.g. trigeminal ganglion, 5Gn in (**B**). Outside the brain, a fainter expression was detected in ventral spinal cord (SC), dorsal root ganglia (DRG) (**A**). Low expression was seen in several organs, like (**A**) heart (Ht) and (**C**) kidney (Kd). Cb, cerebellum; IC, inferior colliculus; In, intestine; Lu, lung; NRe, neural retina; Thyr, thyroid gland; Pit, pituitary gland.

***Zbtb20* expression in the embryonic brain**

The highly restricted expression of *Zbtb20* in E16.5 brain motivated to examine the dynamics of *Zbtb20* expression in developing brain, at stages E12.5, E14.5 and E18.5 (Fig. 14).

At E12.5 (Fig. 14A-C) *Zbtb20* transcripts were detected in the telencephalon, with selective staining of VZ and SVZ of the subpallium: the medial (MGE), lateral (LGE) (Fig. 14A), caudal (CGE) (Fig. 14B) ganglionic eminences. Notably, *Zbtb20* was also expressed in VZ of small area of the medial pallium, consisting of the dorsal half of the cortical hem and

the hippocampal anlage (arrows in Fig. 14A, B). Furthermore, the VZ of diencephalon, mid- and hindbrain were *Zbtb20* positive (Fig. 14C).

At E14.5 (Fig. 14D-G) *Zbtb20* mRNA was detected within the entire germinal zone of the cortex showing a faint gradient (Fig. 14D), more strongly expressed caudomedially (Fig. 14F). In the hippocampal anlage, the expression of *Zbtb20* became much more prominent and was observed in cells in VZ and in the mantle zone (Fig. 14E, F). Strong signal was seen in the VZ of di- and mesencephon, whereas the VZ of cerebellum displayed low level of *Zbtb20* expression (Fig. 14G).

At E18.5 (Fig. 14H-L) *Zbtb20* showed a consistent expression in germinal zones of the developing cortex at a slightly lower level as compared to stage E16.5 (Fig. 9). The hippocampus, which has been further advanced in its differentiation, showed a very strong *Zbtb20* expression, in the entire Ammon's horn as well as in DG (Fig. 14J). At E18.5, several amygdalar nuclei were additionally demarcated by *Zbtb20* expression (Fig. 14J). The mesencephalon (Fig. 14K) and the cerebellum (Fig. 14L) were even more faintly labeled than at E16.5 (D and not shown).

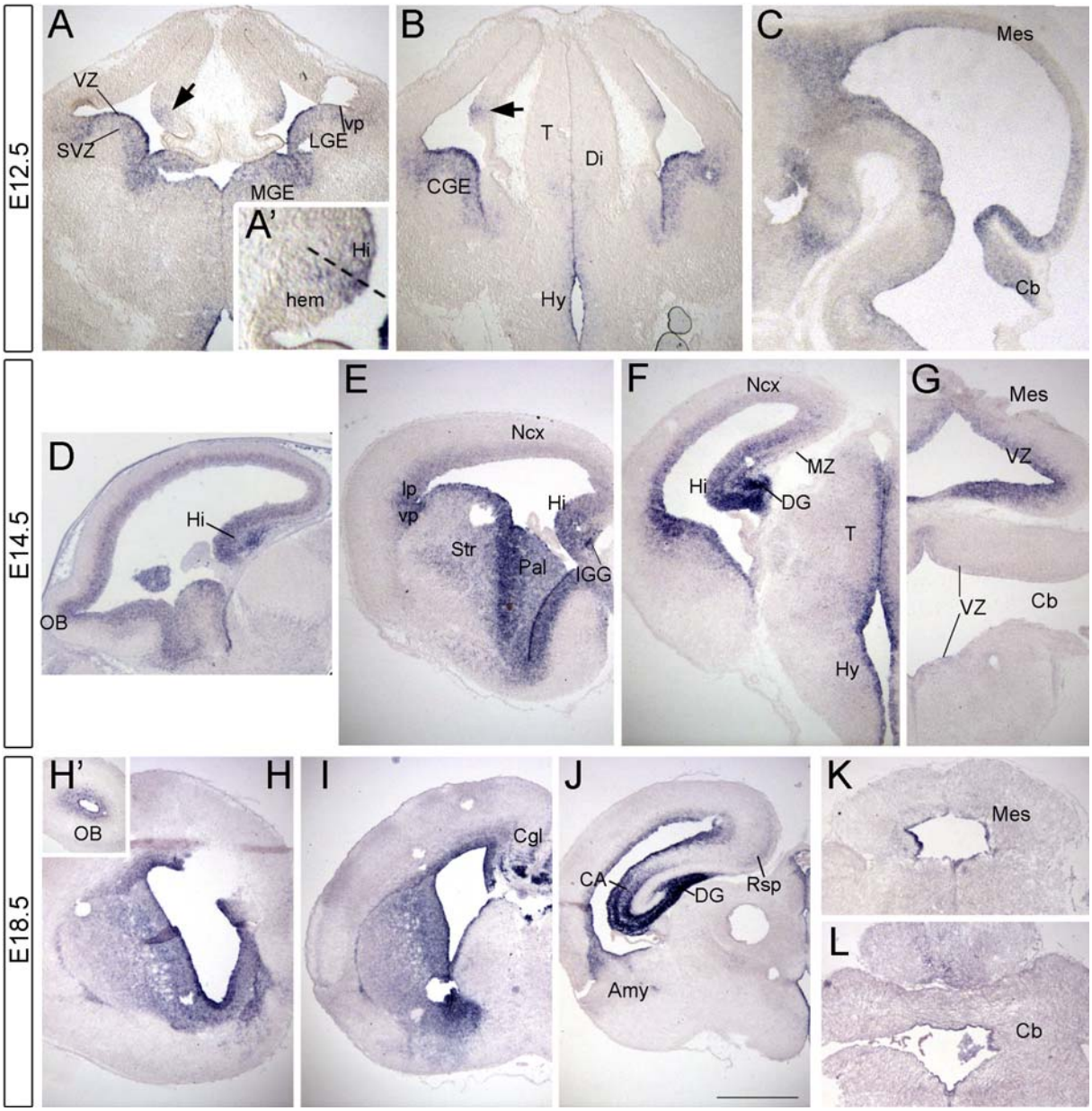

Fig. 14. *Zbtb20* expression in E12.5-18.5 mouse brain sections. In situ hybridization on coronal sections shown from rostral to caudal, except (**C**) and (**D**) showing sagittal sections. E12.5 (top row): (**A/A'**) In the telencephalon, *Zbtb20* was expressed in a domain consisting of the anlage of hippocampus (Hi) and dorsal half of the hem. (**A, B**) *Zbtb20* transcripts were also detected in the VZ/SVZ of the subpallium (MGE, LGE and CGE) as well as in ventral pallium (vp). (**B, C**) *Zbtb20* was also expressed in VZ of diencephalon (Di), mesencephalon (Mes) and cerebellum (Cb). (**D-F**) At stage E14.5, *Zbtb20* showed expression in the entire telencephalic germinal layer, including olfactory bulbs (OB). In VZ/SVZ and MZ of the cortex, this expression was slightly graded, with a higher levels caudomedially. Strongest *Zbtb20* signal was seen in the anlage of Hi (**F**). (**D-G**) Furthermore, high to moderate levels of *Zbtb20* expression were detected in the basal ganglia (Str, striatum and Pal, pallidum) and VZ of di- and mesencephalon. (**J**) At stage E18.5, *Zbtb20* showed abundant and restricted expression in CA-regions (CA) and dentate gyrus (DG) of hippocampus, mostly in postmitotic pyramidal neurons. Note the expression in upper layers of the cortical plate (CP) in cingulate (Cgl) (**I**) and retrosplenial cortex (Rsp) (**J**). Additionally, some amygdalar nuclei (Amy) were labeled. (**A'**) is a close up of

(**A**). CGE, caudal ganglionic eminence; Hy, hypothalamus; LGE, lateral ganglionic eminence; lp, lateral pallium; MGE, medial ganglionic eminence; MZ, marginal zone; Ncx, neocortex; SVZ, subventricular zone; T, thalamus; VZ, ventricular zone. Scale bar: 1 mm.

2.2.2. Targeted disruption of *Zbtb20*

The genomic locus of the murine *Zbtb20* gene (Fig. 15A) is localized on chromosome 16 between 42,875,994 and 43,619,250 basepairs (NCBI: NC_000082.5; Ensembl gene ENSMUSG00000022708). The gene locus encompasses 743.256 kb comprising 11 exons. To date, 5 different transcripts have been detected (http://www.ensembl.org). Eight alternative splicing variants give rise to two different protein isoforms, Zbtb20L and Zbtb20S, which are of 741 or 688 aa long, respectively (Mitchelmore et al., 2002). The start codons of Zbtb20L and Zbtb20S are located in exon 4 and exon 6, respectively. Both protein isoforms (Fig. 15B) contain the BTB/POZ domain and the domain comprising the 5 zinc fingers, which are transcribed from exon 6 and exon 7. As it is hardly feasible to delete all exons, it was decided to knockout the exon 6, encoding the functionally important BTB/POZ domain, a stretch of low homology and the first zinc finger.

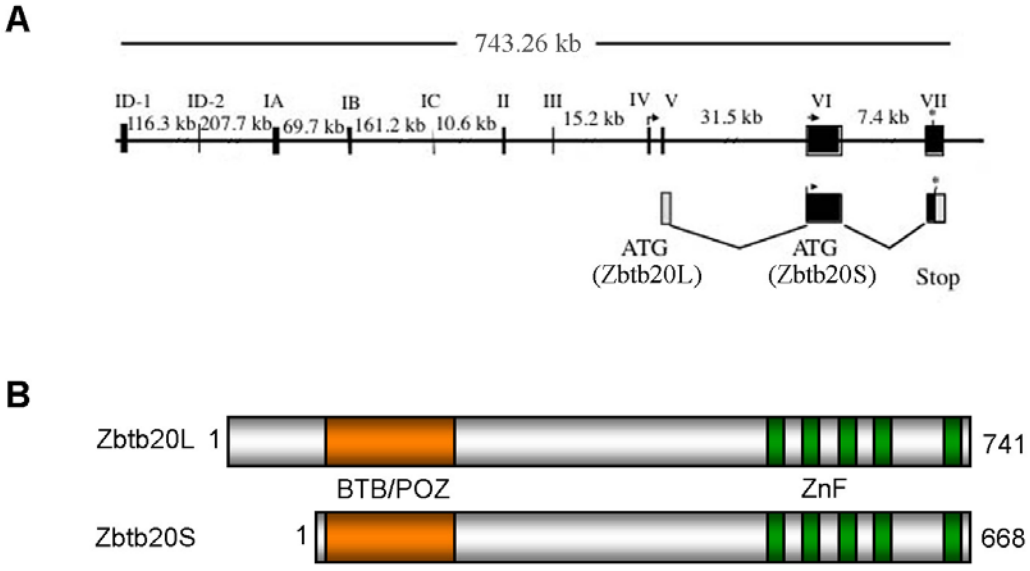

Fig. 15. Structure of the *Zbtb20* gene and Zbtb20 protein in the mouse. (**A**) genomic structure of the murine *Zbtb20* locus is shown above. Exons are depicted as black boxes. (**B**) The translated region comprises exon 4, 5, 6 and 7. B, The protein sequence of two protein isoforms of Zbtb20. (Adapted from Mitchelmore et al., 2002)

2.2.2.1. Generation of knockout construct

To gain insight into the functional role of *Zbtb20* during development, a targeted inactivation of the *Zbtb20* gene was carried out in mouse.

Given the expression pattern of *Zbtb20*, primarily restricted to the developing brain, the possibility of lethal phenotype of the knockout (KO) mice was considered to be low. Therefore, *Zbtb20* was disrupted by the classical knockout approach, which would lead to the ablation of *Zbtb20* function in all cells, in which this gene is expressed. In order to obtain the desired genomic sequence containing the exon 6 of the *Zbtb20* locus, a Lambda FIX II library (Stratagene) was screened. The targeting vector was created according to a method termed recombineering or recombinogenic engineering (Copeland et al., 2001; Lee et al., 2001; Liu et al., 2003; Muyrers et al., 2001). This method exploits the homologous recombination activity via the gap repair mechanism by the λ phage Red proteins in *E. coli*, a fact making the need for restriction enzymes or DNA ligases dispensable during the cloning steps.

All cloning products (Fig. 16A) were verified by restriction enzyme digestion. Additionally, the DNA products were sequenced to exclude that mutations were inserted into the genomic *Zbtb20* locus. In Fig. 16B, an analytic agarose gel is shown, demonstrating the correct cloning of the knockout construct (pER4).

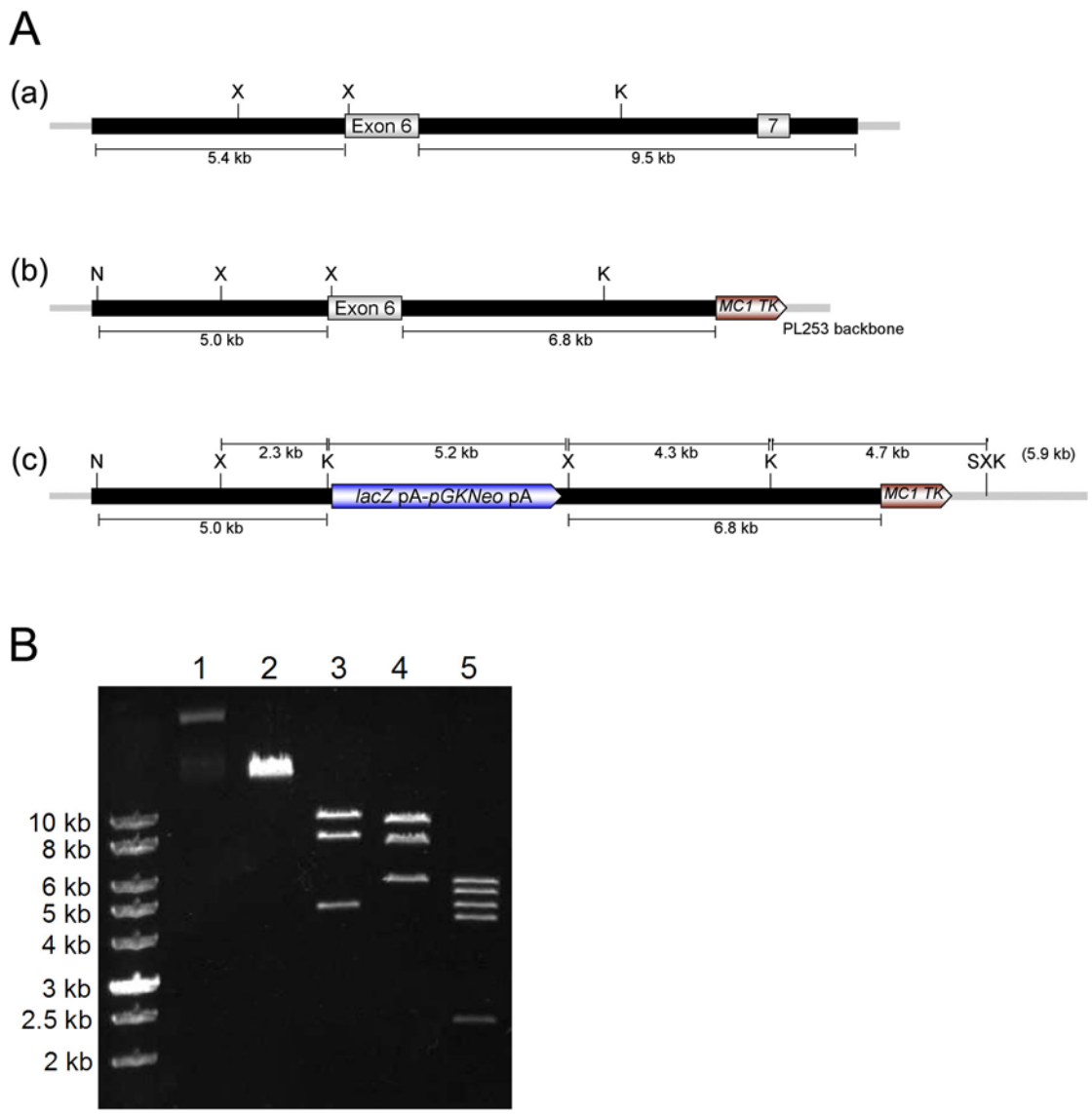

Fig. 16. Construction of the *Zbtb20* knockout vector (pER4). (**A**) Retrieving and targeting of the 16.5 kb genomic region containing the *Zbtb20* exon 6. Targeting region is depicted in bold black. Grey boxes indicate exons 6 and 7. TK- and *LacZ*polyA-*pGKNeo*polyA-cassettes are shown in brown and blue, respectively. Important restriction sites are labeled with K, *KpnI*; N, *NotI*; S, *SalI*; X, *XhoI*. (**a**) pERλ2, (**b**) GRV, (**c**) pER4. (**B**) Agarose gel showing the correct cloning of the knockout construct pER4. Lane 1: undigested vector; lane 2: *SalI* linearized vector (22.5 kb); lane 3: *KpnI* digest (9.6, 8.2, and 4.7 kb); lane 4: *XhoI* digest (9.0, 7.6, and 5.8 kb); lane 5: *KpnI*/*XhoI* digest (5.9; 5.2, 4.7, 4.3, and 2.3 kb).

2.2.2.2. Generation of homologous recombinant ES-cells

Embryonal stem cells (ES cells), isolated from the inner cell mass of the mouse blastocyste, can be cultured in vitro. In presence of the supplement Lif (leukemia inhibiting factor), which inhibits the differentiation of ES cells, their pluripotency is preserved. The culturing of cells in the following was carried out by S. Mahsur, as described previously (Mansouri, 2001).

The targeting strategy of the *Zbtb20* locus is depicted in Fig. 17A. The linearized *Zbtb20* knockout construct was electroporated into the MPI-II ES cells (mouse strain 129/Sv) (Doetschman et al., 1985), which were subsequently submitted to positive/negative selection with G418 and gancyclovir (Ganc), respectively. Cells containing the *Neo* cassette and which survived the exposure to gancyclovir were assumed to have undergone homologous recombination. In total, 399 of such clones were isolated and cultivated. To test for homologous targeting event, DNA from each clone was isolated and subjected to southern blot analysis. By PCR amplification, two probes were generated detecting DNA stretches located outside or within the 5' and 3' homology arm region, respectively. For southern blot analysis, genomic DNA from each clone was at first digested with *KpnI* and hybridized with the 5'-external probe, because the insertion of the targeting-cassette into the correct locus should generate an additional *KpnI* restriction site. Consequently, a 15.4 kb band revealed the wild type allele and an additional 9.5 kb band indicated the homologous recombined allele (Fig. 17B). Thus four clones were identified with this combination. Their 3' region flanking the targeting-cassette was subsequently analyzed by means of the 3'-internal probe and previous *XhoI* digestion. As the correct integration of the targeting cassette produced another *XhoI* restriction site in the locus, a 12.8 kb and 11.2 kb band was obtained in case of a positive, revealing the wild type or recombined allele, respectively. From 243 ES cell clones that had been screened two positive ES cell clones emerged revealing the correct bands with 5' and 3' probe, corresponding to a recombination frequency of 1/122. The two clones (ER31 and ER42) were used to generate mouse chimaeras.

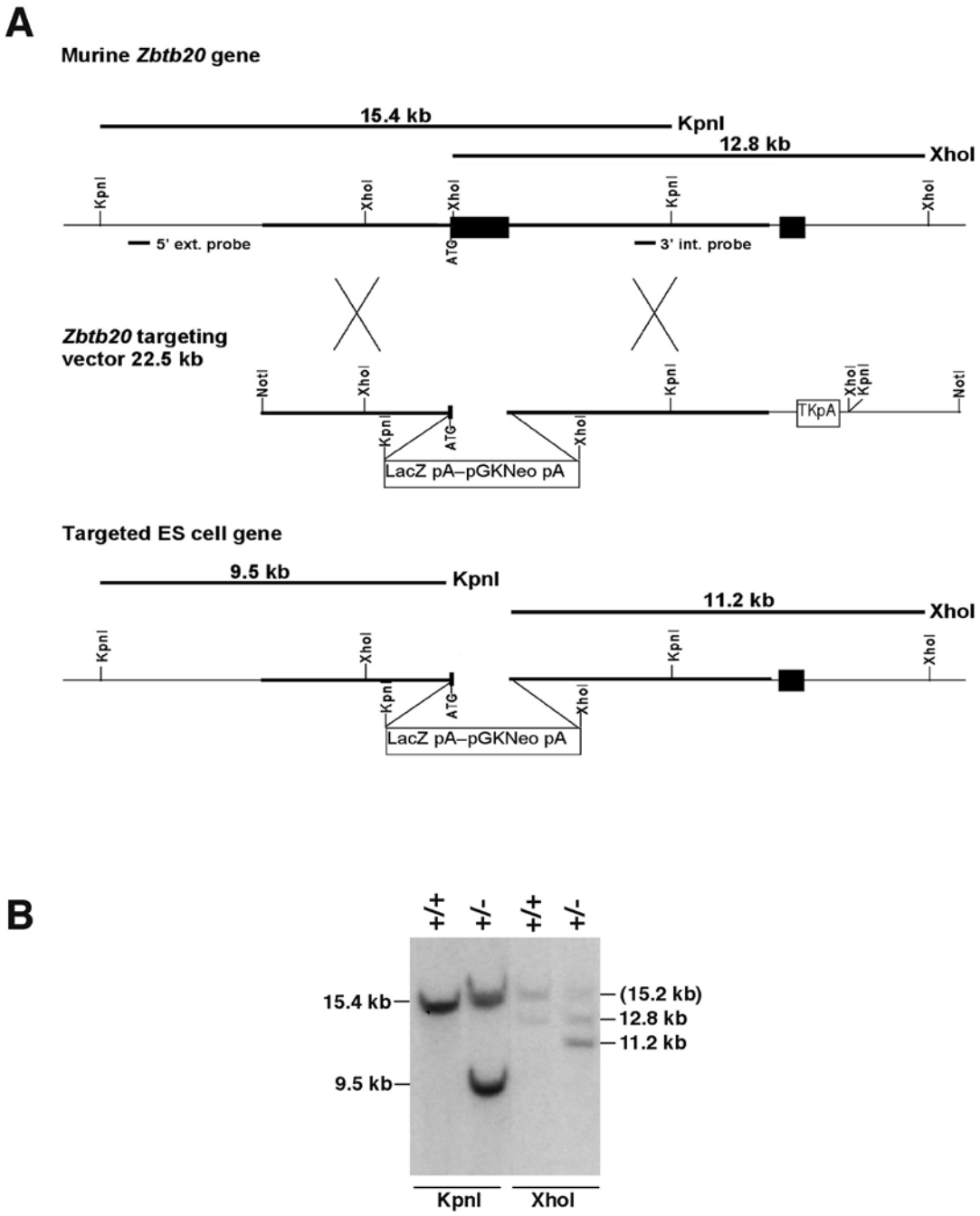

Fig. 17. Targeted disruption of the *Zbtb20* gene and identification of ES cell clones with correctly inserted targeting cassette. (**A**) Homologous recombination between the targeting (KO) construct and the genomic *Zbtb20* locus. Correctly targeted ES cell DNA revealed a 15.4 kb wild type and a 9.5 kb KO band after *KpnI* digestion and subsequent southern blot analysis using a 5'-external probe. Similarly, a 12.8 kb wild type and 11.2 kb KO band was obtained with the same DNA when *XhoI* digested and analyzed by southern blot using 3'-internal probe. (**B**) Result of Southern blot analysis of ES cell clone ER42 demonstrating that targeting occurred correctly. *KpnI* (left) or *Xho*I (right) digestion followed by analysis with 5' external or 3' internal probe, respectively. Digestion by CpG methylation-sensitive enzyme *XhoI* produced an unexpected additional 15.2 kb band, probably resulting from incomplete cleavage. The *XhoI* restriction site located 49 bp downstream of exon 6 start codon was part of a CpG island as revealed by software http://www.ebi.ac.uk/Tools/emboss/cpgplot/. As *XhoI* is a CpG methylation-sensitive enzyme, this suggests that this region is partially methylated in ES cells.

2.2.2.3. Generation of mouse chimaeras and screening for germline transmissions

To obtain chimeric mice, the two positive clones (mouse strain 129/Sv, agouti fur, black eyes) were expanded separately to 16-cell stage and aggregated with morulae, isolated from the CD1 albino mouse strain (white fur, red eyes) (Wood et al., 1993). On the next day those embryos that had reached the blastocyst stage (developmental day 2) were chosen to be transferred into the oviduct of pseudopregnant foster mothers. The pups were either born naturally or by Caesarean. In total, 31 animals reached adulthood and could be used for further matings:

ES cell clone	Number of chimaeras
ER31	6
ER42	15

The grade of chimaerism in these animals could be easily detected based on the coat color. The higher the proportion of dark (agouti) coat color, the higher will be the chance that a chimaeric mouse carries the transgenic information in its germ cells. In this case, the information can be transmitted to its offspring. After six weeks, primarily highly chimaeric mice, having at least 50% agouti coat color, were mated to CDI wild type mice. Germline transmission in the offspring from these test breedings was noticeable by means of the eye color. Pups with black eyes were descendants of the transgenic ES cell line (129/Sv strain), whereas red-eyed pups originated from the non-transgenic ES cell line (CDI strain). From both ES cell clones (ER31; 42) germline transmissions were accomplished. Heterozygous animals from this F1 generation (mixed 129/Sv/ CDI background) were intercrossed to obtain *Zbtb20*-/- mice. This was done for first phenotype analysis. Chimaeras giving germline transmission were crossed with 129/Sv mice to generate *Zbtb20* mutants of pure 129/Sv background. In order to investigate the phenotype under homogeneous inbred background, backcrossings on the C57 BL/6 inbred strain were initiated. ER31 and ER42 derived *Zbtb20* mutant mice produced an identical phenotype.

2.2.2.4. Confirmation of homologous recombination into the *Zbtb20* gene locus

2.2.2.4.1. PCR

For genotyping, DNA was extracted from tail biopsies, followed by PCR amplification of distinct fragments. Forward primers ER_*Zbtb*_F, ER_*Neo*_F and reverse primer ER_*Zbtb*_R

were designed to complement 3' end of exon 6, a part in *Neo* gene and an intronic stretch 249 bp downstream of exon 6, respectively. The combination of these primers allowed to distinguish between the wild type (313 bp, primers ER_*Zbtb*_F and ER_*Zbtb*_R) and the knockout allel (518 bp, primers ER_*Neo*_F and ER_*Zbtb*_R) (Fig. 18A), thereby providing further evidence (on the genomic DNA-level) that exon 6 of *Zbtb20* had been successfully replaced by the *LacZ/Neo* cassette.

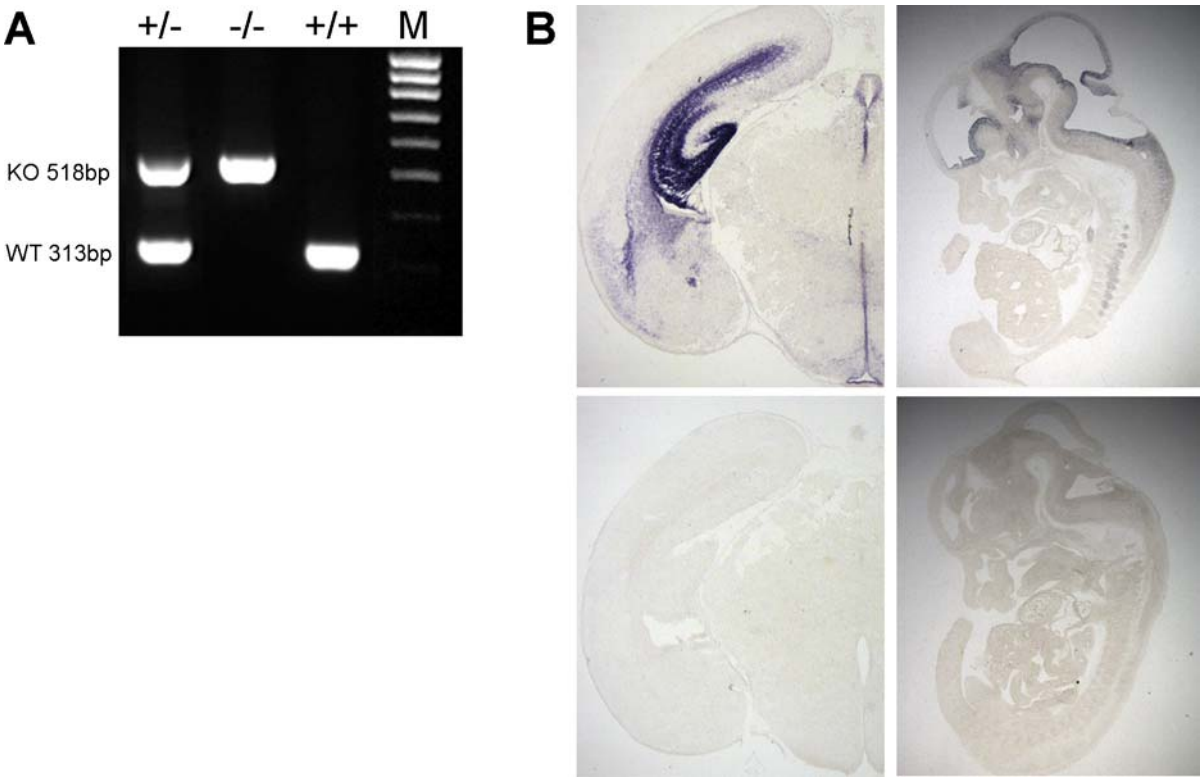

Fig. 18. Confirmation of homologous recombination into the *Zbtb20* gene locus. (**A**) PCR amplified products specific to the wild type (313 bp) and knockout alleles (518 bp) in homozygous and heterozygous animals. (**B**) ISH analysis on sections from E18.5 brain (left) and E12.5 embryo (right) from wild type (above) and homozygous (below) mice were performed using a *Zbtb20* specific probe detecting the deleted part (exon 6). Specific *Zbtb20* expression pattern was revealed in the wild type, but not in the homozygous *Zbtb20* deficient mouse. Furthermore, the *in situ* probe, which has been generated, obviously did not cross-react with transcripts from other genes.

2.2.2.4.2. RNA-ISH

A RNA-ISH on E18.5 brain sections from *Zbtb20*+/+ and *Zbtb20*-/- mice was carried out using a probe recognizing the deleted exon 6 (Fig. 18B). The typical *Zbtb20* expression pattern was delivered by the wild type, but not by the mutant, proving the absence of the *Zbtb20* exon 6 specific transcript in the mutant mice brain.

2.2.3. Expression analysis of *Zbtb20* in developing embryo based on *LacZ* reporter activity of *Zbtb20*+/- mice

To gain more detailed information about the temporal and spatial expression of *Zbtb20*, advantage was taken of the *LacZ* reporter gene included in the vector generated for targeted inactivation of *Zbtb20.* The *LacZ* reporter gene, which is under the control of the endogeneous *Zbtb20* promoter, allows an accurate detection of even low levels of *Zbtb20* expression.

Whole mount X-gal staining of *Zbtb20* heterozygous animals from embryonic stages E9.5-E12.5 facilitated to get an overview of the *LacZ* reporter gene expression. The earliest *LacZ* expression was detected at E9.5, when X-gal staining was strong in the heart and weaker in the somites (Fig. 19A). The expression of *Zbtb20* in the brain started at stage E10.5 in the anlage of the basal ganglia (Fig. 19B). From E10.5 onwards, abundant expression was detected in the entire central nervous system (CNS), including telencephalon, diencephalon, mesencephalon, hindbrain and spinal cord (Fig. 19B-D), dorsal root ganglia and all cranial ganglia (Vth, trigeminal, VIIth, facial, XIth, glossopharyngeal) were also strongly *Zbtb20* positive (Fig. 19B, C).

Analysis of sagittal sections of E12.5 embryos after X-gal staining revealed in addition expression in the rostral dorsal telencephalon (anlage of cortex) and mediocaudal telencephalon (anlage of hippocampus), as well as the regions of cerebellum and hypothalamus (Fig. 19E). Notably, the expression pattern in *Zbtb20*+/- E12.5 embryos revealed by X-gal staining accorded closely with the patterning revealed by in situ hybridization analysis, indicating that the activity of the *LacZ* transgene mimics endogeneous wild type *Zbtb20* expression faithfully (Fig. 19F).

In order to get more detailed information about the regional distribution of the *LacZ* signal, cross sections from previously X-gal stained embryos were examined. This helped to reveal additional expression domains of *Zbtb20* in E10.5-12.5 embryos. Interestingly, the early expression of *Zbtb20* in the telencephalon clearly outlined the regions of the hem and hippocampus (Fig. 20H). Because the hem is an inductive center with important role for the patterning of the medial telencephalon, these results suggest a role for *Zbtb20* in hippocampal morphogenesis. Furthermore, the expression of *Zbtb20* in the spinal cord showed a regionalized expression in the basal plate, including the motor neuron column (Fig. 20D). Faint expression was also detected in notochord, sympathetic chain (Fig. 20D, L), otic vesicle (Fig. 20E), neural retina (Fig. 20I), vomeronasal organ (Fig. 20J), and kidney (Fig. 20K).

Notably, ribs (L) and sclerotome (D), structures giving rise to part of the axial skeleton, were *Zbtb20* positive as well. A summary of the observed expression patterns is shown in Table 3.

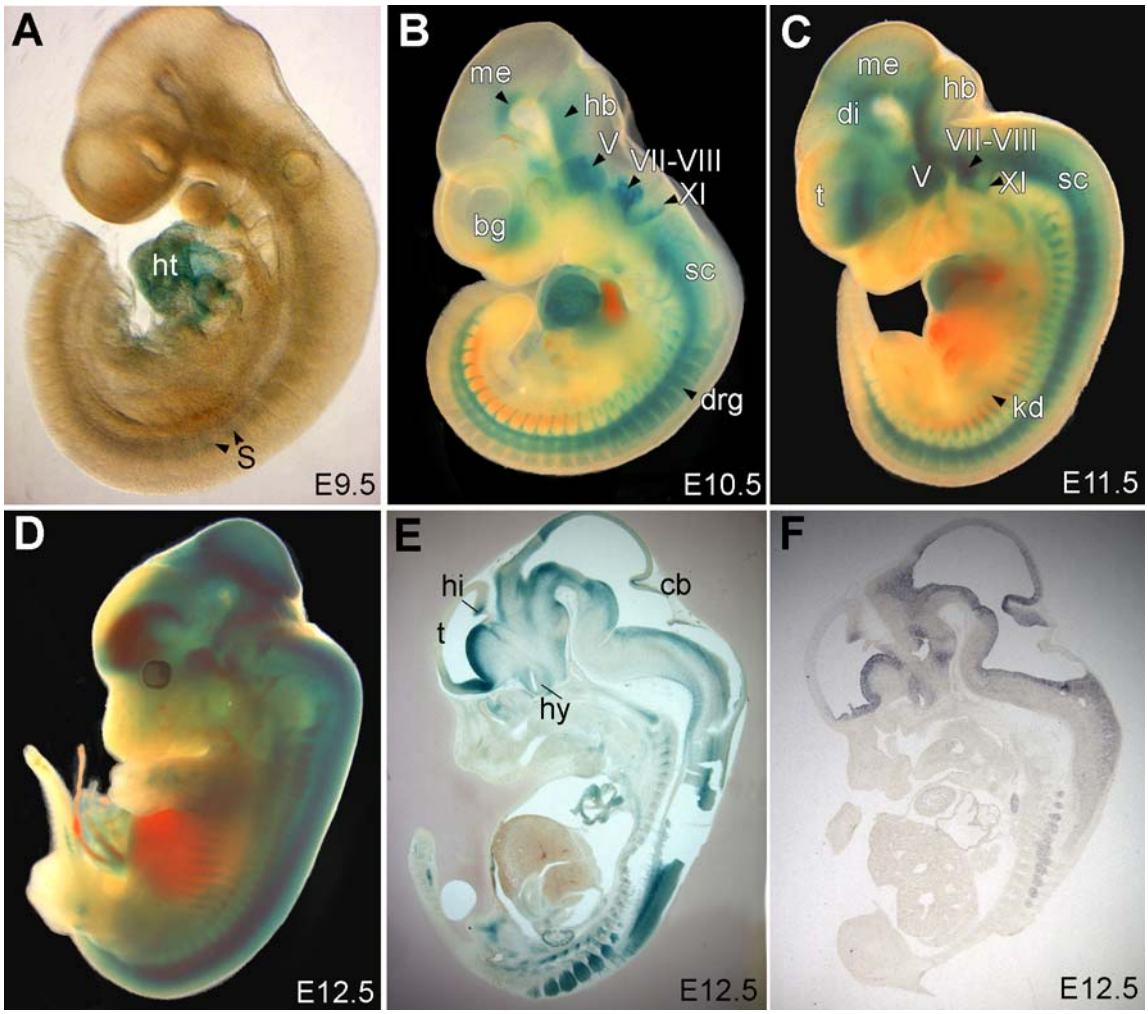

Fig. 19. *Zbtb20* expression pattern revealed by X-gal staining or ISH. *Zbtb20*+/- embryos, isolated at E9.5-E12.5, were subjected to whole-mount X-gal staining. The transgene was first expressed at E9.5 (**A**) in the heart (ht) and in the somites (s). (**B-H**) Note the progressively increased expression of *Zbtb20* in the entire CNS and PNS at later stages. (**F**) ISH, performed on sagittal sections of E12.5 embryo with a *Zbtb20* situ probe revealed almost identical expression with the X-gal staining patterns shown in (**E**). V, trigeminal ganglion; VII-VIII, facio-acoustic ganglion; IX, glossopharyngeal ganglion; bg, basal ganglia; di, diencephalon; drg, dorsal root ganglion; hb, hindbrain; kd, kidney; me, mesencephalon; sc, spinal cord; t, telencephalon.

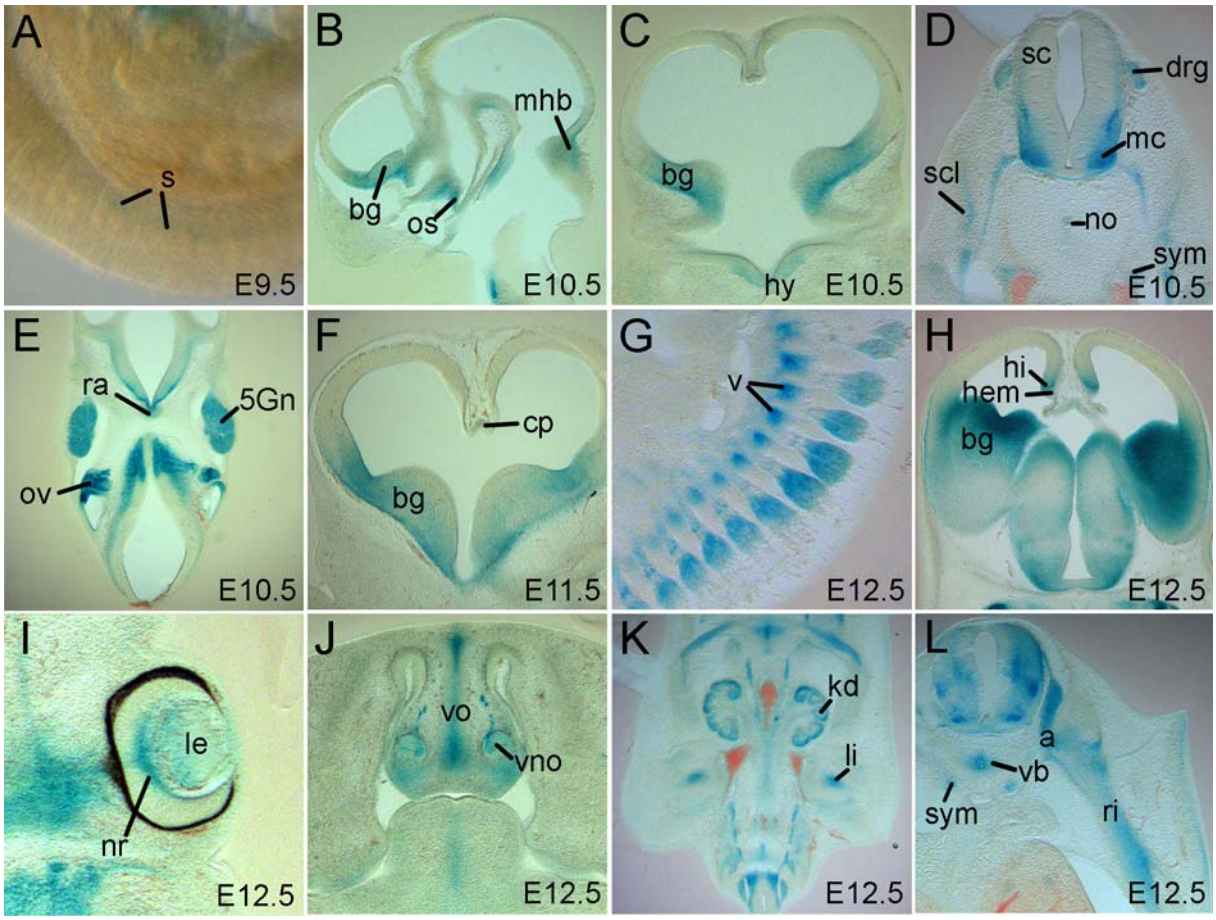

Fig. 20. Details of *Zbtb20* expression pattern revealed by X-gal. Shown are a close up of Fig. 19A (**A**), cross (**C-F**, **H**, **K** and **L**) or sagittal (**B**, **G** and **I**) sections (100 µm) after whole mount X-gal staining of *Zbtb20*+/- embryos at different stages: (**A**) E9.5; (**B-E**) E10.5; (**F**) E11.5; (**G-L**) E12.5. In (**D**) note the restricted X-gal staining in the basal plate of the spinal cord (sc) and motoneuronal column (mc), as well as in notochord (no), sympathetic chain (sym). In addition to somites (s) (**A**), and notochord (no) (**D**), X-gal staining was also seen in the sclerotome (scl) (**D**) and later in the vertebrae (v) (**G**) and the ribs (ri) (**L**), suggesting a role in skeleton formation. In (**H**) note the highly regionalized and strong expression within the regions of the hem, hippocampus anlage (hi) and basal ganglia (bg), suggesting a role of *Zbtb20* in early patterning of telencephalon. 5Gn, trigeminal ganglion; a, neural arch; bg, basal ganglia; cp, commissural plate; drg, dorsal root ganglion; hy, hypothalamus; kd, kidney; le, lens; li, limb; mhb, midbrain hindbrain boundary; nr, neural retina; os, optic stalk; ov, otic vesicle; ra, Rathke's pocket; vb, vertebral body; vno, vomeronasal organ; vo, vomer.

Table 3. Summary of *Zbtb20* expression based on *LacZ* gene reporter activity in *Zbtb20*+/- embryos (E10.5-12.5)

	E9.5	E10.5	E11.5	E12.5
CNS		++	++	++
Telencephalon		++	++	++
Commissural plate			+	
Hippocampus/hem				+++
Basal ganglia		++	++	+++
Diencephalon		++	++	+++
Mesencephalon		++	++	++
Midbrain hindbrain boundary		++	++	+++
Cerebellum		++	++	++
Neural tube		++	++	++
DRG		++	++	++
Sympathetic chain		++	++	++
Cranial ganglia		++	++	++
Motor column		++	+	+
Ribs				+
Optic stalk		+	+	++
Neural retina			+	++
Lens				+
Olfactory neuroepithelium				++
Vomer				++
Vomeronasal organ				+
Otic vesicle		++	++	++
Heart	++	++	++	++
Kidney			+	++
Thyroid gland		++	++	++
Submandibular gland				+
Notochord		+	+	++
Somites	+			
Sclerotome			+	
Intervertebral disk				+
Vertebrae				+

Relative intensity indicated as follows: +, low; ++, moderate; +++, high.

The emerged *LacZ* expression pattern in skeleton elements in the course of time E9.5- E12.5 was solidified at later stages. As shown in Fig. 21 at stage E17.5, very strong X-gal signal was observed in vertebrae, intervertebral disks, trachea, limbs, digit bones, and the ribs. These findings further implicate a possible role of *Zbtb20* for skeleton development.

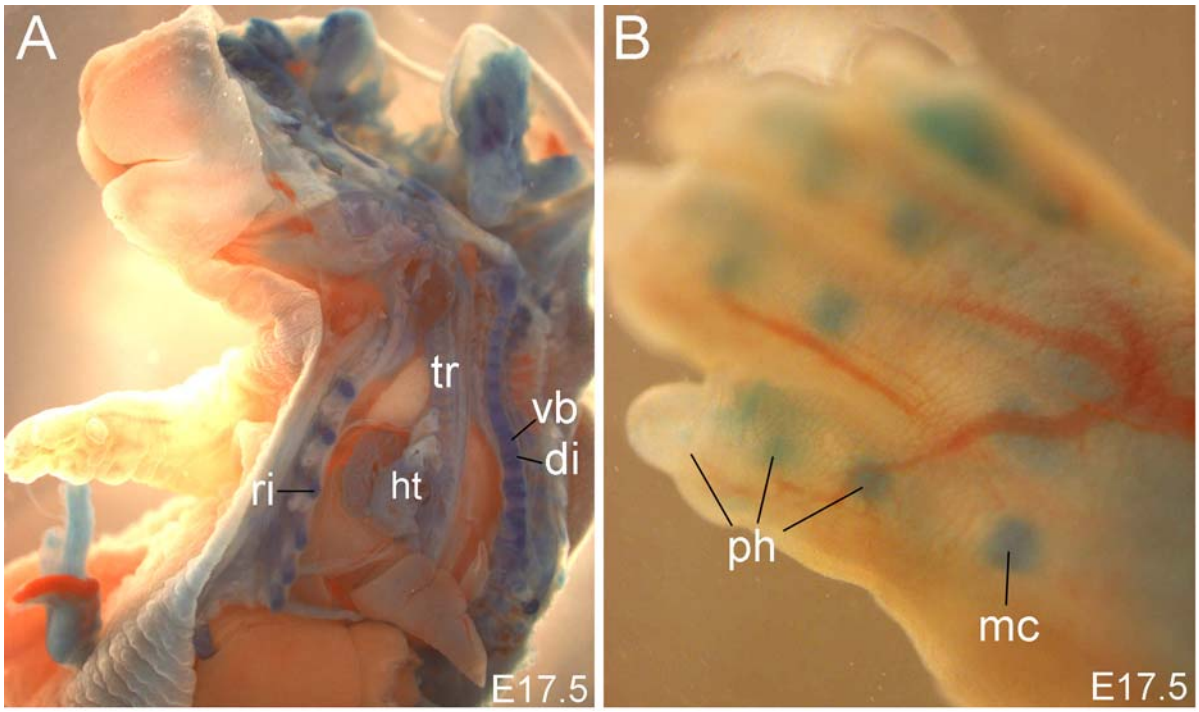

Fig. 21. *Zbtb20* expression in the developing skeleton at E17.5 based on *LacZ* reporter activity. (**A**) *Zbtb20* +/- E17.5 embryo, cut sagittally in half before X-gal staining. (**B**) Manus of a whole mount X-gal stained *Zbtb20*+/- embryo. Strong *LacZ* signal was detected in the ribs (ri), vertebrae (vb) and intervertebral disks (di) (**A**) and digit bones (**B**). ht, heart; mc, metacarpal; ph, phalanx; tr, trachea.

2.2.3.3. Expression in postnatal brain

The discovered restricted expression of *Zbtb20* in several brain regions (hippocampus, basal ganglia, cerebellum) during embryogenesis lead to the motivation to investigate whether the expression pattern was preserved in the adult brain. Therefore, the X-gal staining on sections (1 mm) of adolescent (P30) *Zbtb20+/-* animals was examined. Interestingly, the *LacZ* reporter gene activity revealed that *Zbtb20* expression is maintained in regions of the mature brain, corresponding to the embryonic *Zbtb20* positive domains. Notably, in the medial cortex, the strong expression of *Zbtb20* in the domain of Rsp delineated a sharp border with the neighboring Ncx (arrows in Fig. 22D). Subiculum and parasubiculum (together designated here as S), and cingulate cortex (Cgl, Fig. 22C) showed a moderate staining, while a very strong X-gal staining was confined to the entire Ammon's horn (CA1-CA3 areas of hippocampus (Hi) proper) and DG (Fig. 22D, E). Even the indusium griseum, the rostral part of the hippocampus, was clearly *LacZ* positive (Fig. 22C). In addition, a faint signal was detected in the upper layers of the somatosensory area (Fig. 22C). In accordance with the embryonic patterns, the basal ganglia, particularly the caudate putamen nucleus, exhibited a strong X-gal staining (Fig. 22C). Further strongly stained telencephalic structures included

diverse structures of the paleocortex, including the olfactory bulb (Fig. 22A, B), olfactory tubercle (Fig. 22C), several subnuclei of amygdala, and the piriform cortex (Fig. 22C, D). In the diencephalon (Fig. 22D, E), *LacZ* signal was confined the VZ of 3rd ventricle and some hypothalamic nuclei. Only faint signal was detected in the midbrain and medulla oblongata (Fig. 22A). Highly restricted expression was seen in the cerebellum (Fig. 22F), labeling only the Purkinje cell layer. Notably, this expression pattern was maintained during later adulthood, in adult 8 months old mice.

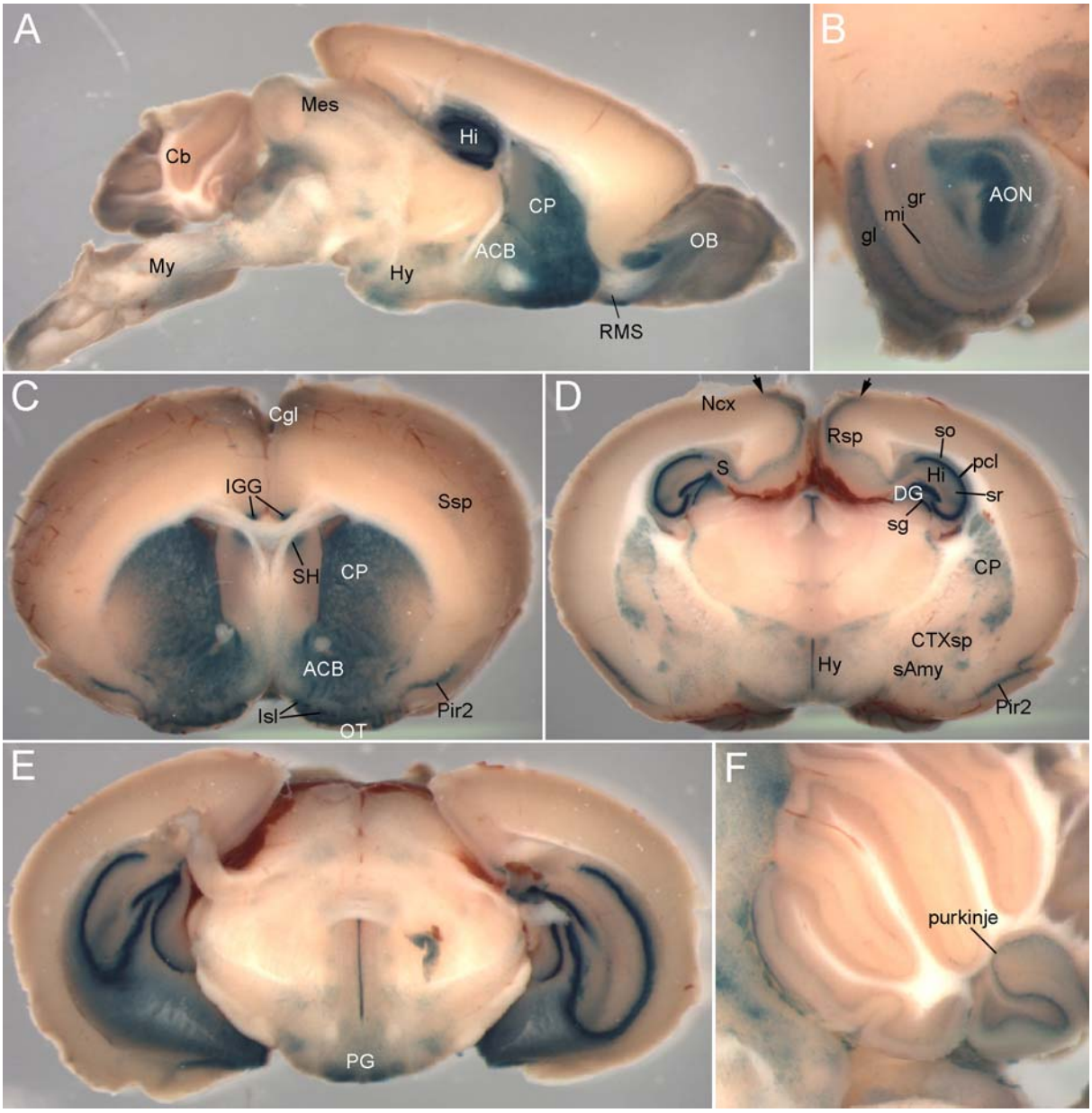

Fig. 22. Analysis of *Zbtb20* expression in adult mouse brain based on *LacZ* reporter activity. X-gal staining of 1mm thick brain slices from *Zbtb20*+/- mice at P30. (**A**) Overview of mid-sagittal brain section illustrating restricted expression of *Zbtb20* in the forebrain, midbrain, hindbrain. (**B-E**) cross sections from rostral to caudal levels of sectioning. (**B**) In olfactory bulb (OB), *Zbtb20* showed expression in granular (gr), mitral (mi),

glomerular layer (gl) and anterior accessory olfactory nucleus (AON) as well as all along the rostral migratory stream (RMS) (**A**). In (**D, E**) note the abundant expression of the *LacZ*-reporter in hippocampus proper (Hi), dentate gyrus (DG), and retrosplenial cortex (Rsp). Arrows in (**D**) indicate the sharp border between strongly *Zbtb20*$^{+}$ Rsp domain and residual neocortex (Ncx). (**C**) The caudate putamen (CP) was *LacZ* positive, except for its lateral subdivision. ACB, nucleus accumbens; Cb, cerebellum; Cgl, cingulate cortex; CTXsp, cortical subplate; CP, caudate putamen; Hy, hypothalamus; IGG, indusium griseum glia; Isl, islands of Calleja; Mes, mesencephalon; My, medulla oblongata; OT, olfactory tubercle; Pir2, pyramidal layer of piriform cortex; pcl, pyramidal cell layer; PG, pontine gray; purkinje, Purkinje cell layer, S, subiculum; sAMY, striatum-like amygdalar nuclei; sg, dentate gyrus granule cell layer; SH, septohippocampal nucleus; so, *stratum oriens*; sr, *stratum radiatum*; Ssp, primary somatosensory area.

2.2.3.4. Expression in different organs in adulthood

LacZ staining in heterozygous *Zbtb20* adult animals revealed that *Zbtb20* is expressed at different levels in several organs (Table 4). Strong to moderate X-gal staining intensity was detected in the peripheral nerves, cartilage of the nose and the ribs, kidney, testis, and heart, whereas eye, stomach, liver and lung displayed weak signal. The pancreas and the skin, as well as wild type control, were *LacZ* negative.

Table 4. *Zbtb20* expression in tissues at adulthood on the basis of *LacZ* reporter activity

Peripheral nerves	++	Pancreas	-
Eye	+	Heart	+++
Stomach	+	Spleen	(u)
Liver	+	Nose cartilage	+++
Lung	+	Rib	+++
Kidney	+++	Skin	-
Testis	++		

Relative intensity indicated as follows: +, low; ++, moderate; +++, high, u, undiscernible.

2.2.4. Gross abnormalities in the *Zbtb20* KO mice

2.2.4.1. Prenatal viability

Heterozygous *Zbtb20*+/- mice were viable and appeared phenotypically normal. To gain insight into the role of *Zbtb20* during development, homozygous *Zbtb20* (*Zbtb20*-/-) mutants were analyzed at embryonic and postnatal stages. From a total of 205 newborn (P0) pups generated through mating of heterozygous parents, 65 (32%) were wild type, 104 (51%) were heterozygous and 36 (18%) were homozygous for the mutant alleles (Table 5). Notably, the

ratio of *Zbtb20-/-* mutant newborns (18%) was significantly below the expected Mendelian ratio of 25% (chi-square, p>0.025), indicating in-utero death. To determine the time point of lethality, embryonal stages E9.5 to E18.5 were analyzed. Until E18.5, a total of 417 embryos were obtained from 59 litters. From these embryos 103 (25%) were wild type, 226 (54%) heterozygous, and 88 (21%) homozygous mutant *Zbtb20* embryos. This result did not significantly deviate from the expected Mendelian 1:2:1 ratio (chi-square, p>0.05), and the ratios of *Zbtb20*-/- embryos at latest gestational stages appeared normal. These findings indicate that the observed decreased number of *Zbtb20*-/- animals involves perinatal or early postpartum death and suggest that *Zbtb20* gene function might be dispensable for perinatal embryo survival.

Table 5. Genotype of offspring from *Zbtb20* +/- heterozygote matings

			Genotype		
Age	Litters	Animals	+/+	+/-	-/-
E9.5	2	19	7	10	2
E10.5	2	19	4	14	1
E11.5	4	37	12	20	5
E12.5	14	102	30	53	19
E13.5	4	31	8	14	9
E14.5	2	15	2	8	5
E15.5	14	77	11	47	19
E16.5	6	41	9	20	12
E17.5	2	16	5	7	4
E18.5	9	60	15	33	12
Total (E9.5-18.5)	59	417	103	226	88
			(25%)	(54%)	(21%)
P0			65	104	36
			(32%)	**(51%)**	**(18%)**

Most of the homozygous *Zbtb20*-/- mutants survived till birth.

2.2.4.2. Growth retardation, premature death and other defects in postnatal *Zbtb20*-/- mice

To investigate further the reason for the premature death in *Zbtb20* KO mice, the postnatal weights of all three genotype were measured. The average body weight was determined at 11 postnatal stages is shown in Fig. 23D. The weights of heterozygous animals did not show any deviation from that of the wild type controls. However, starting at stage P6, the weight of the

homozygous *Zbtb20* animals showed a progressive decrease, especially profound at the latest studied stages P18, P20, at which the weight of *Zbtb20*-/- animals represented only about 50% of the normal values (Fig. 23D). Within the second postnatal week, the axial growth in *Zbtb20*-/- was arrested. At this time, all *Zbtb20*-/- mice displayed a noticeably smaller body size (dwarfism) and a lower body mass in comparison to their normal littermates (Fig. 23B). However, the brain size of the mutant was not or only slightly reduced (Fig. 23C). The health status of the *Zbtb20*-/- mice progressively worsened as seen by loss of weight, clotty eyes and ragged fur. At the same time, they showed hyperactive behavior by running around in the cage more quickly and more often than their heterozygous or wild type littermates. Lifespan monitoring of wild type, *Zbtb20*+/- and *Zbtb20*-/- mice revealed that all mice homozygous animals died between P5 and P24, with an average lifespan of only approx. 16 days. (Fig. 23E). Lethality among wild type or *Zbtb20*+/- mice was not observed during this period of time. Death of *Zbtb20*-/- mutants was preceded by a dramatic loss in body weight, suggesting starvation may be the cause of death. However, autopsy revealed that the majority of the dying *Zbtb20*-/- pups still contained milk in their stomach while large accumulations of air were found in the intestines. Together, these findings indicate that *Zbtb20* plays an essential role in animal survival, vital functions, possibly related to regulation of important metabolic function.

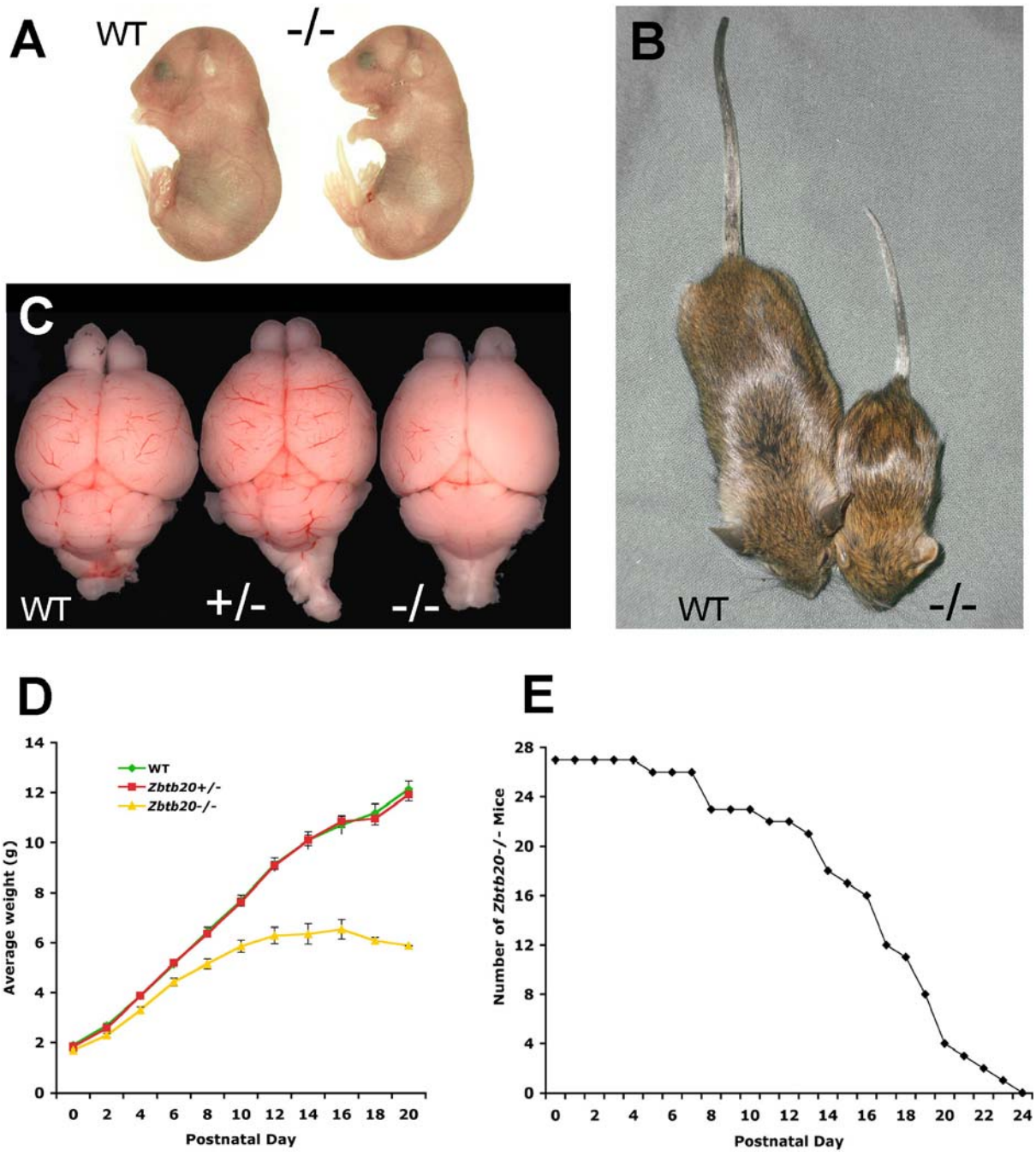

Fig. 23. Life span and growth rate of *Zbtb20* knockout mice was severely diminished. (**A**) At E18.5, *Zbtb20* -/- embryos appeared normal and did not display gross abnormalities compared to wild type littermates. (**B**) *Zbtb20*-/- mice at P19 display dwarfism compared to the control. (**C**) At stage P20, homozygous *Zbtb20*-/- brains appeared normal or slightly reduced in size as compared to wild type and heterozygous (+/-) *Zbtb20* brains. (**D**) Average weights for wild type (n=30), *Zbtb20*+/- (n=53) and *Zbtb20*-/- (n=17) mice at P0, P2, P4, P6, P8, P10, P12, P14, P16, P18 and P20. Error bars indicate SEM (standard error of means). (**E**) Individual life spans of *Zbtb20*-/- mice. The *Zbtb20*-/- mice survived 5-24 d after birth, with an average lifespan of 16.3d (n=27).

2.2.5. Analysis of the brain phenotype in *Zbtb20* KO mice

2.2.5.1. Morphological defects of the postnatal brain

Given the interesting expression pattern of *Zbtb20* in developing and postnatal brain, first the gross morphology of the brain of *Zbtb20* KO mice at postnatal stage P10 was examined. At this stage, the generated neurons have accomplished their migration towards the cortex and they have found their location in the cortical layers. Remarkably, examination of cresyl violet (Nissl) stained sections from mutant and control brains revealed a severely impaired cytoarchitecture, specifically of the hippocampal formation. The size of the hippocampus in *Zbtb20* mutants, including the whole Ammon's horn with its CA1, CA2, CA3 areas as well as the DG, was drastically reduced and appeared hypocellular. The morphological abnormalities were more severe at rostral levels, seen by the absence of the indusium griseum (arrows in Fig. 24A/A'), the rostralmost part of the hippocampus, and severe malformations of CA1-CA3 regions of hippocampus proper. In addition, DG appeared misshaped due to a shortened enclosed blade (black arrowheads in Fig. 24B', C'). Notably, the typical compact stratified pyramidal cell layer (pcl, arrow in Fig. 24B) of CA1 seen in the controls (Fig. 24B, C) could not be identified in the *Zbtb20*-/- mutant (Fig. 24B'). The characteristic six-layered morphology of the Ncx is not easily detectable in the Cgl and retrosplenial cortex (Rsp) domain of the medial cortex (Fig. 24A, B), except for the uppermost layers that show a similar compact appearance in both neo- and archicortex. Interestingly, similarly to Ncx, the Rsp domain in the *Zbtb20-/-* brain exhibited very well defined layer 5 neurons, consisting of large pyramidal neurons. The subiculum (S), a transitory domain intercalated between the Cgl (rostrally) or Rsp (caudally) cortex and the CA1 domain of hippocampus, is characterized by loosely arranged pyramidal cells better recognizable at more caudal level (arrow in Fig. 24C). Intriguingly, S domain in *Zbtb20-/-* mutant looked much more compact as compared with the matching controls and exerted a gross morphology resembling to the adjacent Rsp domain (arrows in Fig. 24C/C'). The mutant cerebellum was proportionally smaller than the wild type counterpart (not shown).

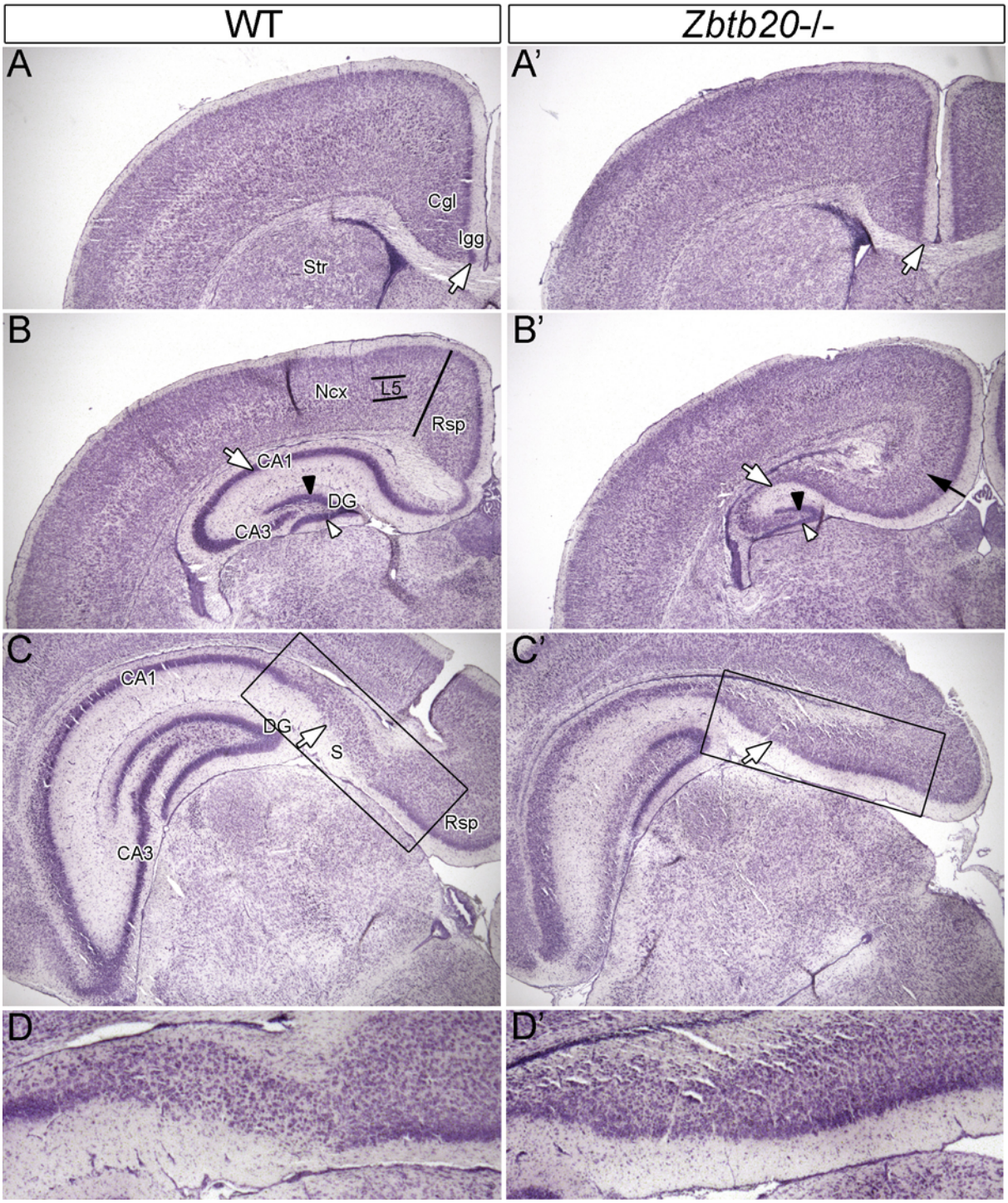

Fig. 24. Morphological defects of archicortex in *Zbtb20*-/- mice. Cresyl violet stained coronal sections from P10 brains of *Zbtb20*+/+ (**A, B, C**) and *Zbtb20*-/- (**A', B', C'**) mice at rostral (**A, A'**) and caudal (**B-C'**) levels of sectioning. (**A/A'**, arrows) The indusium griseum glia (Igg), were absent in the *Zbtb20*-/- mutant. (**B/B'**) In the mutant brain, the compact pyramidal cell layer (pcl), indicated by a white arrow in (**B, C**) was virtually absent (**B', C'**), while the defined layer 5 (L5) indicative of neocortex (Ncx) outside retrosplenial cortex (Rsp) (**B**) extended into the presumptive Rsp domain . In (**B'**) black arrow points at medial border of defined neocortical L5 in mutant brain. In **C/C'** note that the subiculum (S), easily identifiable in the controls by its loosely packed and wide pcl, adopted a laminate morphology in the *Zbtb20*-/- brain, similar to that of the adjacent Rsp (arrows in **C, C'**). (**D, D'**) are close ups of (**C, C'**). The dentate gyrus (DG) showed a reduction in size (**B/B'**, **C/C'**).

Note that compared to the controls, the enclosed blade (black arrowhead in **B/B'**) of the mutant DG is shorter that the free blade (white arrowhead in **B/B'**). CA1-3, CA fields; Cgl, cingulate cortex; Igg, indusium griseum glia; Str, striatum.

In order to obtain more detailed information about above mentioned abnormal cytoachitecture and lamination within hippocampus, Golgi stainings were performed with P20 wild type and *Zbtb20*-/- brains (Fig. 25). At this age, the hippocampus has reached maturity. The Golgi's method enables the visualization of a limited number of cells at random in their entirety (Nicholls et al., 2001). Instead of the large homogeneously arranged neurons extending densely branched apical and basal dendrites seen in the control CA1 region, the CA1 area of *Zbtb20*-/- mice comprised a variety of cell types normally seen in Rsp. Collectively, the results from these histological experiments suggested that the regionalization of the medial pallium is severely affected.

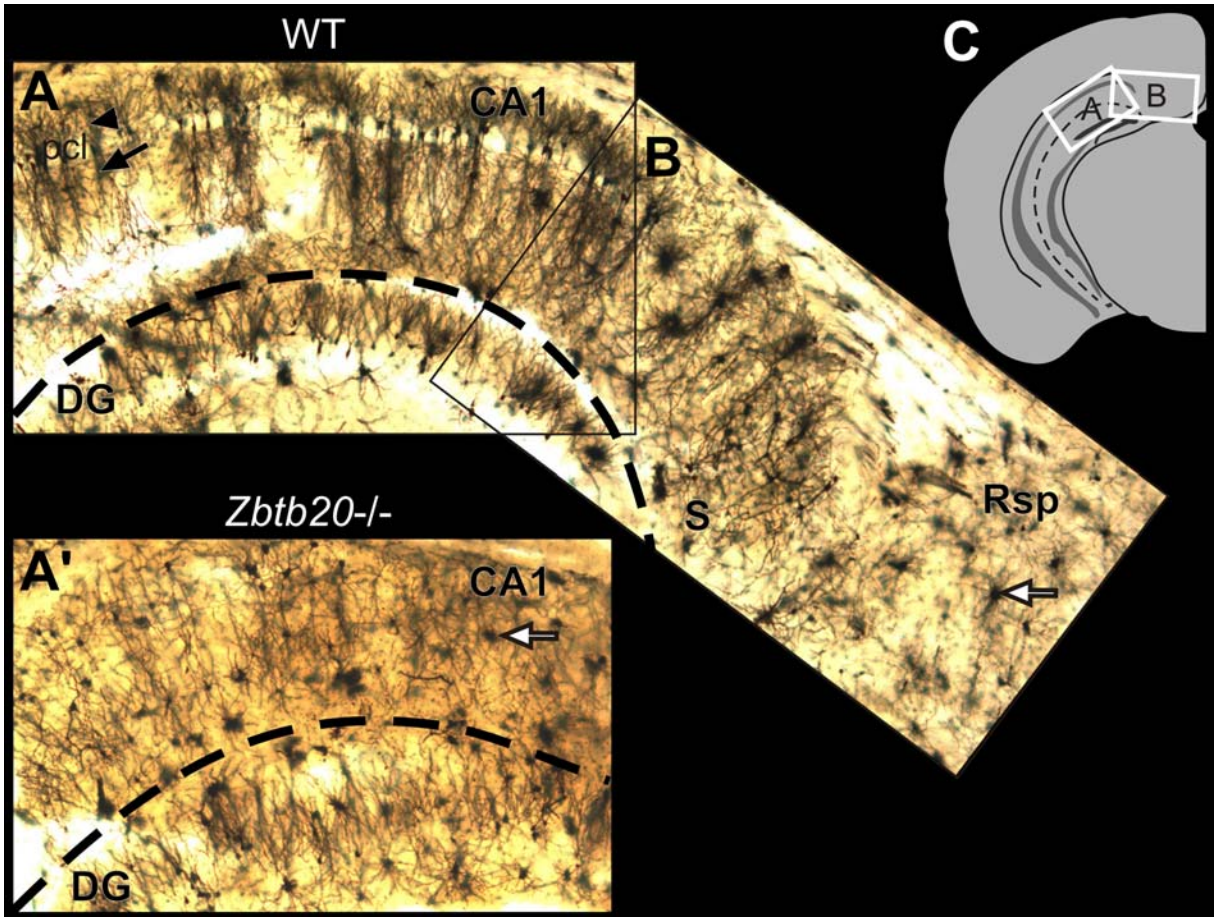

Fig. 25. Golgi impregnation of wild type and *Zbtb20*-/- hippocampus. (**A/B**) is a compilation consisting of two separate photos showing CA1, S and Rsp in the control brain, which is a close up of (**C**). (**C**) A coronal brain hemisection drawn as a schema. (**A'**) is the corresponding region of (**A**) in the *Zbtb20*-/- brain. The single compact layer of pyramidal cells (pcl) seen in the CA1 of control (**A**) is undetectable in the mutant (**A'**). The mutant CA1 was infiltrated by cells (arrow in **A'**) with appearance resembling Rsp (arrow in **B**), which replaced

the CA1 pyramidal neurons. Arrowhead and arrow in (**A**) point at a basal and an apical dendrite tree of a pyramidal cell in the normal brain, respectively. The dashed line indicates the hippocampal fissure. CA1, CA1 region; DG, dentate gyrus; Rsp, retrosplenial cortex, S, subiculum.

2.2.5.2. Analysis of the molecular patterning of cortex in *Zbtb20* KO embryos at stage E12.5

The performed expression analysis revealed that *Zbtb20* expression begins at stage E12.5 (Fig. 14A/A') and that it is strictly confined to the hem and the anlage of Hi. The hem is a small region at the medial edge of the medial telencephalic neuroepithelium, which lies between the dorsal midline roof and the cortical VZ (Fig. 14A, A'; Grove et al., 1998). Together with the detected abnormalities restricted to the hippocampus in *Zbtb20*-/- animals as described above, these findings suggested that *Zbtb20* might have a role for the early molecular regionalization of the developing cortex. To study this issue, by using a set of pallial markers, extensive in situ hybridization analysis was performed on sections from E12.5 *Zbtb20-/-* and control embryo brains.

To study features of the general patterning along AP and ML axis of the cortex of *Zbtb20* mutants, the expression pattern of the homeodomain–containing transcription factors (TFs) *Emx1*, *Emx2*, and *Pax6* was examined first. These TFs were shown to play decisive roles for the early patterning of the cortical anlage (Muzio et al., 2002; Muzio and Mallamaci, 2003). *Emx1* and *Emx2* are expressed in a graded manner in the pallial progenitors having highest levels in the MP, but progressively diminishing in the dorsal and lateral cortex (Fig. 26A, B and C, D, respectively; Cecchi and Boncinelli, 2000). On the contrary, TF *Pax6*, whose expression is confined to the pallial pluripotent RG progenitors (Götz et al., 1998; Walther and Gruss, 1991) shows an opposite expression gradient, namely rostrolateral-high to caudomedial-low (Fig. 26E, F). In the *Zbtb20* mutant, the expression of all these three markers, *Emx1*, *Emx2* and *Pax6,* appeared normal (Fig. 26A-F'), indicating that *Zbtb20* is not involved in the AP patterning across the cortex.

Given the restricted expression of *Zbtb20* in the hem, next, the expression of *Foxg1* (formerly *Bf1*), *Lhx2*, *Bmp4* and *Wnt3a* was examined. All of these genes normally exhibit a specific expression pattern in MP. The TF Foxg1 is crucial for normal telencephalic and cortical morphogenesis (Xuan et al., 1995). *Foxg1* is expressed with a rostrolateral-high to caudomedial-low gradient in the dorsal and ventral telencephalic neuroepithelium, but excluding specifically the domain of the hem (Fig. 26G; Tao and Lai, 1992). Similarly, the TF *Lhx2*, although exerting a strong expression in MP progenitors, is not expressed in the

hem (Fig. 26I). In absence of *Lhx2*, the identity of MP and DP is lost at the expense of an enlarged anlage of the hem and choroid plexus (Mangale et al., 2008; Monuki et al., 2001). Notably, in the *Zbtb20-/-* embryo cortex, the expression of both *Foxg1* and *Lhx2* was not altered, suggesting that the early regionalization of the germinal neuroepithelium of MP is not affected.

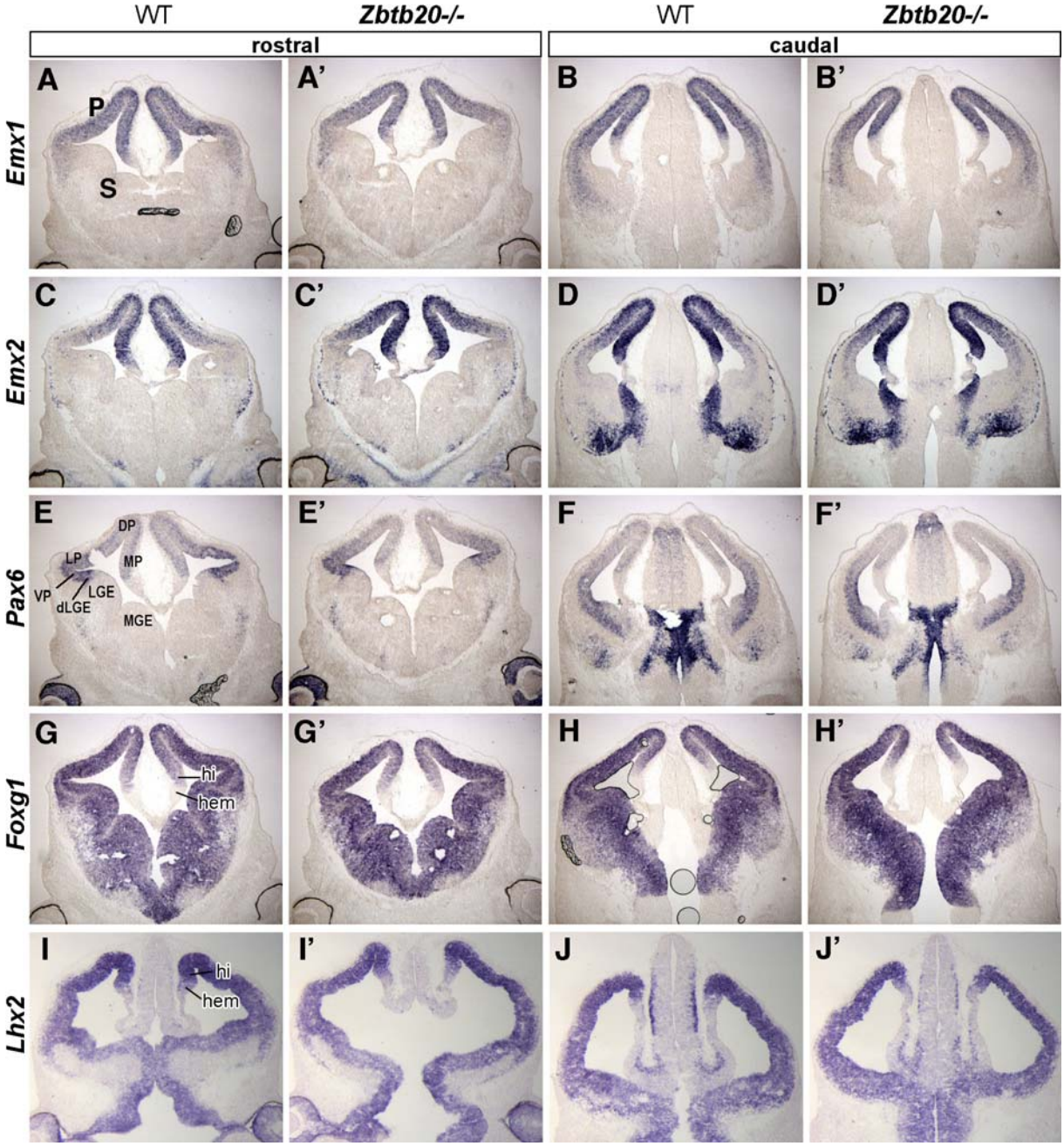

Fig. 26. Patterning of telencephalon of *Zbtb20-/-* embryos at stage E12.5. RNA in situ hybridization on rostral (left two columns) and caudal (right two columns) coronal sections from E12.5 wild type and *Zbtb20-/-* mutant brains was performed with probes as indicated. The pattern-forming genes, *Emx1* (**A-B'**), *Emx2* (**C-D'**), *Pax6* (**E-F'**), *Foxg1* (**G-H'**) and *Lhx2* (**I-J'**) exerted normal expression patterns in *Zbtb20-/-* embryo brains. DP, dorsal pallium; dLGE, dorsal lateral ganglionic eminence; LGE, lateral ganglionic eminence; LP, lateral pallium; MGE, medial ganglionic eminence; MP, medial pallium; P, pallium; S, subpallium; VP, ventral pallium.

Next, the expression of *Bmp4* and *Wnt3a* was examined, two powerful morphogens, produced by the dorsal midline of the forebrain, including the hem (Furuta et al., 1997; Grove et al., 1998; Shimogori et al., 2004). *Bmp4* normally shows a restricted expression confined to the cortical hem and the developing choroid plexus epithelium (Fig. 27A, B; Furuta et al., 1997; Grove et al., 1998). In partial ablation of *Bmp4*, only residual choroid plexus epithelial cells are generated from the medial neuroepithelium (Hébert et al., 2002). Noteworthy, the level of *Bmp4* expression in the *Zbtb20*-/-mutant (Fig. 27A'/A''', B'/B''') was markedly decreased in comparison to the control (Fig. 27A/A'', B/B''). Evidences were shown that secretion of *Wnt3a* from the hem is indispensable for the generation of the hippocampus (Grove et al., 1998; Lee et al., 2000). Importantly, the hem-specific expression of *Wnt3a* (Fig. 27C/C'', D/D'') was clearly significantly diminished in the telencephalon of *Zbtb20*-/- mutant (Fig. 27C'/C''', D'/D'''). Together, these findings suggest that in absence of *Zbtb20*, deficiency of *Wnt3a* and/or *Bmp4* controlled pathways could impart the defect in development and differentiation of the archipallium.

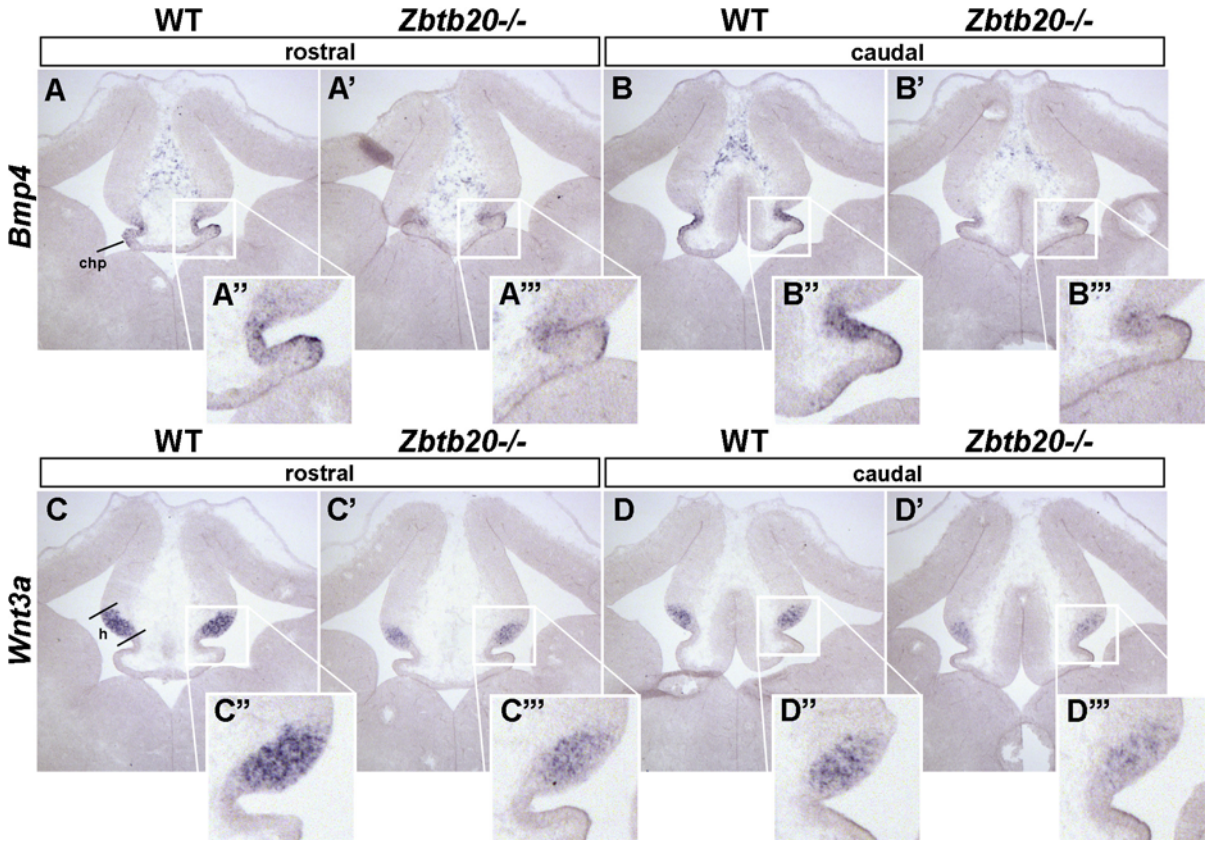

Fig. 27. Patterning defects in the MP of *Zbtb20*-/- embryos at stage E12.5. RNA in situ hybridization on rostral (left two columns) and caudal (right two columns) coronal sections from E12.5 wild type and *Zbtb20*-/- mutant brains was performed with probes as indicated. Note that both, *Bmp4* (**A-B'''**) and *Wnt3a* (**C-D'''**) hybridization signal was significantly diminished in the hem and hippocampus anlage of the *Zbtb20*-/-

telencephalon. Close ups of *Bmp4* (**A''-B'''**) and *Wnt3a* (**C''-D'''**) expression are shown. Chp, choroid plexus; h, hem.

2.2.5.3. Defect of the regional organization of the medial pallium at stage E16.5-18.5

2.2.5.3.1. Medial displacement of the border retrosplenial cortex/subiculum, Rsp/S

The observed down regulation of *Wnt3a* and *Bmp4* expression in the hem of *Zbtb20*-/- mice suggested that morphological abnormalities in the medial pallium may occur at later stages, when the differentiation has been advanced. Therefore, by using a number of regional markers for hippocampal subregions (Tole et al., 2000), the patterning and the morphology of the *Zbtb20*-/- telencephalon were studied at stage E18.5.

Restricted expression of an increasing number of markers was shown to outline the borders between different neocortical functional domains (e.g. motor/somatosensory, visual/ somatosensory areas) along the AP axis of developing cortex in VZ/SVZ (reviewed by (Rash and Grove, 2006), but also in CP (Joshi et al., 2008). Unfortunately, no markers were so far available to study the regionalization of the subdomains of the archicortex. The CP of the Ncx is extending medially over the domains of the cingulate (Cgl) (rostrally) and Rsp (caudally) cortex. As mentioned above, the neurons in both Cgl and Rsp are distributed into layers, although not so well visible as in the Ncx. In the medial pallium, the region of subiculum (S, Fig. 28) is intercalated between the Cgl or Rsp and CA1 area of hippocampus proper. As described below, we identified several novel marker genes that demarcate expression borders between Rsp/S, and S/CA1 domains of archicortex. These were successfully applied to characterize the *Zbtb20*-/- cortical phenotype.

The TF genes *Id2* and *Math2* are expressed at equally high level in postmitotic neurons of the entire depth of CP of the Ncx, including Cgl and Rsp (Fig. 28A, B, C, D; Rubenstein et al., 1999; Schwab et al., 1998; Tzeng and de Vellis, 1998). Due to the loosely dispersed cells in the S, the expression of both markers looks fainter in this domain. Similarly, TF gene *Foxg1* is strongly expressed by the majority of the densely packed neurons of the neocortical CP, Cgl and Rsp domains, and at a lower level in the domain of S (Fig. 28E, F; Hanashima et al., 2004). Strikingly, in the *Zbtb20*-/- mice, the robust and compact expression of *Id2*, *Math2*, *Foxg1*, a characteristic trait of their expression in the CP of Ncx and Rsp, was extending ectopically over S and even over the CA1 area of hippocampus (compare Fig. 28A/A', B/B', C/C', D/D', E/E', F/F').

To test furthermore the defective patterning of S, the riboprobes for *Nef3* and *Odz3* (Julien et al., 1986; Young and Leamey, 2009) were used. Rostrally, S was negative for both *Nef3* and *Odz3* (Fig. 29A, C), showing only weak signal caudally (Fig. 29B, D). In the *Zbtb20-/-* brain, a very strong and wide band of *Nef3* expression, resembling the expression characteristics of *Nef3* in Ncx and Rsp, was ectopically extended over the entire S and CA1 domain of hippocampus (compare Fig. 29A/A' and B/B'). Similarly, *Odz3* signal showed ectopic and compact extension into S in *Zbtb20-/-* brains, very much resembling to the patterning of the adjacent Rsp (Fig. 29C/C', D/D').

To sum up, based on the described region-specific expression traits of *Id2*, *Math2*, *Foxg1*, *Nef3* and *Odz3*, these genes appear to be useful markers in outlining the putative border Rsp/S of MP. Furthermore, the results suggest in the *Zbtb20-/-* brain, an ectopic extension of Rsp into the domain of S and CA1 of hippocampus occurred.

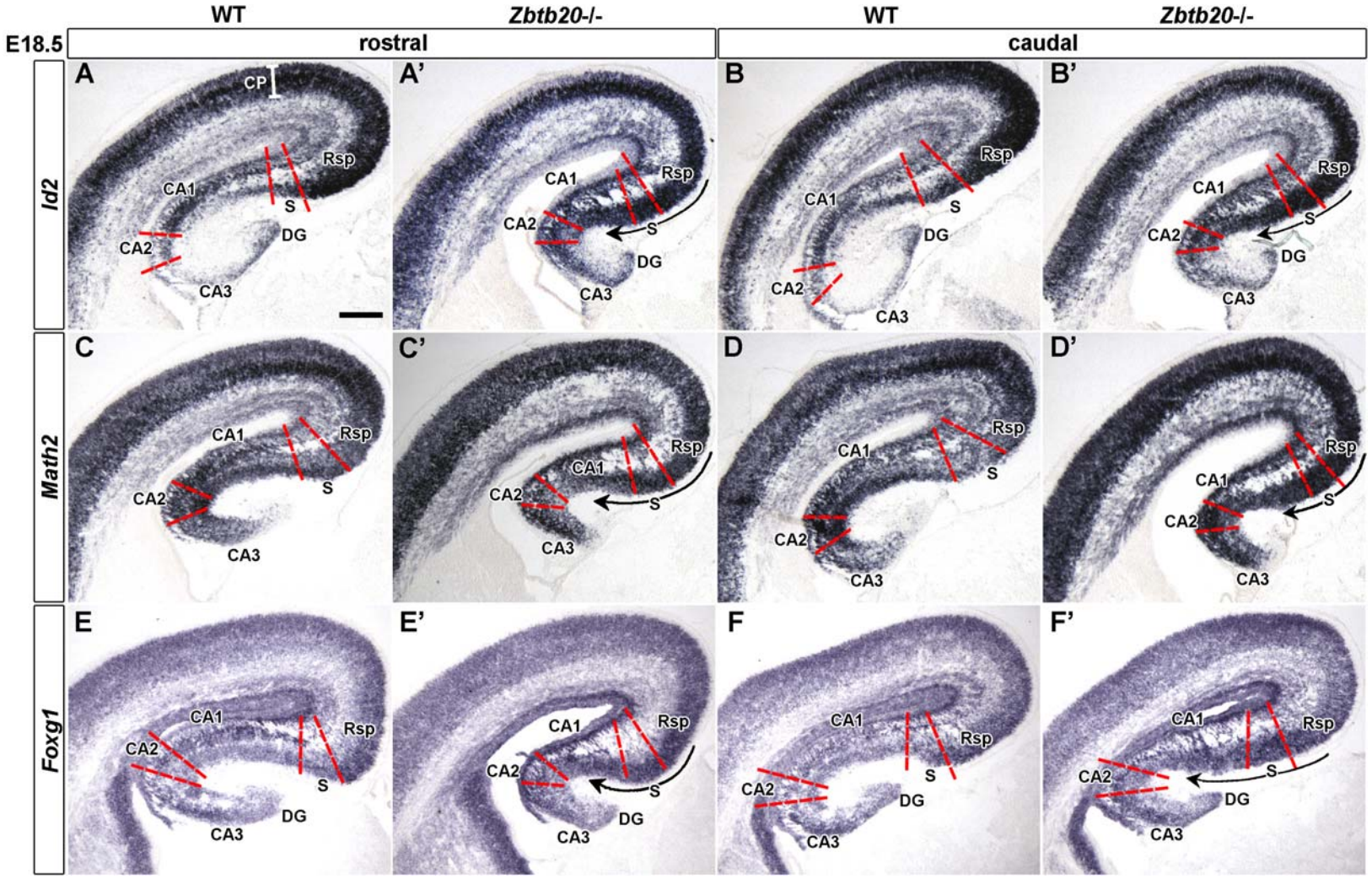

Fig. 28. Medial shift of the borders Rsp/S and S/CA1 area in the *Zbtb20*-/- brain.

ISH on rostral (left two columns) and caudal (right two columns) coronal sections of wild type and *Zbtb20*-/- mutant brain at E18.5 with in situ probes as indicated. In (**A/A'**) and (**B/B'**) note that in the mutant the domains of Rsp, S, and CA1 showed a discontinuous, compact, strong and wider *Id2* expression band as compared to the control, similar to the *Id2* expression pattern in the Ncx. Very similar pattern defect was detected also with *Math2* (**C/C'**, **D/D'**) and *Foxg1* (**E/E'**, **F/F'**) riboprobes. Red dashed lines indicate presumptive boundaries between adjacent regions. Arrows indicate the medial expansion of the strong expression domains in the mutant Abbreviations: CA, CA region; CP, cortical plate; DG, dentate gyrus; Rsp, retrosplenial cortex; S, subiculum. Scale bar 500 µm.

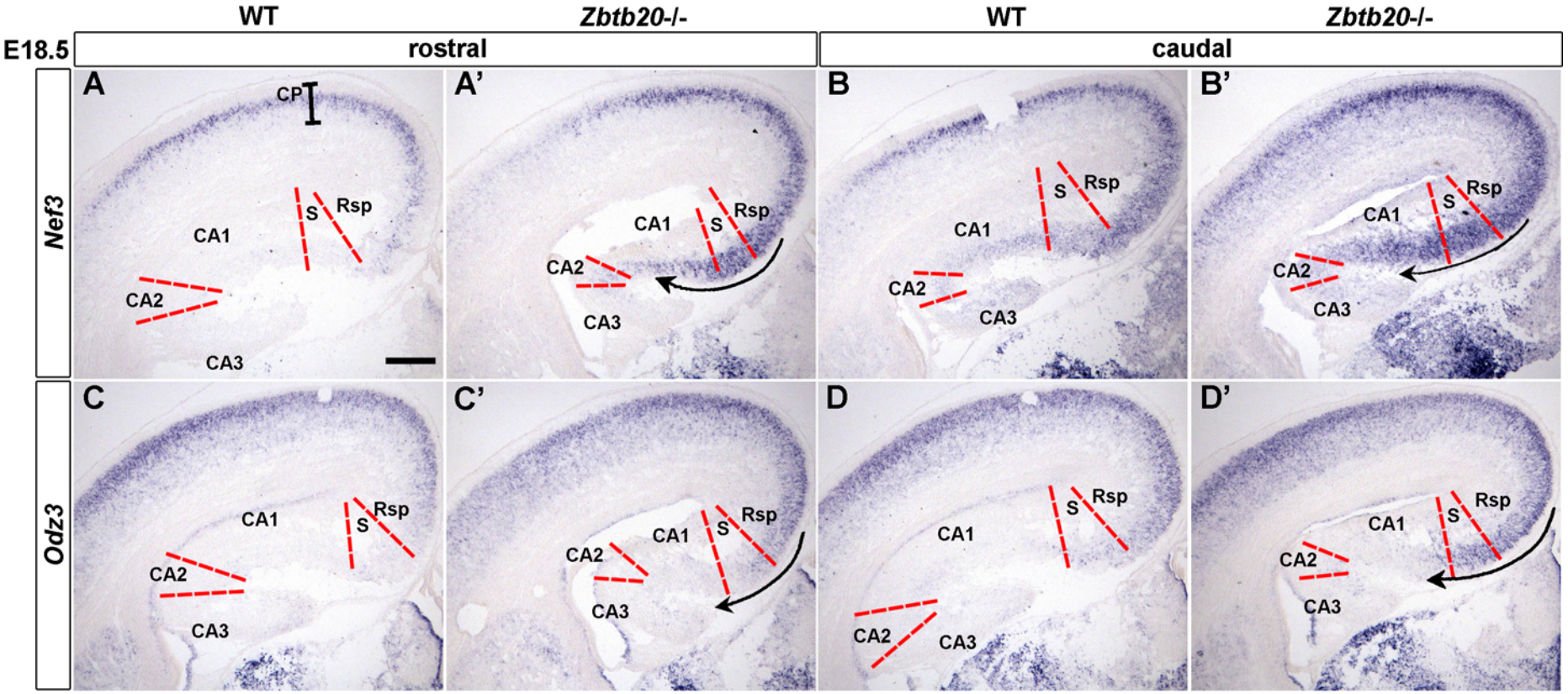

Fig. 29. Medial shift of the borders Rsp/S and S/CA1 area in the *Zbtb20*-/- brain.

ISH on rostral (left two columns) and caudal (right two columns) coronal sections of wild type and *Zbtb20*-/- mutant brain at E18.5 with in situ probes as indicated. In (**A-B'**) note that while normally devoid of *Nef3* transcripts, the S and CA1 area in *Zbtb20*-/- brain showed an ectopic and wide band of *Nef3* expression. (**C–D'**) Similar pattern defect was observed with *Odz3* in situ probe. In **C'** and **D'** note that the ectopically extended expression of *Odz3* into the S of *Zbtb20*-/- brain was confined to the upper layers in the Ncx. Red dashed lines indicate presumptive boundaries between adjacent regions. Arrows indicate the medial expansion of the strong expression domains in the mutant. CA, CA region; CP, cortical plate; DG, dentate gyrus; Rsp, retrosplenial cortex; S, subiculum. Scale bar 500 µm.

2.2.5.3.2. Medial displacement of the border S/CA1 of hippocampus

The pattern disturbance at the border S/CA1 described above was based on the detected distinct strength of the expression in these two adjacent domains. To gain better evidence that in *Zbtb20*-/- brain the patterning at this border was indeed affected, molecular markers were chosen, showing highly restricted expression in these two domains. The orphan nuclear receptor gene ***Nurr1*** was expressed at a high level in the cortical subplate, as well as in differentiating cells of the basolateral cortex and in S (Fig. 30A, B; Zetterstrom et al., 1996). The adjacent domain of Rsp cortex was, however, negative for *Nurr1 t*ranscripts. Interestingly, in the *Zbtb20* KO mice, the expression of *Nurr1* in the presumptive normal location of S was absent, while a faint residual *Nurr1* signal was detected in much more medial position, namely, in the presumptive normal location of the CA1-field of hippocampus (Fig. 30A', B'). These results strongly suggest that in absence of *Zbtb20*, there is a medial displacement of the Rsp into S domain, and subsequently, the S into CA1 domain. In a further support, similar pattern disturbance was observed with the *Er81* in situ probe. The TF gene ***Er81*** (also named *Etv1*) is a specific marker not only for a subpopulation of layer 5 projection neurons (Brown and McKnight, 1992), but also for S at stage E18.5 (Fig. 30C, D), demonstrated as well as for the rat at P5 (Yoneshima et al., 2006). Thus, although expressed at much lower level than *Nurr1* in S, *Er81* is a useful marker to analyze this region. Notably, in *Zbtb20-/-* mice, the expression of *Er81* was specifically abolished in the S (arrowheads in Fig. 30C', D'), but not in layer 5 of CP. Together, these pattern disturbances suggest that in absence of *Zbtb20*, the Rsp extends into the normal domain of S, which is displaced into the normal domain of CA1 of hippocampus.

As an additional approach to study mispatterning of the MP, immunohistochemistry against the calcium-binding protein, **calretinin** (Fig. 30E-F'), was applied. Besides interneurons in the marginal zone (MZ) and subplate (SP), the calretinin antibody labels also axon fibers of the thalamocortical and/or corticofugal projections to and from the Ncx (arrowhead in Fig. 30; DeFelipe, 1997). At stage E17.5, these axons reach the subplate thus outlining the limits of the neocortical and Rsp domains. Interestingly, while in the control brain these axon fibers were almost excluded from the S region, in the *Zbtb20*-/- embryos, the anti-calretinin positive zone was extended far more medially beyond the S domain.

It is important to note that in accordance with the described restricted early expression of *Zbtb20* in the hem, the expression of *Nurr1*, *Er81* and calretinin as well as the pattern of the five markers described above (*Id2*, *Math2*, *Foxg1*, *Nef3* and *Odz3*) was affected only

within the region of MP (see Fig. 28A', B', C', D', E', F', Fig. 29A', B', C', D'). Thus, by controlling the molecular patterning within MP, *Zbtb20* plays a role for the regionalization across the ML axis of dorsal telencephalon.

2.2.5.3.3. Medial displacement of the border CA1/CA2-3

The detected mispatterning at the border Rsp/S suggested medial displacement of subregions of the archicortex. Medially to S, the hippocampus proper is located with its three subdomains CA1, CA2, CA3. The principal cell layer of the Hi proper, the *stratum pyramidale*, or the pyramidal cell layer (pcl), can be easily recognized by its prominent C-shape. Laterally, the dense pcl ends into subiculum, where it widens, appearing much less compact. The CA3 and CA2 fields are composed of large pyramidal cells while CA1 contains smaller pyramidal cells. At E18.5, however, these differences are not yet morphologically distinct (Altman and Bayer, 1990b). The proximal end the pcl is capped by the dentate gyrus (DG), which is "U" or "V" shaped. The DG comprises the molecular layer, the granule cell layer and the polymorphic layer. The principal cell type of the DG are the granular neurons, which form the granular cell layer, gcl.

Given the discovered ectopic expansion of Rsp and S markers into more medial cortical domains in *Zbtb20-/-* mice, next it was examined whether the different Hi-subdomains were correctly patterned.

SCIP (also *Pou3f1*, *Oct-6, Tst-1*), which encodes a POU transcription factor (Suzuki et al., 1990), is strongly expressed in the upper cortical layers of Ncx, including the Rsp area. Only a fainter signal was detected for *SCIP* in S and CA1 of Hi (Fig. 31A, B; Tole et al., 1997). Interestingly, in the *Zbtb20-/-* mutant, the strong *SCIP* expression, characteristic for CP of the neo- and Rsp cortex, was medially expanded over the presumptive domain of S (filled arrows in Fig. 31A'/B'). As shown in Fig. 31A/B, the wild type expression of *SCIP* in CA1 is much stronger as compared to the adjacent S domain, reflecting the difference in the packing of the pyramidal neurons, as described above. Notably, in the *Zbtb20-/-* brain, the stronger expression of *SCIP* in CA1 was severely diminished, acquiring an expression level normally seen in the adjacent S (dashed arrows in Fig. 31A'/B'). These findings suggest therefore that in the *Zbtb20-/-* mutant the S is not lost, but displaced more medially into the normal area of CA1 of hippocampus proper. Consequently, the tight packing of the cells in pcl of CA1 in *Zbtb20-/-* brain is lost (see also Fig. 24B/B', C/C' and Fig. 25).

Finally, to get more convincing evidence for this assumption, next several molecular markers were used that do not label S, but are expressed in the adjacent domains, the Rsp and/or CA1 of Hi.

As a marker to study the patterning at the S/CA1 border, ***Steel*** was used, encoding a ligand for the Kit receptor, involved in hippocampus-dependent learning (Motro et al., 1996). Abundant *Steel*/*Kitl* transcripts were detected in lower layers of CP of Ncx and Rsp, as well as in CA1 area of Hi and in DG. As S is a *Steel*-negative domain (Fig. 31C/D), this regionalized expression helps to outline the two borders, Rsp/S and S/CA1. In the *Zbtb20* mutant, this *Steel*-negative domain (thus with a "subicular-like" characteristic) was expanded over the CA1 area, which became a *Steel*-negative region (dashed arrow in Fig. 31C'/D'). At the same time, ectopic *Steel* signal with a strength similar to that seen in Rsp was displaced into the location of the normally negative S in the *Zbtb20-/-* mutant (filled arrows in Fig. 31C'/D'). Furthermore, the normal *Steel* expression in CA1 was displaced into the presumptive domain of CA2/CA3, regions that are normally devoid of *Steel* transcripts (arrowheads in Fig. 31C'/D').

Neuropilin-2 (*Nrp2*), the receptor for semaphorins E and IV, is highly expressed in all three domains CA1, CA2, CA3 of hippocampus proper, dentate gyrus (DG), and olfactory cortex (Chen et al., 2000; Chen et al., 1997). In the hippocampus proper, the expression of *Nrp2* is confined to the pcl of CA1-3 and IZ (Fig. 32A, B; Chen et al., 2000). Because CA1 but not the adjacent S expresses *Nrp2*, the *Nrp2* in situ probe was used as an indicator of the boundary between S and CA1 (S/CA1 border). Surprisingly, in the *Zbtb20-/-* mutant, the *Nrp2* signal in CA1 was fully abrogated and severely diminished in CA2 region. Thus these two hippocampal domains seemed to have become *Nrp2* negative, having acquired a trait typical for the adjacent S (Fig. 32A', B').

Similarly to *Nrp2,* the probe for basic helix-loop-helix transcription factor gene *Neurod1* (Liu et al., 2000a) labeled the CA1-3 pyramidal cell layer, but not S (Fig. 32C, D; Miyata et al., 1999). In the *Zbtb20-/-* embryos, the negative S domain expanded over the CA1/2 area, which became a *Neurod1* negative region as well (indicated by the dashed arrows in Fig. 32C', D').

Finally, the expression of *Nk3* (also termed *Tacr3*) was tested, encoding the neurokinin 3 receptor, a member of the tachykinin family (Shigemoto et al., 1990). In the controls, *Nk3* transcripts were confined to a contiguous region including mostly CA1 and CA2 areas (Tole et al., 2000), while S normally is a *Nk3* negative region (Fig. 32E/F). Noteworthy, *Nk3*

expression in CA1 and CA2 was undetectable in the *Zbtb20*-/- mutant (Fig. 32E', F'), thus seeming to have acquired patterning of the S.

Together, these results strongly suggest that in absence of *Zbtb20*-/- subdomains of the archicortex were ectopically displaced into more medial areas: Rsp into S, S into CA1, and CA1 into CA2.

2.2.5.3.4. Mispatterning of the CA2/CA3 area of hippocampus

To get insight for the mispatterning at the CA2/CA3 border, in addition the *KA1* and *EphB1* in situ probes were utilized. ***KA1/Grik4*** (kainate class ionotropic glutamate receptor gene) labeled all cells of pcl of CA2 and CA3 (Fig. 33A, B; Tole et al., 1997; Tole et al., 2000), and at a lower level the hippocampal IZ (IZh). In the *Zbtb20* mutant, *KA1* signal was abrogated in the region CA2, suggesting that the *KA1* negative domain of CA1 was expanded over the CA2 (dashed arrow in Fig. 33A', B'). Supporting evidence for such a conclusion was found after application of the ***EphB1*** in situ probe. *EphB1* codes for the Eph receptor B1, a member of the Eph family of receptor tyrosine kinases (Friedman and O'Leary, 1996). *EphB1* showed a moderate expression in the lower layers of the CP of Ncx, Cgl, Rsp, and S. The highest expression of *EphB1* was confined to CA3 area and DG, while both CA2 and CA1 areas appeared negative. (Fig. 33C, D). Thus this marker outlined well two hippocampal borders between: a) S (positive area) and CA1 of Hi (negative area) and b) the CA2 (negative) and CA3 (positive) areas. Notably, in the *Zbtb20*-/- brain, ectopic and very strong *EphB1* expression signal was observed in CA1, similar to the normal pattern seen in the adjacent S (filled arrow in Fig. 33C', D'), indicating a medial shift of the border S/CA1. Furthermore, in the mutant, *EphB1* expression in CA3 was strongly inhibited, which is possibly related to the expansion of the negative CA2 into CA3. The latter appeared to be contracted laterally (C', D').

Together, these findings indicate that in *Zbtb20*-/- mice, in addition to the above-described mispatterning at the border S/CA1, the region with molecular characteristics of CA2 is expanded into presumptive hippocampal CA3.

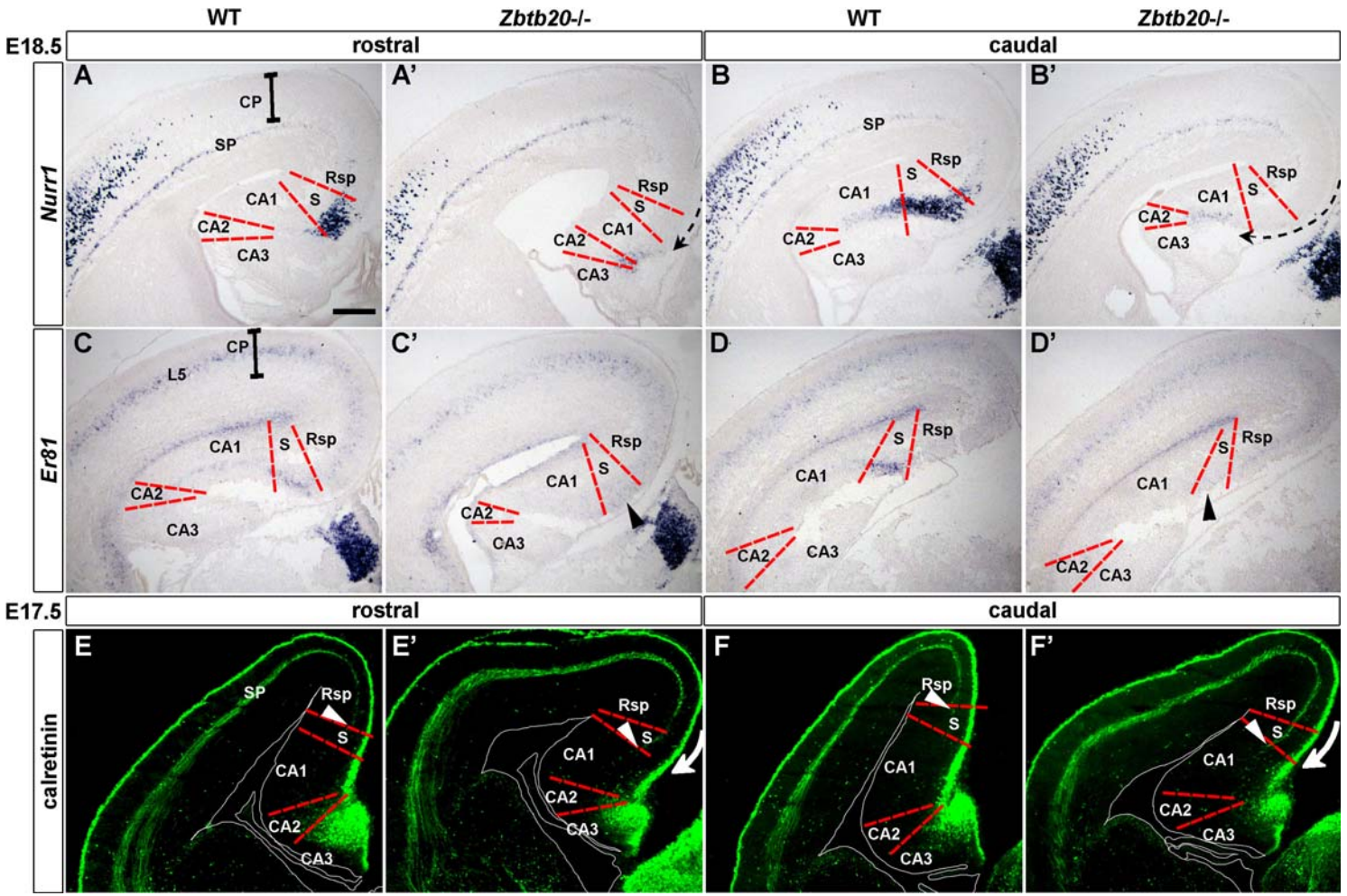

Fig. 30. Mispatterning of subiculum in *Zbtb20*-/- cortex. ISH (**A-D'**) and IHC (**E-F'**) on rostral and caudal coronal sections of wild type and *Zbtb20* -/- mutant brain at E18.5 (**A-D'**) and E17.5 (**E-F'**) with markers as indicated. Note the highly restricted expression of *Nurr1* (**A, B**) and *ER81* (**C, D**) in the subiculum (S). In *Zbtb20*-/- mutant, the expression of both *Nurr1* (**A'**, **B'**) and *Er81* (**C'**, **D'**) was abolished in the normal location of S, which acquired expression characteristic of the adjacent retrosplenial cortex (Rsp) (compare **A/A'**, **B/B'**, **C/C'**, **D/D'**). Red dashed lines indicate approx. boundaries between subregions of Hi. Dashed arrows in **A'** and **B'** indicate the medial expansion of the *Nurr1* negative domain, characteristic for the Rsp area, into S of the mutant brain. Arrowheads in **C'**, **D'** point to the S of *Zbtb20*-/- brain, in which the expression of *Er81* was lost, thus resembling the expression characteristic of the adjacent Rsp cortex. The pictures in (**E-F'**) illustrate the immunohistochemical signals detected with calretinin antibody on sections from control and *Zbtb20*-/- mutant, as indicated. Arrowheads in **E-F'** point to the dorsomedial border of calretinin-positive axons that have reached the subplate (SP) in the region of Ncx and Rsp. In **E'** and **F'** arrows indicate the far more medial extension of anti-calretinin positive zone beyond the S domain in the *Zbtb20*-/- mutants. White lines in **E-F'** outline the lumen of lateral ventricle. CA, region; CP, cortical plate; L5, layer 5.

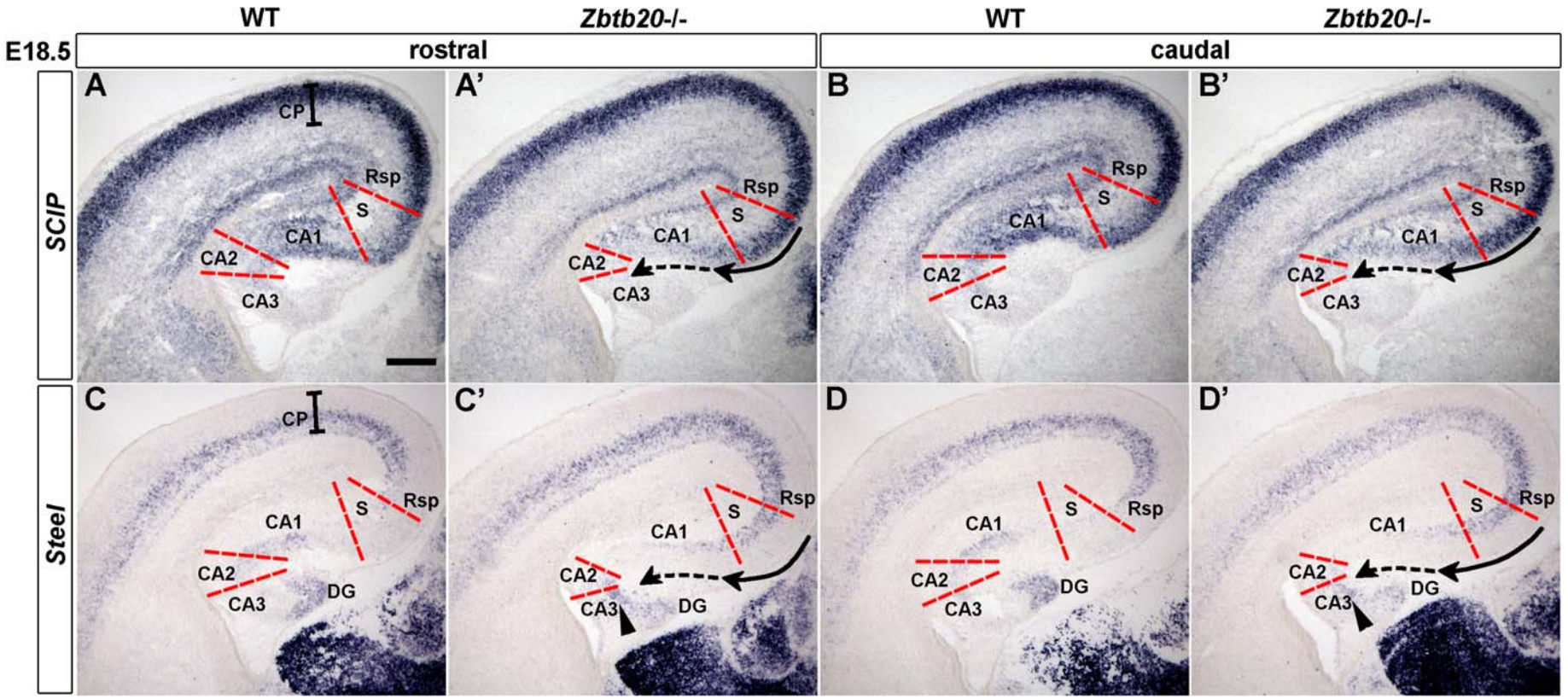

Fig. 31. Medial expansion of the CA1 region into CA2/CA3 of Hi in the *Zbtb20*-/- cortex. ISH on rostral and caudal coronal sections of wild type and *Zbtb20*-/- mutant brain at E18.5 with region-specific markers as indicated. In the control, *SCIP* (**C**, **D**) marked the upper cortical layers of Ncx, retrosplenial cortex (Rsp) and CA1 region of Hi proper; *Steel* (**E**, **F**) labeled lower cortical plate (CP) of dorsal pallium (DP) and CA1, but not the subiculum (S). In the *Zbtb20*-/-mutant, the S seemed to expand into the domain of CA1, while the CA1 area appeared to be displaced into the normal domain of CA2 and CA3, as demonstrated by the abnormal expression characteristics of the used markers, indicated in 2nd and 4th column of the panel (see also the text in results). Red dashed lines indicate approx. boundaries between Rsp/S, S/CA1, CA1/CA2 and CA2/CA3. Arrowheads in **C'/D'** point to ectopic *Steel* expression in CA3 in the mutant. Dashed arrows in 2nd and 4th column indicate the medial expansion of the normally moderately *SCIP* positive or *Steel* negative subiculum (see the text) over the CA1 in the *Zbtb20*-/- mutant. The filled arrows indicate the medial expansion of Rsp expression traits into S, detected with the applied markers. Abbreviations: CA1, CA2, CA3 region; DG, dentate gyrus.

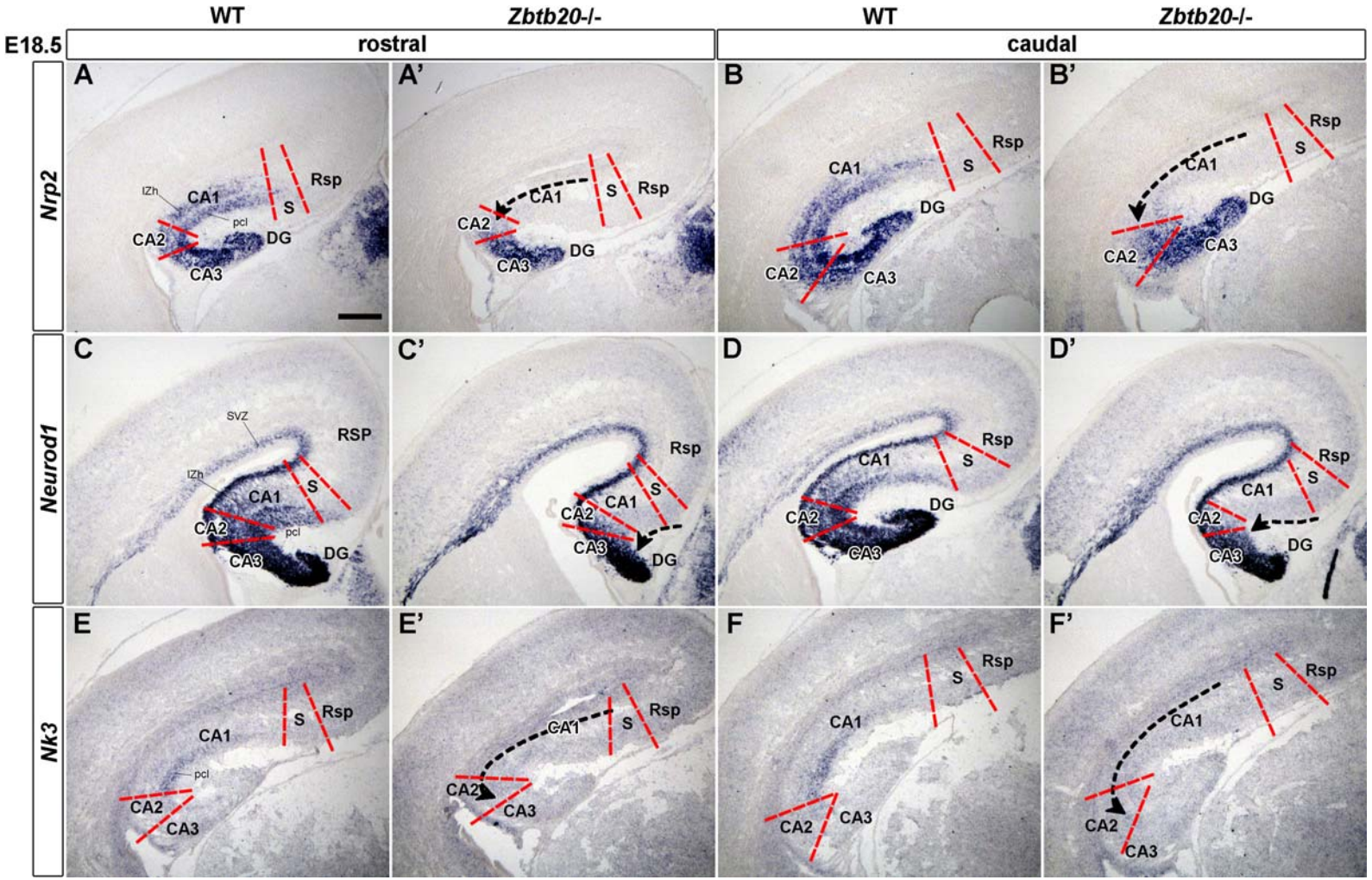

Fig. 32. Medial expansion of the CA1 region into CA2/CA3 of Hi in the *Zbtb20*-/- cortex. ISH on rostral and caudal coronal sections of wild type and *Zbtb20*-/- mutant brain at E18.5 with region-specific markers as indicated. In the control, *Nrp2* (**A**, **B**) and *Neurod1* (**C**, **D**) outlined the Hi proper and dentate gyrus (DG). Both (**A, B, C, D**) were expressed in pyramidal cell layer (pcl) and hippocampal intermediate zone (IZh) of CA1-3, while *Neurod1* (**C, D**) showed additional signal in subventricular zone (SVZ) of dorsal pallium. *Nk3* (**E, F**) signal was confined to CA1-2 pcl. In the *Zbtb20*-/- mutant, the subiculum (S) seemed to expand into the domain of CA1, while the CA1 area appeared to be displaced into the normal domain of CA2 and CA3, as demonstrated by the abnormal expression characteristics of all used markers, indicated in 2nd and 4th column of the panel (see also the text in results). Red dashed lines indicate approx. boundaries between Rsp/S, S/CA1, CA1/CA2 and CA2/CA3. Dashed arrows indicate the medial expansion of the normally negative S for all used markers over the CA1 in the *Zbtb20*-/- mutant. CA1, CA2, CA3 region; Rsp, retrosplenial cortex.

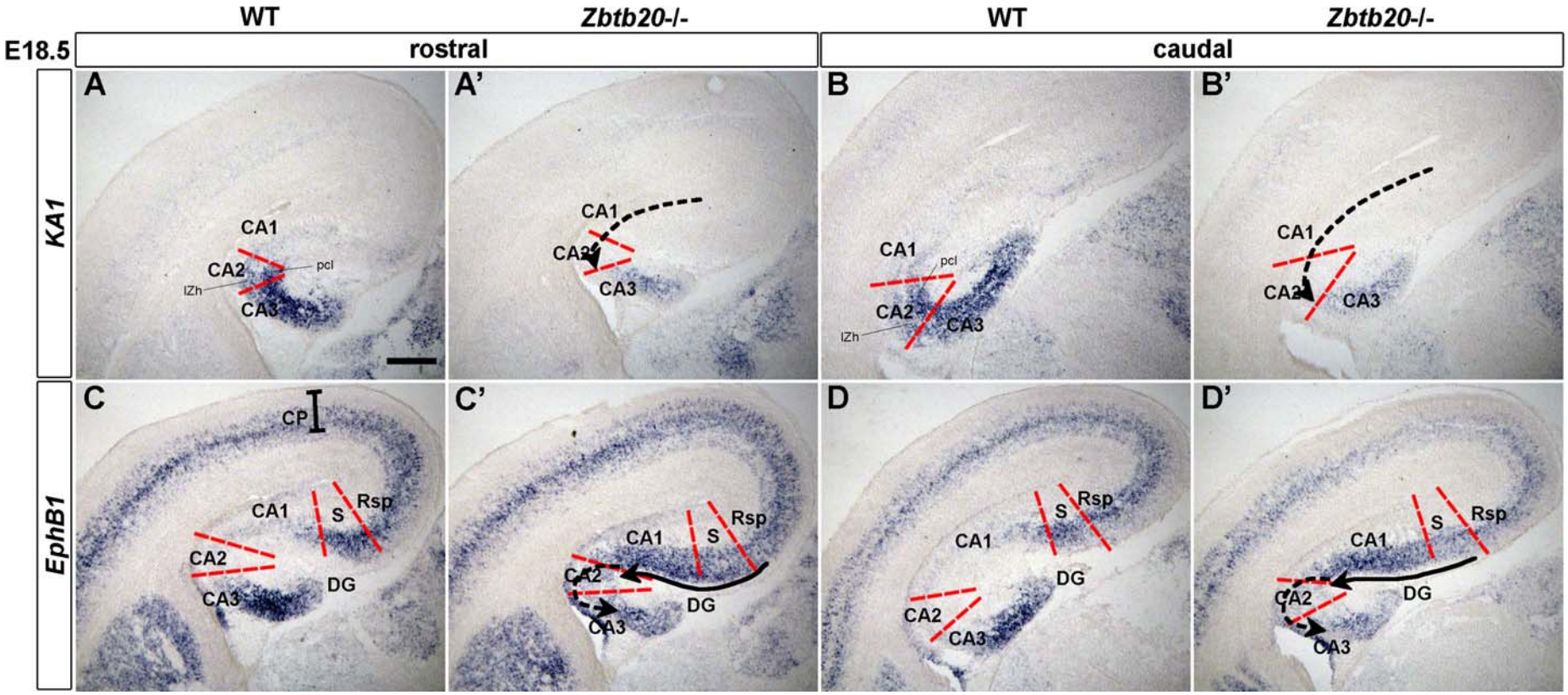

Fig. 33. Medial displacement of the CA1/CA2 border in Hi in the *Zbtb20*-/- cortex.

ISH on rostral (left panel) and caudal (right panel) coronal sections of *Zbtb20* wild type and mutant brain at E18.5 with region-specific markers as indicated. In the control, the expression of *KA1* (**A, B**) outlined a contiguous domain containing CA2 and CA3. *EphB1* expression (**C, D**) was confined to the CA3 of Hi and dentate gyrus (DG) as well as to subiculum (S). In the mutant, expression domains of these markers in CA regions appeared smaller due to lateral shrinkage (**A', B', C', D'**), whereas the highly *EphB1* positive S domain was expanded far into the normal CA1 region of Hi, indicated by filled arrows in (**C', D'**). Red dashed lines indicate approx. boundaries between labeled brain regions. Dashed arrows in 2nd and 4th column indicate the medial expansion of negative domains of these markers in the mutant brain. CA1, CA2, CA3 region; CP, cortical plate; DG, dentate gyrus; IZh, hippocampal intermediate zone; pcl, pyramidal cell layer; Rsp, retrosplenial cortex.

2.2.5.3.5. Patterning defects in the *Zbtb20*-/- medial pallium – a summary

The performed detailed ISH analysis demonstrated that a range of molecular markers was misexpressed in the MP and hippocampus of the *Zbtb20*-/- mutant. Generally, dorsolateral pallial domains expanded ectopically into more ventromedial regions of the mutant cortex.

Firstly, these results indicate that in the *Zbtb20* mutant, the transitory neocortical Rsp area expands into the adjacent area of subpallium (archicortex). The shift of the patterning with characteristic for the Rsp into S domain in *Zbtb20-/-* animals was reflected by the ectopic expression into S of regional markers, that normally label either more strongly the Rsp as compared to S (e.g. *Id2, Math2, Foxg1*), or such that label specifically the Rsp, but not S (e.g. *Nef3*, *Odz3*, *SCIP*, *Steel* and *EphB1*). In opposite, when the used markers showed restricted (or much stronger) expression in the S domain (e.g. *Nurr1*, *Er81*), in the *Zbtb20*-/- mutant the expression characteristics of the S area were replaced by patterns, normally observed in the adjacent Rsp domain.

Secondly, the border between the S and CA1 region of hippocampus was also displaced ventrally in the *Zbtb20-/-* mutant. This abnormality was evident by the medial ectopic expansion of the strong *Nurr1* and *SCIP* signal (characteristic only for S) into the CA1 of hippocampus proper, which is normally negative for these two markers. In contrast, in the *Zbtb20* mutant, the expression of markers, which normally delineate the CA1 but are not labeling the S domain (e.g. *Nrp2, Steel, Neurod1, Nk3*) was abolished in the CA1 area, thus acquiring a pattern, characteristic for the adjacent S.

Finally, in addition to mispatterning at the border subiculum/hippocampus proper (S/CA1), pattern defects were also registered within the hippocampus proper itself, affecting establishment of the borders between the three subdomains CA1, CA2, CA3. In the *Zbtb20-/-* mutant, the CA1 region negative for *KA1* expression was medially displaced into the CA2 domain, and the expression of *Nk3* confined to CA1 was fully abolished. In this line of evidence, the specific expression of *Steel* in CA1 exhibited clearly ectopic expression into CA2/CA3 in the *Zbtb20-/-* mice, while the CA2 that normally lacks any *EphB1* transcripts appeared displaced into CA3, contributing to substantial diminishing of the normal expression of *EphB1* in this area.

Thus, similarly to TF *Emx2* and *Pax6*, involved in distribution of distinct functional areas (M, SS, V) across A-P axis of the neocortex, the TF Zbtb20 exerts an essential function in regionalization of functional subdomains across the D-V axis of the medial pallium, including S and CA1-CA3 areas.

In fact, these results show for the first time that a differential expression of TF (predominantly in postmitotic cells) plays an essential role in mediating regional specification of medial pallium.

2.2.5.3.6. Abnormality of dentate gyrus in the *Zbtb20*-/- mutant brain

The granule cell layer (gcl) of DG is specifically marked by the *Steel* in situ probe. (Fig. 31C, D; Tole et al., 2000). Based on the detected expression of *Steel*, the V-shaped DG was generated in the *Zbtb20* mutant, although being considerably underdeveloped (Fig. 31C', D'). In order to study the patterning and differentiation of the granule cells (gc) of DG, the expression of the homeobox TF **Prox1** (Oliver et al., 1993) was examined. *Prox1* is an early marker of the DG, expressed in gcl (Oliver et al., 1993; Pleasure et al., 2000; Fig. 34A). At E18.5, *Prox1* was expressed in DG of *Zbtb20*-/- brain but, however, revealed a much shorter gcl in the mutant as compared to the controls (Fig. 34A/A'). The reduction of the size of the DG was also evident by the expression of the anti-neurogenic bHLH TF gene *Id3* (Fig. 34B/B'; Pleasure et al., 2000).

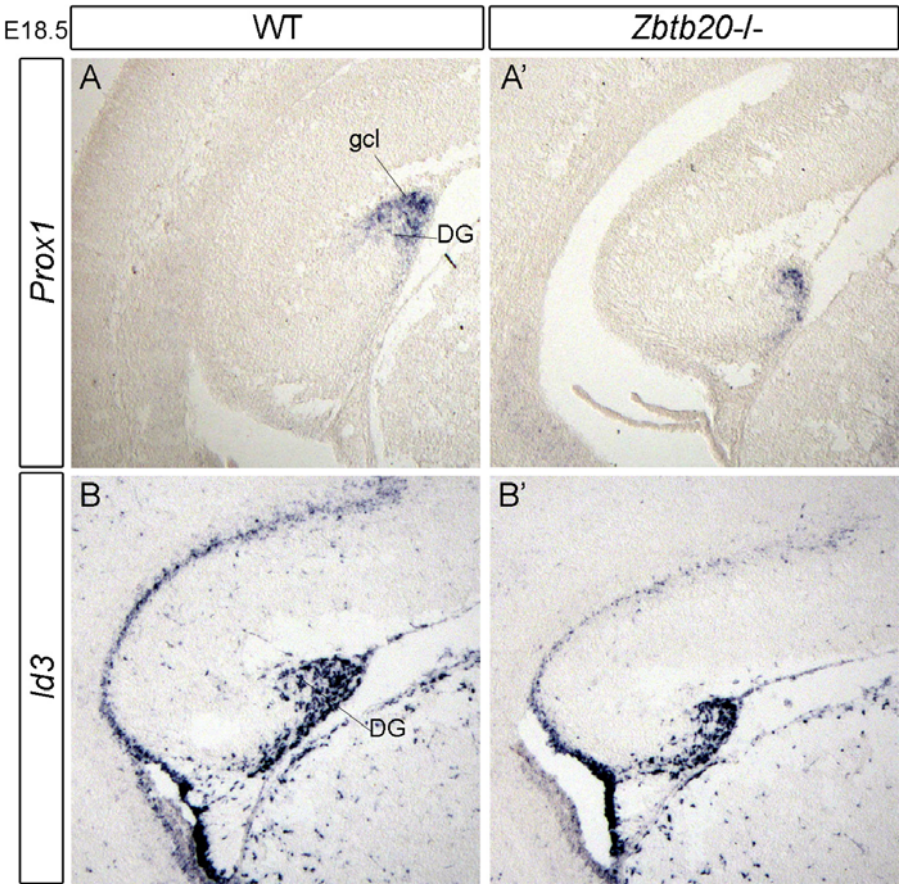

Fig. 34. Malformations of the dentate gyrus in *Zbtb20*-/-.
ISH on coronal sections of *Zbtb20*-/- wild type (A, B) and mutant (A', B') brain at E18.5 with DG-specific markers as indicated. All shown markers revealed a smaller dentate gyrus (DG) compared to the control. gcl, granule cell layer.

2.2.5.3.7. Failure of neuronal differentiation in *Zbtb20*-/-

The present study revealed that *Zbtb20* is strongly expressed in progenitors in VZ/SVZ of the developing telencephalon. Neural stem cells initially proliferate, while later on they divide asymmetrically to produce first neurons, followed by glial cells.

In order to study aspects of differentiation of cortical progenitors in the absence of *Zbtb20*, the pattern of expression of several differentiation markers on sections from E18.5 mutant and control brains was examined. The expression of TF ***Sox2*** is restricted to the proliferating cells, including neural stem and progenitor cells, glial precursors and proliferating astrocytes (Bani-Yaghoub et al., 2006). By inhibiting the progenitor differentiation, *Sox2* plays a crucial role in maintaining neural progenitor identity in developing CNS (Graham et al., 2003). Intriguingly, in the *Zbtb20* mutant, the expression of *Sox2* was clearly upregulated in VZ/SVZ of the entire dorsal and ventral telencephalon (Fig. 35A/A').

The homeobox TF gene ***Emx2*** exerts a strongly regionalized expression in the cortical progenitors, confined mostly to the mediocaudal cortex, the anlage of the hippocampus proper (Fig. 35B; Simeone et al., 1992). Noteworthy, the expression of *Emx2 in* the MP progenitors and especially in those of the hippocampus proper was clearly enhanced in the *Zbtb20* mutant (arrow in Fig. 35B'), suggesting that in absence of *Zbtb20* cell differentiation is delayed.

The bHLH TF gene ***Mash1*** (*Ascl1*) is expressed in a limited number of telencephalic cells (Britz et al., 2006), representing a population of committed neural precursors before their differentiation (Torii et al., 1999). In the dorsal telencephalon, *Mash1* is required to promote neuronal versus astrocytic differentiation of these multipotent progenitors (Nieto et al., 2001). Surprisingly, in the entire dorsal pallium of the *Zbtb20*-/- mutant, the number of *Mash1* positive cells was clearly reduced (Fig. 35C') compared to the control (Fig. 35C). The ventral telencephalon in the mutant, however, showed no obvious changes in *Mash1* positive cell numbers (not shown).

In the wild type, bHLH TF gene ***Id3*** showed highest expression within the population of migrating precursors of the DG (Fig. 35D), as reported earlier (Pleasure et al. 2000). Moreover, *Id3* was moderately expressed in the proliferating zones (VZ/SVZ) of dorsal pallium, while other layers contained few *Id3*+ cells (Fig. 35D). *Id3* is reported to be confined to the less differentiated neuroblasts throughout the mouse nervous system (Jen et al., 1997). Notably, in the dorsal pallium of *Zbtb20*-/- mice, *Id3* expression was clearly reduced (Fig. 35C'), implicating a defect in neuronal differentiation in absence of *Zbtb20*.

Taken together, these findings indicate that in absence of *Zbtb20* not only the regionalization of the pallium, but also the differentiation of progenitors of Ncx and archicortex appears to be compromised.

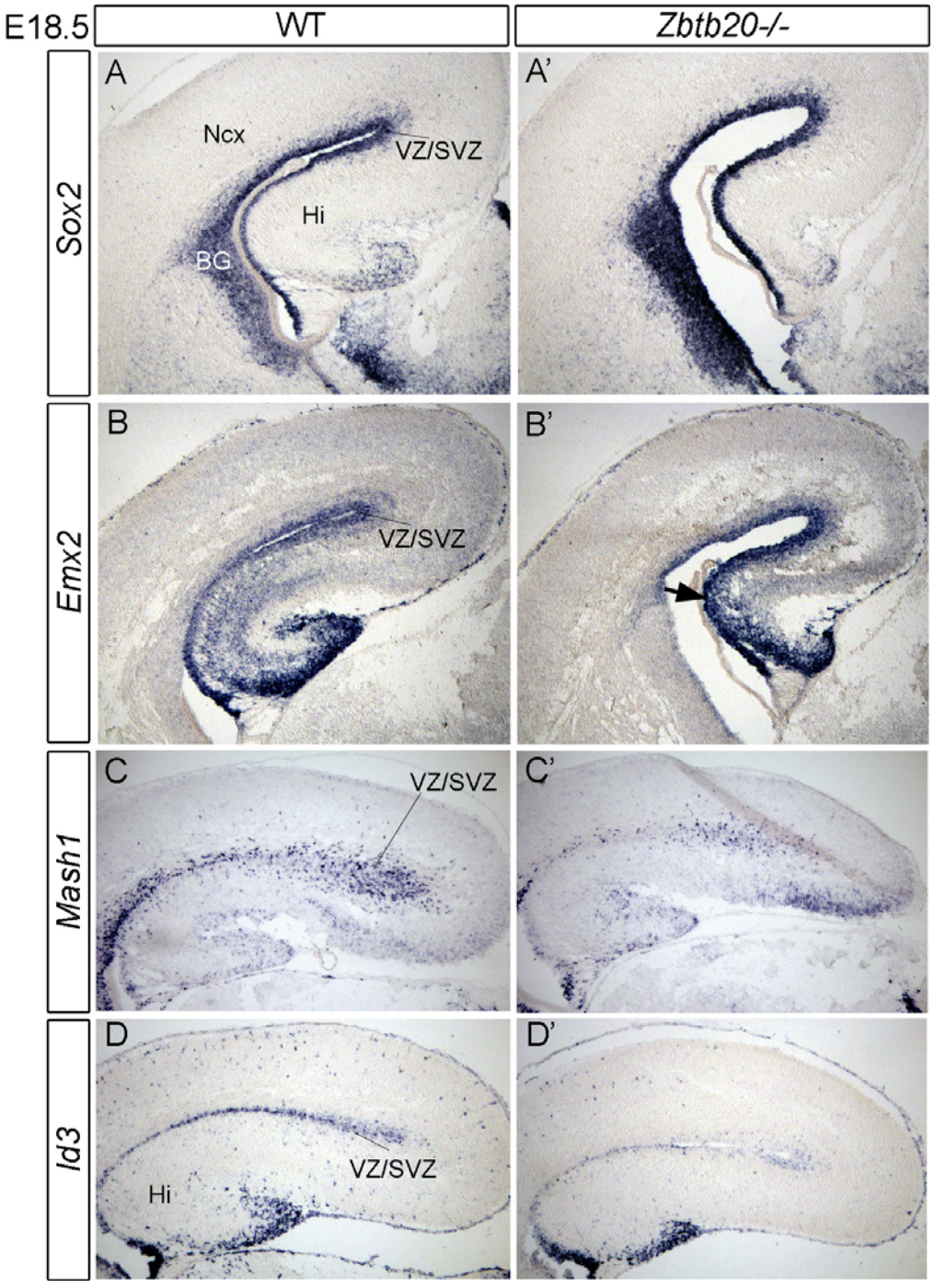

Fig. 35. Altered neuronal differentiation in *Zbtb20*-/- brains. ISH on coronal sections of wild type (**A, B, C, D**) and *Zbtb20*-/- mutant (**A', B', C', D'**) brain at E18.5 with markers as indicated. Altered *Sox2* (**A'**), *Emx2* (**B'**), *Mash1* (**C'**) or *Id3* (**D'**) signal in the mutant may indicate altered differentiation. See also text. BG, basal ganglia; Hi, hippocampus; Ncx, neocortex; SVZ, subventricular zone; VZ, ventricular zone.

2.2.6. Defects of skeleton of *Zbtb20* KO mice

The results from the analysis of the expression of the *LacZ* reporter indicated that *Zbtb20* exerts a restricted expression in a number of skeletal elements (see Fig. 20, Fig. 21). Although not directly related to the main research focus, namely the control of cortical neurogenesis, it was decided to characterize also the skeleton phenotype of the *Zbtb20* KO mice. Skeletons from wild type and homozygous mutant animals at different embryonic and postnatal stages (E18.5-P24) were prepared, and cartilage and bone were visualized by alcian blue and alizarin red staining, respectively.

2.2.6.1. Defect in the composition of vertebral elements in absence of *Zbtb20*

The vertebral column of the mouse is organized into seven cervical vertebrae (C1-C7), 13 rib-carrying thoracic vertebrae (T1-T13), of which the first seven ribs are fused to the sternum ventrally, six lumbar vertebrae (L1-L6), four sacral (S1-S4), of which the first three are fused, and a variable number of caudal vertebrae. Precise definition of the vertebrae is facilitated by small morphological differences. Cases of vertebrae displaying adjacent element identity are referred to as homeotic transformation, which is defined as transformation of one body part into the likeness of something else (Bateson, 1894).

Skeletons isolated from mice of a mixed (129SV/CDI) background were analyzed. Vertebral transformations were identified by morphologic characteristics described formerly (Kessel and Gruss, 1991; Li et al., 1997). A certain proportion of the control mice showed deviations from the axial formula, as a naturally occurring variation (Kessel and Gruss, 1991). Notably, skeletons of *Zbtb20*-/- mutants showed much more frequently alterations of the axial formula as compared to the controls (Table 6). Characteristic traits of the sacral vertebrae are the enlarged transverse processes, which are directed toward the ileum, forming the sacral articular surface with the pelvis (Menegola et al., 2001). The lumbar vertebrae are missing direct connections with the pelvis. Interestingly, in the *Zbtb20*-/- mutants, the lumbar vertebra six (L6) often appeared with transverse processes, resembling sacral vertebra one (S1) (Fig. 36B, D), which suggests a “transformation”-like change. Thus, the *Zbtb20* mutants carried only five “true” lumbar vertebrae instead of six. The rate of observed transformations in the mutant animals was more than twofold higher than in wild type (Fig. 36A, C)**.** The L6 fully or partially transformed into S1, showing the new identity bi- (Fig. 36B) or unilaterally (Fig. 36D), respectively.

It should be noticed, however, that despite the fact that the vertebrae in *Zbtb20*-/- animals showed twice more often alteration of the identity of lumbar vertebrae than the controls, these differences did not reach formal levels of statistical significance (Fisher's exact test p=0.34). Examination of a higher number of animals will be required to verify this conclusion.

Table 6. Transformation-like changes in axial skeleton in *Zbtb20*-/- mutants

Transformation	+/+ (n=13)	-/- (n=18)
C7→T1	1 (7.6%)	1 (5.6%)
T11→T10	0 (0%)	1 (5.6%)
L6→S1	1 (7.6%)	3 (16.7%)

Definitions:

C7→T1: vertebra carrying a minute rib of one or both sides;

T11→T10: with a rib as long as seen normally on T10;

L6→S1: The 6th lumbar vertebra is fused by transverse processes to the pelvis form the first sacral bone.

2.2.6.2. Malformations of elements in the axial skeleton

Examination of skeletal preparation of P7-P24 animals, when bone formation is more advanced, revealed a range of malformations in the skeleton of the *Zbtb20* mutant, predominantly restricted to the vertebral arches. In the normal mouse, the arch of thoracic vertebra two (T2) is characterized by a prominent processus spinosus (ps). In the majority of *Zbtb20*-/- animals, the ps of T2 was clearly reduced or absent (Fig. 36H), which is statistically significant difference (Fisher's exact test p=0.0105). Frequently, the xiphoid process (xp, Fig. 36F) harbored a hole (not shown), or one or more vertebra were asymmetric (Fig. 36L, J).

At later postnatal stages (P13-24, n=5), tooth defects were detectable in the *Zbtb20* KO mice. In four out of five *Zbtb20*-/- inspected animals, lower incisors were positioned more anteriorly than seen in the control situation (Fig. 36N). In the most extreme cases, the lower incisors protruded the upper incisors, which was not seen in the control (n=4). As nine out of ten analyzed *Zbtb20*-/- mice displayed at least one of the described defects in tooth or skeletal elements (Table 7). These results suggest that *Zbtb20* is required for the normal morphology of the skeleton.

Table 7. Abnormalities of axial skeleton in *Zbtb20*-/- mutants.

	+/+ (n=6)	-/- (n=10)
C2 vertebral arch malformed	0 (0%)	1 (10%)
T2 processus spinosus strongly reduced or absent	0 (0%)	7 (70%)
T11, T12, T13 vertebra arch malformed	0 (0%)	1 (10%)
Intersternebrae connecting sternebrae 4 and 5 fully ossified	0 (0%)	1 (10%)
Hole in xiphoid process	0 (0%)	2 (20%)

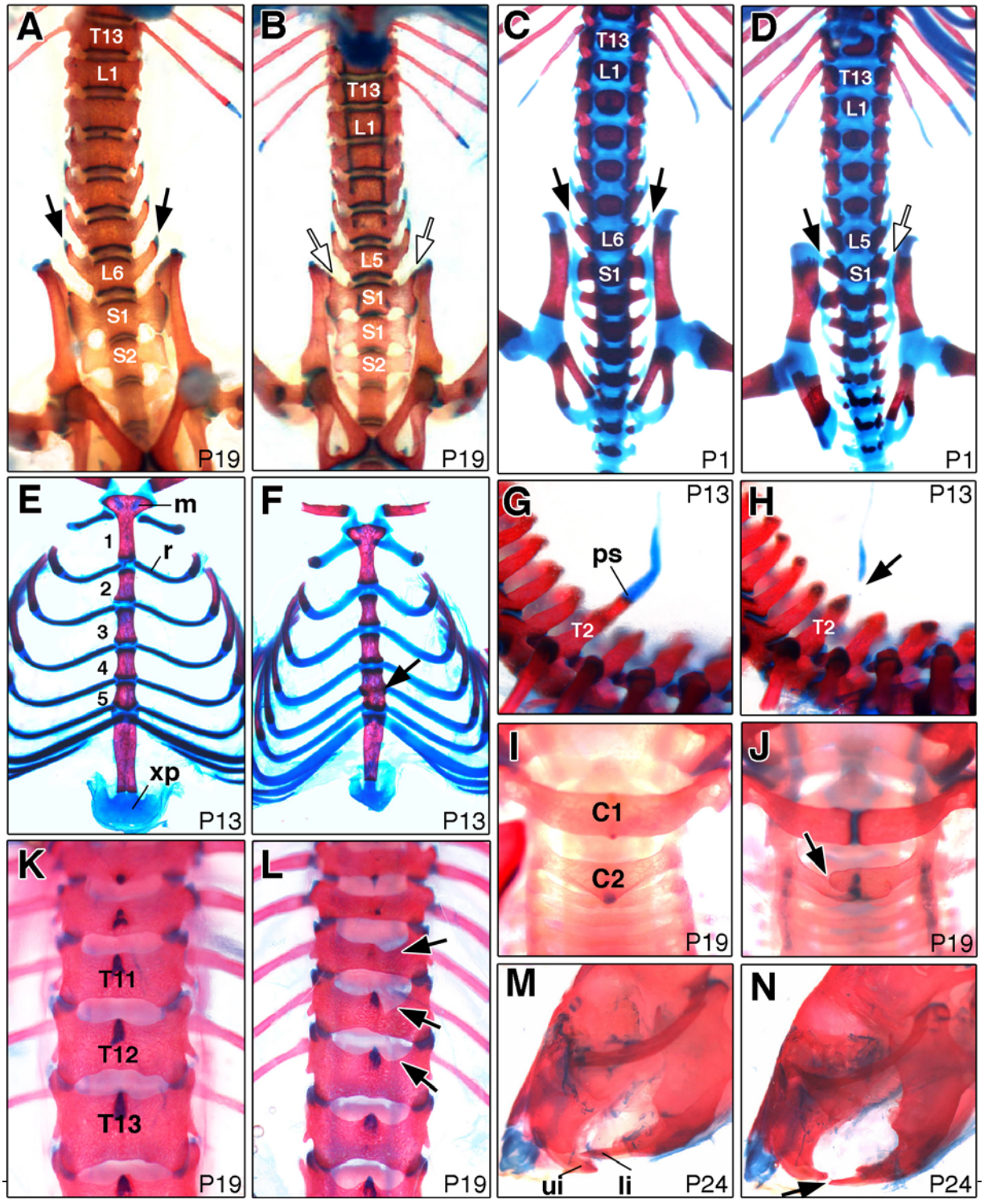

Fig. 36. Transformation-like changes and malformations in skeletons of *Zbtb20*-/- mice. Skeletons from wild type (**A, C, E, G, I, K, and M**) and mutant mice (**B, D, F, H, J, L, and N**) were stained with alizarin red and alcian blue. Ventral views of vertebral column from the posterior thoracic to the anterior caudal region at P19 (**A, B**) or at P1 (**C, D**). In (**A-D**) note that in the *Zbtb20*-/- specimen the sixth lumbar vertebra (L6) has been transformed into the first sacral vertebra (S1) on both sides (**B**) or alternatively, at one side only (**D**), evident by the sacro-iliac joints (white arrows in **B, D**). Black arrows point to normal L6 vertebral elements. (**E, F**) Ventral view of the sternum at P13. (**E**) In the controls, the ossified sternebrae 1-5 were clearly separated by cartilaginous intersternebrae, to which the ribs (r) attach. (**F**) The *Zbtb20*-/- sternum showed a complete ossification of the intersternebrae connecting sternebrae 4 and 5 (black arrow). (**G, H**) Lateral views of lower cervical to upper thoracic vertebrae at P13. (**G**) In the controls, a prominent processus spinosus (ps) was seen on thoracic vertebra two (T2). (**H**) In the mutant, ps is reduced, due to underdevelopment of both, the bone (red) and cartilage (blue) component. (**I, J**) Dorsal view of the upper cervical vertebrae (C1 and C2) at P19. (**J**) In the mutant, C2 harbors an abnormal incision (arrow in **J**). (**K, L**) Dorsal view of the lower thoracic vertebrae at P19. In contrast to their normal counterparts (**K**), the arches of thoracic vertebrae 11-13 (T11-13) in the mutant (**L**) contains abnormal incisions (arrows in **L**). (**M, N**) Lateral view of skulls at P24. (**M**) In wild type, the tips of lower incisors (li) were positioned posterior to upper incisors (ui), whereas in the *Zbtb20*-/- mouse (**N**), the tips of lower incisors protruded upper incisors (arrow in **N**). M, manubrium; xp, xiphoid process.

2.2.6.3. Delayed ossification of the skeleton

To get a better insight into the role of *Zbtb20* in skeleton ossification, the bone development of the *Zbtb20* KO and control animals was analyzed at stages E18.5, P0, 1, 7, 13, 15, 19 and 24. According to several studies (Patton and Kaufman, 1995; Wirtschafter, 1960), primary and secondary ossification centers (OC) in the mouse skeleton have a normal sequential timing when they first appear. Surprisingly, during all stages analyzed, the status of bone formation was more advanced in wild type animals compared to the *Zbtb20*-/- mice. For simplified analysis it was estimated to which extent the bone formation was delayed in the mutant by focusing on OC absent in the *Zbtb20*-/- animals that were present in the control.

At stage E18.5, the ossification of maxilla and mandible in the mutant (Fig. 37A') was less advanced compared to the controls (Fig. 37A), as seen by smaller calcified portions in the mutant. Furthermore, the mutant (Fig. 37B') was lacking the vertebral bodies of cervical vertebra 2-7, which were present in the control (Fig. 37B). At P0, the OC of sternebra 5 and xiphoid process (xp) in the mutant sternum (Fig. 37C') were smaller than in the wild type (Fig. 37C). Furthermore, inspection of the hind paws revealed presence of OC in the medial phalanges (mp) 2-4 in the controls (Fig. 37D), which were missing in the *Zbtb20*-/- mutants (Fig. 37D').

One week after birth (P7), the periotic capsule (pc), the structure surrounding the internal ear, was largely ossified in the controls (Fig. 37E), while the mutant displayed a much lower level of ossification (Fig. 37E'). Similarly, the forelimb of the control animal contained numerous OC (Fig. 37F), which were missing in the mutant (Fig. 37F'), that is the greater tubercle (gt), head of humerus (hh), epiphyses of metacarpals (mce), proximal phalanges (ppe), distal epiphyses of radius (rde) and ulna (ude). The absence of mce and ppe in the *Zbtb20-/-* mice suggests an approximate ossification delay of 2-4 d for these structures (Table 8). While in the P13 controls, the knee showed well developed OC of the proximal epiphyses of tibia and fibula (Fig. 37G) in the mutant these elements were undetectable (Fig. 37G'). At P15, secondary OC in epiphyses of metatarsals (mte) and proximal phalanges (ppe) were present in the hind paw of the controls (Fig. 37H), whereas in the mutants both structures were missing (Fig. 37H'). As OC of mte and ppe in digits II, III, IV normally appear at P7 (Wirtschafter, 1960), this suggested a delay of at least 9 days in the *Zbtb20* KO mice.

One week after birth, the ventral (costal) ribs and the cartilages of the larynx become calcified and stain well with alizarin red (Barnicot, 1941; Sweet and Green, 1981). In these hyaline cartilageous tissues, calcium carbonate deposits are found early, but only as a result of degenerative process, not as a consequence of chondrocyte maturation or perichondral bone formation (Karaplis et al., 1994). While in normal animals, an axial zone of calcified costal cartilage was present at P7 (not shown), it was missing in *Zbtb20*-/- mutants even at P24 (Fig. 37I'). This suggests a delay by at least 18 days for this structure in the *Zbtb20* mutants. Moreover, alizarin red staining of the thyroid and cricoid cartilages of the larynx was only present in the control (Fig. 37J), not in the mutant (Fig. 37J'). Notably, in the P24 mutant none of the caudal vertebrae (Cd) showed secondary OC at the epiphyses (Fig. 37K). In Cd1, the most rostral caudal vertebra, secondary OC in epiphyses are reported to appear normally at P6 (Wirtschafter, 1960), which suggests an ossification delay in *Zbtb20* KO mice by at least 19 days. Taken together, these findings indicate that in *Zbtb20*-/- mice, ossification is delayed during bone development, a defect that becomes stronger with the time.

Table 8. Summary of absent alizarin red stained (calcified) structures in *Zbtb20*-/- skeletons and hereupon deduced delay of ossification for the corresponding skeletal part.

Stage	Missing calcified structure in Homo	Normal appearance *	Min. delay (d)	Specimen (n)
E18.5	C2 (OC vertebral body)	E18.5	1	2
P0	C7 (OC vertebral body)	E18.5	2	2
	Diaphyses of middle phalanges (digits II-V), forepaw	E18.5	2	2
P1	C3 (OC vertebral body)	E18.5	3	3
	Diaphyses of middle phalanges (digits II-V), hindpaw	E18.5	3	3
P7	Greater Tubercle (humerus)	P4-5	3-4	5
	Epiphyses of metacarpals (digits II-V)	P4-5	3-4	5
	Epiphyses of proximal phalanges (digits II-V), forepaw	P4-6	2-4	5
P13	Proximal epiphyses of tibia	P7	7	2
	Epiphyses of middle phalanges (digits II-V), forepaw	P6	8	2
	Distal epiphyses of femur	P5	9	2
P15	Epiphyses of metatarsals (digits II-V)	P7	9	1
P19	Between vertebral body OC and pedicle OC in L2	P15	5	1
P24	Axial zone in ventral ribs	P7	18	1
	Epiphyses of Cd1	P6	19	1

*reported by Wirtschafter, 1960. C, cervical vertebra; Cd, caudal vertebra; OC, ossification center.

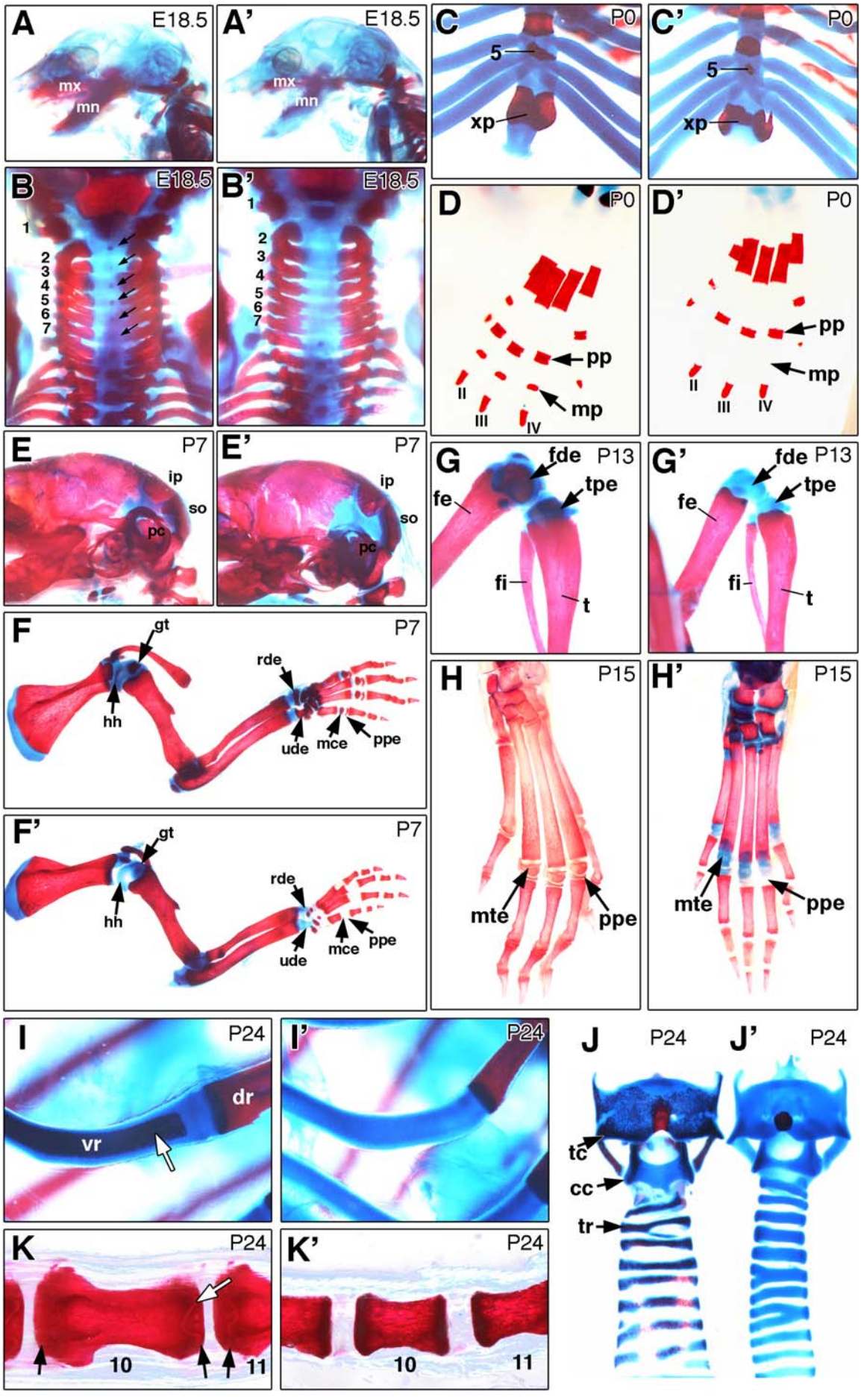
A
E18.5
mx
mn
A'
E18.5
mx
mn
C
P0
5
xp
C'
P0
5
xp
B
E18.5
1
2
3
4
5
6
7
B'
E18.5
1
2
3
4
5
6
7
D
P0
pp
mp
II
III
IV
D'
P0
pp
mp
II
III
IV
E
P7
ip
so
pc
E'
P7
ip
so
pc
G
fde
P13
tpe
fe
fi
t
G'
fde
P13
tpe
fe
fi
t
F
P7
gt
rde
hh
ude
mce
ppe
F'
P7
gt
rde
hh
ude
mce
ppe
H
P15
mte
ppe
H'
P15
mte
ppe
I
P24
dr
vr
I'
P24
J
P24
J'
P24
tc
cc
tr
K
P24
10
11
K'
P24
10
11

Fig. 37. Defects in ossification of skeleton of *Zbtb20*-/- mice, visualized by alcian blue (cartilage) and alizarin red (bone) staining. Stages E18.5 (**A, A', B, B'**), P0 (**C, C', D, D'**), P7 (**E. E', F, F'**), P13 (**G, G'**), P15 (**H, H'**) and P24 (**I, I', J, J', K, K'**) are shown. (**A, A'**) Staining of skulls from control (**A**) and *Zbtb20 KO* animals (**A'**) at E18.5 revealed a lower degree of ossification of maxilla (mx) and mandibula (mn) in the mutant. (**B, B'**) Dorsal view of neck region at E18.5 showing absence of OC in cervical vertebrae 2-7 in the *Zbtb20*-/- animal (**B'**), which were present in the control (**B**, arrows). (**C, C'**) Ventral view of the rib-cage at P0. OC of sternebra 5 and xiphoid process (xp) were much smaller in *Zbtb20*-/ -mice (**C'**) compared to wild type (**C**). (**D, D'**) Hindpaw of wild type (**D**) and mutant (**D'**) at P0. Medial phalanges (mp) of the hind paw in control (**D**) contained primary OC, which were completely lacking in their *Zbtb20*-/- counterparts, while the proximal phalanges (pp) showed also reduced ossification in the mutant (**D'**). (**E, E'**) Staining of skulls of P7 control (**E**) and *Zbtb20*-/- (**E'**) mice revealed a lower degree of ossification of periotic capsule (pc) in the mutant. (**F, F'**) P7, forelimbs. Control forelimb (**F**) exhibited ossification centers of greater tubercle (gt), head of humerus (hh), epiphyses of metacarpals (mce), epiphyses proximal phalanges (ppe), the distal epiphyses of radius (rde) and ulna (ude), and in epiphyses of metacarpals (mce) and proximal phalanges (ppe). In the *Zbtb20*-/- mice (**F'**), ossification in all these structures were undetectable. (**G, G'**) P13, Knee. While the control (**G**) revealed profound OC in proximal epiphysis of tibia (tpe) as well as distal epiphysis of the femur (fde), these structures were absent in the *Zbtb20* KO specimen (**G'**). (**H, H'**) P15, hindlimbs. In the wild type (**H**), clear OC in epiphyses of metatarsals (mte) and proximal phalanges (ppe) were visible, which were absent in the mutant (**H'**). (**I, I'**) P24 ribs. Ventral segments of rib (vr) in controls (**I**) revealed a calcified axial zone in their costal cartilage (arrow in **I**) while this was absent in *Zbtb20*-/- (**I'**). (**J, J'**) Larynx and trachea. Calcified thyroid (tc), cricoid (cc) cartilages of the larynx as well as calcified cartilages of the trachea (tr) were present in the controls (**J**), not in the mutant animals (**J'**). (**K, K'**) Caudal vertebrae. Epiphyseal ossification centers (indicated by black arrows in **K**) were seen in caudal vertebrae (cd No 10 and 11 are shown) in the controls (**K**), while in the mutants (**K'**) this was undetectable. White arrow in (**K**) points at the border between epiphysis and diaphysis. Dr, dorsal segment of the rib; fe, femur; fi, fibula; ip, interparietal bone; so, supraoccipital bone; ti, tibia.

III. Discussion

3.1. Candidate genes acting in Emx2-dependent manner during corticogenesis

The neurons in mammalian cortex are distributed radially in six layers and tangentially in numerous functional domains that integrate and process motor, sensory and cognitive information. The molecular basis of development in general and corticogenesis in particular, is far from being completely understood. It is generally assumed that complex interactions between signaling molecules and transcription factors (TFs) expressed in cortical progenitors in gradients specify the area identities. However, the molecular pathway that leads to this phenotype is unknown. Recent evidence suggests that while such graded expression of molecular determinants in cortical progenitors broadly specifies area identities, regional expression of factors in postmitotic neurons contributes for the acquisition of the final area identities in the cortex (Joshi et al., 2008). Particularly strong evidences were presented for the involvement of TF *Emx2* in cortical arealization (Bishop et al., 2000; Mallamaci et al., 2000b). In *Emx2* deficient mouse cortex, the caudomedial areas are shrunken at the expense of the augmented rostrolateral areas, whose identity is altered (Bishop et al., 2000; Mallamaci et al., 2000b), reviewed by Mallamaci and Stoykova (2006).

The purpose of this study was twofold: firstly, to identify genes, possibly involved in cortical arealization in *Emx2*-dependent manner; secondly, to gain insights into the function of a selected candidate gene in cortical arealization. Therefore, in the first part of this work, selected genes from a previously performed microarray (Mühlfriedel et al., 2007) showing a similar to *Emx2* graded expression (either in progenitors or in cortical plate, CP) were analyzed in wild type and *Emx2*-/- mouse background. Indeed, six of the ten analyzed candidate genes were detected to show altered expression in the *Emx2*-/- cerebral cortex: *Odz3*, *Nef3*, *Zbtb20*, *Flrt3*, *Ebf3*, and *Nrp2*.

Initially, ***Odz3*** appeared to be an interesting candidate for functional analysis. *Odz3* is a member of a highly conserved gene family, consisting of four type II transmembrane proteins (Odz1–4) (Baumgartner et al., 1994; Ben-Zur et al., 2000; Levine et al., 1994; Oohashi et al., 1999). In all species examined to date, *Odzs* are predominantly expressed in the nervous system. Here, it was found that *Odz3* exerts a prominent expression gradient, caudal-high to rostral-low, in postmitotic neurons of CP, but also in brain regions belonging to the visual system (e.g. occipital cortex, dLGE and superior colliculi, see Fig. 7), which is in agreement with recently published data (Leamey et al., 2007). In the E16.5 *Emx2* deficient cortex, only a small residual expression of *Odz3* was detected, suggesting that *Odz3* gene activity is related

to *Emx2* function. In the progress of this study, Li et al., 2006 suggested that all four *Odz* members possibly act as direct *Emx2*-targets in cortical arealization. However, given the fact that *Emx2* and *Odz3* are expressed in cortical progenitors and differentiated neurons of CP, respectively, *Odz3* appears to mediate into CP the encoded *Emx2*-dependent positional information in cortical progenitors. Because another group (Leamey et al., 2007) was already in an advanced stage in the generation of *Odz3* loss-of-function transgenic mouse, the identification of other candidates was pursued.

Nef3 exerted a restricted expression in superficial layers of the occipital CP at E16.5 and E18.5. *Nef3* encodes NF-M (neurofilament, medium polypeptide), one of five major intermediate filament proteins expressed in mature neurons (Lariviere and Julien, 2004). Interestingly, the expression of *Nef3* was down regulated in the CP of *Emx2*-/- mutants, suggesting *Nef3* expression may depend on *Emx2* function. However, in a published description of the phenotype of *Nef3*-/- KO mice, no overt phenotype was found except for a reduction in the thickness of large myelinated axons (Jacomy et al., 1999). Further work might be necessary to address the question whether *Nef3*-/- mice display defects in cortical area formation.

During corticogenesis, newly born neurons leaving the VZ move radially along the processes of the radial glial progenitors, crossing the intermediate zone (IZ) to reach CP. ***Flrt3*** (Fibronectin leucine-rich transmembrane protein 3) was a gene with a marked graded expression in the postmitotic cells in both IZ and superficial layers of occipital CP. Flrt3 belongs to a small subfamily of putative type I transmembrane proteins, conserved in human, mouse, chick and frog (Lacy et al., 1999) with a role as a modulator of cell adhesion (Haines et al., 2006). Indeed, in *Xenopus*, Flrt3 was identified as a high affinity interactor of the netrin receptor Unc5B, both proteins being involved in a mechanism controlling cell adhesion (Karaulanov et al., 2006). Interestingly, in the *Emx2-/-* background, *Flrt3* displayed a down regulation in CP and a pronounced enhancement in the IZ (see Fig. 10), implicating that in absence of *Emx2* cell adhesive properties are disturbed and radial migration of neurons is defective. Despite that, *Flrt3* was not considered for further analysis because work of another group on generation of *Flrt3* KO mice was in advanced stage. As recently reported, *Flrt3* KO mutant mice die at around E10.5 due to defects in ventral closure, headfold fusion and endoderm migration (Maretto et al., 2008), thus excluding possibility to study their cortical phenotype.

The expression of two other candidate-genes, *Ebf3* and *Nrp2,* was also affected in the *Emx2* KO mutant. Specifically, the earliest-born type of cortical neurons, the Cajal-Retzius

(CR) located in MZ, normally expressing both *Ebf3* (this study) and *Emx2* (Mallamaci et al., 2000a) were depleted in the *Emx2*-/- embryo cortex. In tumor cells, *Ebf3* can induce a transcriptional program leading to cell cycle arrest and apoptosis (Zhao et al., 2006). It is conceivable therefore, that *Ebf3* could act downstream of *Emx2* in Cajal-Retzius neurons. During the progress of this work, *Ebf3* KO mice have been generated, which display defects in innervation of the olfactory bulbs (Wang et al., 2004), while a cortical phenotype has not been reported to date. The expression of *Nrp2* (neuropilin 2) was also affected in *Emx2-/-* background, particularly in CA1/CA2 areas. Neuropilins are a family of transmembrane glycoproteins involved in axonal guidance (Pellet-Many et al., 2008). In the *Nrp2-/-* KO mice the gross morphology of Hi was unaffected, major telencephalic and diencephalic axonal tracts were missing and projections from the DG to the CA3 region showed defects corroborating its role for *Nrp2* in guiding axons (Chen et al., 2000).

For further functional analysis, ***Zbtb20*** was favored, a gene coding for a transcription factor belonging to the POK (Poxviruses and Zinc-finger (POZ) and *Krüppel*) family of transcription repressors (reviewed by Costoya, 2007). In an immunohistochemical analysis using a *Zbtb20* antibody, Mitchelmore et al. (2002) suggested that Zbtb20 is expressed only in postmitotic immature neurons. However, as shown by in situ hybridization analysis in the present work, an interesting dynamics of distribution of *Zbtb20* transcripts was registered: While at stage E12.5, in VZ/SVZ, *Zbtb20* mRNA transcripts outlined exclusively the anlage of hem, hippocampal primordium, and the rostralmost domain of Ncx, at stage E14.5, a caudomedial-high to rostrolateral-low expression gradient was observed in cortical VZ. From this stage onward, a strikingly high *Zbtb20* expression was registered exclusively confined to the differentiated Hi proper and DG, which appeared to be involved in mediating D/V patterning in developing medium pallium, as discussed below.

3.2. Function of TF Zbtb20 during development

3.2.1. *Zbtb20* controls body growth

Available data indicate that *Zbtb20* encompasses 743.256 kb, containing 11 exons, which generate two protein isoforms by alternative splicing, Zbtb20L (741aa) and Zbtb20S (668aa) (Mitchelmore et al., 2002). Both proteins contain a BTB/POZ domain and a second domain comprising five zinc fingers, which are transcribed from exon 6 and exon 7. By using homologous recombination approach, the 6th exon, encoding this functionally important part of the Zbtb20 protein was deleted and simultaneously a *LacZ* reporter sequence was

introduced to enable the analysis of the endogeneous expression of *Zbtb20*. The generated heterozygous *Zbtb20*+/- mutant mice were viable and able to transfer the mutation to the progeny. The registered expression of the *LacZ* reporter in heterozygous embryos or juvenile brains was identical with the pattern of *Zbtb20* mRNA distribution, using an in situ probe, confirming the successful gene targeting and functionality of introduced reporter gene. This fact furthermore allowed providing detailed and so far unknown expression characteristics of *Zbtb20* in developing embryo body as well as in the developing, juvenile and adult brain (Chapter 2.2.3.). In addition to brain, presence of *Zbtb20* transcripts was detected in vital organs, such as heart, kidney as well as in other parts of the central and peripheral nervous system (CNS and PNS).

Mice homozygous for the induced mutation in *Zbtb20* gene displayed a clear 100% penetrant phenotype: all *Zbtb20*-/- mutants showed dysgenesis of hippocampus (Hi) and a delay of ossification of the skeleton. Juveniles showed growth retardation and died before the age of 25 days, which is in line with the observations from another recently reported *Zbtb20* full knockout in mice (Sutherland et al., 2009). In the intestinum of the dying *Zbtb20*-/- pups, large accumulations of air (bloatings) were observed, which possibly result from metabolic dysfunction due to reduced blood sugar levels (hypoglycemia) reported for *Zbtb20* KO mice after postnatal stage P10 (Sutherland et al., 2009). Indeed, glucose levels are known to influence gastric motility (Horowitz and Fraser, 1994) and hypoglycemia can lead to accelerated gastric emptying in humans (Schvarcz et al., 1993). Upon rapid gastric emptying, the small intestines fill too quickly with undigested food, leading to gas bloating (Horowitz and Fraser, 1994). Notably, in the current study, the enteric parasympathetic ganglia, generated from vagal and sacral neural crest cells (Pomeranz et al., 1991; Teillet et al., 1987), were detected to express *Zbtb20* (Fig. 20). Thus, the impaired gut motility of the gastrointestinal tract in *Zbtb20*-/- may also result from a dysfunction of the enteric nervous system in the *Zbtb20* mutant mice.

The first part of this discussion deals with the role of *Zbtb20* in the molecular patterning of the mammalian telencephalon with emphasis on hippocampal development. The second part is focused on the role of *Zbtb20* in skeletal development.

3.2.2. Role of *Zbtb20* in developing mammalian cortex

The mammalian cortex (pallium) is generated during development by progenitors of dorsal telencephalon. The progenitors of the dorsal, lateral and ventral pallium (DP, LP, VP)

produce neurons of the neocortex (Ncx) that are distributed radially into six layers as well as in into many functional domains, each with distinct responsibilities. The progenitors of the medial pallium (MP) generate neurons of the archicortex, which includes several subregions, the hippocampal formation, consistent of hippocampus proper (with its CA1-CA3 areas), DG and subiculum. The hippocampus (Hi) (Hi proper and DG) are the most thoroughly characterized brain fields in mammals, because of their crucial role in learning and memory (Hi proper) as well as the unique feature of ongoing neurogenesis in DG even in the adult brain. Molecular patterning of CNS starts yet at a stage open neural plate. After closure of the neural tube, the medial and lateral domains of the open neural plate acquire ventral and dorsal positions in the forebrain vesicle, respectively. In this study it is shown that TF Zbtb20 has a crucial role in molecular dorso-ventral patterning of MP, regulating thereby the morphogenesis of hippocampus proper, subiculum, retrosplenial cortex (Rsp), and dentate gyrus.

3.2.2.1. *Zbtb20* and morphogenesis of hippocampus

In this work, a dramatic alteration in the cytoarchitecture of the hippocampus in the postnatal *Zbtb20-/-* mice is shown. Located posteriorly in MP, the hippocampal formation is composed of subiculum (S), three fields of Hi proper (CA1, CA2, CA3), and the dentate gyrus (DG). Homogeneously arranged pyramidal or granule neurons build up the compact *stratum pyramidale* of CA1-CA3 or *stratum granulosum* of dentate gyrus, respectively. The CA regions are consisting of excitatory pyramidal neurons, which show specific connectivity and physiological properties (Paxinos, 2004). CA2, forming a narrow band of large pyramidal cells between CA1 and CA3, is generally ignored in discussions of hippocampus, being often described as an intermingling (transitory) zone of cells from CA1 and CA3 (e.g. Tole et al., 1997). Although at the level of gene expression CA2 and CA3 are often indistinguishable, more detailed analysis revealed that gene expression in CA2 is distinct from that in CA1 and CA3, indicating that CA2 is a functionally distinct hippocampal subregion (Lein et al., 2004; Woodhams, 1993), also based on the results of the present study as discussed below. The subiculum is the end point of the hippocampal formation, abutting upon the cingulate (Cgl), rostrally, and retrosplenial (Rsp) cortex, caudally. Both regions are assumed to be transitory neocortical domains. The subiculum (S) contains three subtypes of loosely distributed large pyramidal neurons, while in Rsp domain subpopulations of pyramidal neurons are distributed in layers, however, much less defined as compared to the Ncx (Staff et al., 2000).

In the *Zbtb20-/-* mutant mice, the size of Hi proper was significantly diminished, the dense compact pyramidal cell layer of the three CA fields was morphologically undetectable and the DG appeared decreased in size and abnormally shaped, with a shortened enclosed blade. More careful morphological analysis revealed alteration of the cytoarchitecture of several adjacent domains in the medial cortex. Because the subiculum has cell-sparse appearance, while the Rsp has compact upper layers, the border between S and Rsp cortex is recognizable after Nissl staining. Remarkably, in postnatal (P10) *Zbtb20*-/- mice, the subiculum showed cell compactness, similar to that seen in the uppermost layers of the neighboring Rsp cortex (see Fig. 24C/C´). Even more intriguingly, in CA1-CA3 domains of *Zbtb20*-/- mice, the large pyramidal neurons normally stacked into a compact layer were replaced by loosely distributed small pyramidal neurons, resembling the neuronal components in the supragranular layers of Rsp and Ncx (Fig. 25).

3.2.2.2. *Zbtb20* and patterning of medial pallium

As noticed several times in this work, multiple evidence supports the view that during development, combinatorial graded expression of TFs along cortical A-P and M-L axis specifies positional information in the germinative zones, intrinsically encoding an area "proto-map" that foreshadows the final arealization of the neocortex (reviewed by O`Leary et al., 2007; O'Leary and Nakagawa, 2002; Mallamaci and Stoykova, 2006). In contrast to the gradient-like expression of such factors in VZ/SVZ, the boundaries between distinct cortical areas in the mature CP are sharply outlined, either by specific morphology of their cell constituents and/or by restricted gene expression pattern of the neighboring domains. The mechanism involved in the establishment of such restricted borders in postmitotic neurons of CP is still unclear.

By using in situ hybridization analyses, in this work it was shown that the expression of *Zbtb20* begins around E12.5 in germinative zones of MP, outlining mostly the anlage of the hem and hippocampus, while later on, the expression is progressively extending into the pallial progenitors in such way that at E16.5, a medial-high to lateral-low expression gradient is established. Despite the early regionalized expression of *Zbtb20* in cortical progenitors across the M-L axis, the expression of TF *Emx2*, the most important player in area patterning in M-L direction, was not affected in midgestational *Zbtb20-/-* embryos. In addition, at stage E12.5, the regions of choroid plexus, hem and/or hippocampal anlage, outlined by the restricted expression of both TF genes *Foxg1* and *Lhx2,* were correctly located within MP of

Zbtb20-/- embryos. TF Lhx2 acts cell autonomously in specification of progenitor identity of the neocortex by suppressing the alternative hippocampal fate in MP (Mangale et al., 2008). Importantly, in absence of *Zbtb20,* the expression of *Lhx2* was unchanged, strongly suggesting that *Zbtb20* does not exert an early control in selection of the identity of MP versus that of neocortex in the germinative zone. Even using the advantage of the incorporated *LacZ* reporter sequence, allowing a more sensitive registration of the endogeneous *Zbtb20* expression pattern in *Zbtb20+/-* embryos, the earliest detected expression of *Zbtb20* in the hem was at E12.5 (Fig. 20). Because most of the patterning of the forebrain is already done at stage E10 (Mallamaci and Stoykova, 2006), the beginning of *Zbtb20* expression in the hem at E12.5 is indeed too late for a dramatic influence of the early patterning events in the pallial progenitors across the medial wall. In support of this notion, in *Zbtb20-/-* mutants, several markers (e.g. *SCIP* for CA1, *KA1* for CA3, and *EphB1* for DG/CA3), assumed as indicative for a correct field-specification of hippocampus proper, showed unchanged patterns.

Despite that the hem, hippocampal anlage and choroid plexus seemed correctly located in VZ of MP in *Zbtb20-/-* embryos, Hi of the adult mutant brain showed a severely diminished size. The hem is an important inductive forebrain center that secretes Wnts and Bmp family molecules (Furuta et al., 1997; Grove et al., 1998; Shimogori et al., 2004). The present analysis revealed that particularly the expression of *Wnt3a* was substantially diminished in E12.5 *Zbtb20*-/- embryonic brains. Wnt signaling is involved in regulation of a number of developmental processes including proliferation, fate determination and late differentiation of the vertebrate CNS (Ciani and Salinas, 2005; Hirabayashi and Gotoh, 2005; Hirabayashi et al., 2004; Hirsch et al., 2007). Distinct signaling molecules belonging to the Wnt family bind to a membrane receptor complex composed of one of ten frizzled (FZD) G-protein coupled receptors and one of two low-density lipoprotein (LDL) receptor-related proteins (Lrps) (Logan and Nusse, 2004; Moon et al., 2004). In this way, distinct Wnts members regulate several intracellular signaling pathways. In the canonical Wnt signaling pathway, the signal is firstly transduced to cytoplasmic ß-catenin, which then enters the nucleus to form a complex with members of the TCF/LEF family TFs to promote specific gene expression (Miller et al., 1999). In telencephalon, six *Wnt* genes (*Wnt2b*, *Wnt3a*, *Wnt5a*, *Wnt7a*, *Wnt7b* and *Wnt8b*) are expressed. Particularly interesting is the fact that targeted disruption of *Wnt3a* causes a full dysgenesis Hi and DG (Lee et al., 2000). Similarly, analysis of dominant-negative *Lef1* mice, or mice with a conditional depletion of ß-catenin, revealed that both Hi and DG are strongly reduced or absent, while the cell proliferation in respective

progenitor domains was significantly decreased (Galceran et al., 2000; Lee et al., 2000; Machon et al., 2003).

Developmental events, both endowing positional information and regulation of regional growth, are considered as components of the patterning. The available data are still not conclusive enough to give a satisfactory answer to the question, which is the leading role of the Wnt signaling pathway in these two interconnected processes. A question arises, therefore, what might be the contribution of the detected decreased Wnt3a signaling from the hem in *Zbtb20-/-* mutant? The prevailing view is that even though the final differentiation of Hi occurs after stage E15.5 (Tole and Grove, 2001), the specification of the distinct hippocampal fields must have occurred already by E12.5, the stage when the *Zbtb20* expression in the hem was registered. Thus, eventual *Zbtb20* - *Wnt3a* genetic interaction appears not to be able to influence the early progenitor patterning in MP. In the same line of evidence, although *Emx2* acts downstream of *Wnt3a,* the graded expression of this factor decisive for Ncx arealization was largely unaltered in the *Zbtb20-/-* mutant.

In *Zbtb20*-/- mice, the hippocampus showed severely diminished size, strongly suggesting that in *Zbtb20* deficiency, inhibition of *Wnt3a* expression could account for a general cell growth defects in all hippocampal subfields (CA1-CA3) and DG. These findings further implicate that after stage E12.5, TF Zbtb20 could be acting upstream in Wnt signaling pathway in regulation of cellular growth of hippocampus.

Taken together, the findings from the performed analysis of cortical patterning in *Zbtb20-/-* mutants at early developmental stages strongly suggest that while possibly not directly involved in areal progenitor specification of MP, the growth of Hi and DG appears to depend on still unknown molecular interactions between TF Zbtb20 and Wnt3a signaling pathway.

3.2.2.3. *Zbtb20* controls acquisition of archicortical areal identity

Results from previous immunohistochemical study indicated that at later developmental stages (E16.5 onwards) Zbtb20 is expressed only in immature post-mitotic neurons, derived from Ammonic and dentate neuroepithelium (Angevine, 1965; Mitchelmore et al., 2002). In agreement with these data, in the present study, strong expression of *Zbtb20* transcripts was detected not only in neurons of Hi proper and DG, but also in the compactly packed upper layers neurons of Cgl and Rsp cortex (e.g. Fig. 22C, D). Thus, the results of the current study indicate that the dorsal limit of *Zbtb20* expression in postmitotic pallial neurons actually

demarcates the Rsp/Ncx boundary. Furthermore, expressed at distinct levels - faintly in CA1 and strongly in CA2+CA3 areas - in developing (Fig. 14J) and in adult brain (Fig. 4G-J in Mitchelmore et al., 2002), *Zbtb20* expression appears to mark the border CA1/CA2+CA3 within hippocampus proper. Recent work provided the first convincing evidence that acquisition of areal identities involves expression of molecular determinants in postmitotic neurons of CP, acting downstream of the encoded "proto-map" in VZ/SVZ (Joshi et al., 2008). Specifically, these authors reported that Bhlhb5, a member of Olig subfamily of bHLH TFs, is selectively expressed in postmitotic CP neurons and regulates the postmitotic acquisition of area identities of SS and M areas. As discussed below, our findings strongly suggest that TF Zbtb20 may also play an important role in acquisition of regional identities in postmitotic neurons, specifically within the medial pallium.

As noticed, the constituents of CA1-CA3 areas are the homogeneous cell type of pyramidal neurons. In absence of convincing morphological traits, boundaries between cortical domains could be demarcated only through the restricted areal expression of specific markers. For instance, in Ncx the border between motor (M) and somatosensory (SS) areas is outlined by the expression of *cadherin 8* only in the upper layer neurons of M area, and the expression of *cadherin 6* in Layer 5 neurons of SS cortex (Suzuki et al., 1997). Similarly, the border between SS and visual cortex (Vi) is marked by the restricted expression of *COUP-TF1* (now *Nr2f1*) or *Chl1* (Liu et al., 2000b) in Vi area, which escapes the neighboring SS domain. However, systematic analyses on establishment and regulation of molecular borders between neo- and archicortex and especially between the distinct CA subregions (CA1, CA2, CA3) of Hi proper have been failing so far. Therefore, in order to evaluate whether region specific expression of *Zbtb20* in postmitotic neurons of MP might influence acquisition of intrinsic area identity, detailed expression analyses were performed at stage E18. This approach allowed to distinguish between distinct archicortical subdomains either by the restricted expression of a given marker in a specific region, or alternatively, through the distinct strength of the in situ hybridization signal between adjacent domains. The results of this extensive analysis are summarized in Table 9 and in Fig. 38. These findings indicate that in absence of *Zbtb20*, the patterning at four molecularly specified borders, namely Rsp/S, S/CA1, CA1/CA2, and CA2/CA3 (see schema in Fig. 38) was severely distorted. In general, markers of more dorsolateral domains were expanded ectopically into the neighboring subregions. How the patterning of a given MP subregion changes in the *Zbtb20* KO mutant (e.g. abolishment, diminishing or enhancement of its normal expression level for the applied marker) appeared to be strictly dependent on the normal (or already changed in case of CA1-

CA3) patterning of the neighboring domain, located more dorsally that the studied one (Table 9). For instance, in the control cortex, *Odz3, Nef3* (Fig. 29A, C), and *Steel* (Fig. 31C, D) were strongly expressed in distinct layers of CP in Ncx and Rsp with expression limit at the border with subiculum, outlining thereby the Rsp/S border at rostral levels. In the *Zbtb20*-/- mutants, the S showed ectopic expression of all these three markers at a strength, similar to that detected in the adjacent Rsp and Ncx areas (Fig. 29A/A´, C/C´; Fig. 31C-D´). On the contrary, while in control sections *Nurr1* and *Er81* expression selectively labeled only S (bordered by Rsp that is normally negative for these markers), in *Zbtb20*-/- mice, S became a negative domain for both markers, suggesting expansion of the Rsp into S domain. Moreover, morphologically, the cell sparse domain of S seemed to be replaced by densely packed neurons that are a normal component of the upper layers in the adjacent Rsp and Ncx (see Fig. 24D/D´).

Subiculum is the major output structure of the hippocampus, involved in processing information about space, movement and memory (O'Mara et al., 2001), but little is known about the molecular control for development of this field. Analyses of knockout mutants for *Wnt3a*, *Emx1*/*Emx2* and *Lef1* suggested that these factors may be involved in the early specification of the subicular and hippocampal anlage (Lee et al., 2000; Shinozaki et al., 2004). The results from the analysis presented here further indicate that the late expression of TF Zbtb20 in the hippocampal anlage and differentiating S and Rsp areas is important for maintenance of the subregional specification of these domains.

Similarly to the registered mispatterning at the border S/Rsp, in the *Zbtb20* KO mutant, each of the more dorsally located hippocampal CA1-CA3 fields appeared to be expanded into the adjacent, more ventromedially located domain. In other words, the molecular characteristics, specific for CA1, were found expanded into CA2 area and subsequently into CA3 area. For instance, because of the expansion of Rsp into S domain in *Zbtb20* KO mice, the normal strong *Nurr1* signal in S was almost lost (Fig. 30A', B'). Consequently, the adjacent CA1 region (normally negative for *Nurr1*) started to exhibit ectopic *Nurr1* expression in *Zbtb20* mutant, suggesting a displacement of S area with a residual identity into the CA1 field. Similarly, in *Zbtb20*-/- mice, the CA1 and CA2 subregions lost their normal strong *Nrp2* and *Neurod1* expression, thus acquiring the patterning that is normally characteristic for the adjacent area of the S, which was ventromedially expanded in the mutant (Fig. 32A', B' and C', D', respectively).

The proposed ventral displacement of the hippocampal areas was better demonstrated after the application of markers showing a distinct intensity of the expression signal in CA1,

CA2, and CA3 subregions. For instance, in *Zbtb20* deficiency, the normal faint expression of *SCIP* in S was replaced by a stronger expression signal, similar to that of the adjacent Rsp (Fig. 31A', B'). In addition to that, the CA1 subregion in the mutant showed a decrease of its normal expression to a level, characteristic for the normal S, suggesting that CA1 has acquired a subicular identity in *Zbtb20* KO mice. Similarly, the detected changes of the patterning with in situ probes for *KA1* and *EphB1* at the borders CA1/CA2 and CA2/CA3 led to the conclusion, that these domains are displaced more ventrally.

Remarkably, however, in most cases, although diminished, the CA3 area seemed to be present in the *Zbtb20-/-* mice, evident by the preserved expression of *Nrp2*, *Neurod1*, *KA1*, *EphB1* (Fig. 32, Fig. 33). Generally, shift of gene expression patterns is indicative of respecification of area identity. For instance, in developing Ncx of *Emx2-/-* mice, expansion of the rostral M area in expense of more caudally located SS and Vi domains is a consequence of defects in specification of area identities. For reasons already discussed above, however, rather exerting control functions in the progenitors (e.g. like Emx2), the TF Zbtb20 seems to act preferentially in postmitotic neurons. Further experiments are necessary to answer the question whether change of the molecular profile of the archicortical subdomains in *Zbtb20* KO mice shown in this study, leads to corresponding alteration of region-specific functions of each area.

Given the role of *Zbtb20* in patterning of hippocampal CA1-CA3 area, which was discovered in this study, it will be important to investigate in future the axonal connectivity of the hippocampus proper. The pyramidal neurons of CA3 normally send projections (Schaffer projections) to the basal and apical dendrites of CA1 pyramidal neurons in *stratum oriens* and *stratum radiatum* of Hi. Due to altered molecular patterning and morphological appearance of the cellular components of the CA1 and CA3 fields in *Zbtb20* mutant, it is to be expected that the Schaffer collateral projections possibly will have a wrong direction of growth. Experiments are in progress to address this issue.

The idea that expression of *Zbtb20* has a decisive role for maintenance of the hippocampal regional identity is fully supported by results of recent analysis of another type of transgenic mice that misexpress *Zbtb20* under the control of a forebrain specific promoter/enhancer D6 (Nielsen et al., 2007). In these experiments, the ectopic expression of *Zbtb20* transgene in non-hippocampal progenitors of cortex caused a transformation of both, subiculum and Rsp into Hi-like cortex. Consequently, the two regions contained a compact CA1-like pyramidal cell layer, leading to formation of an extremely large CA1-domain (Nielsen et al., 2007).

Taken together, the findings presented in this study suggest: firstly, expression of TF Zbtb20 in postmitotic neurons of the two transitory regions, the subiculum (archicortex) and Rsp (transitory Ncx) plays a crucial role for acquisition/maintenance of archicortical versus neocortical fate, and secondly, the expression of *Zbtb20* in the archicortex controls the subregional identity (CA1-CA3) of hippocampus proper.

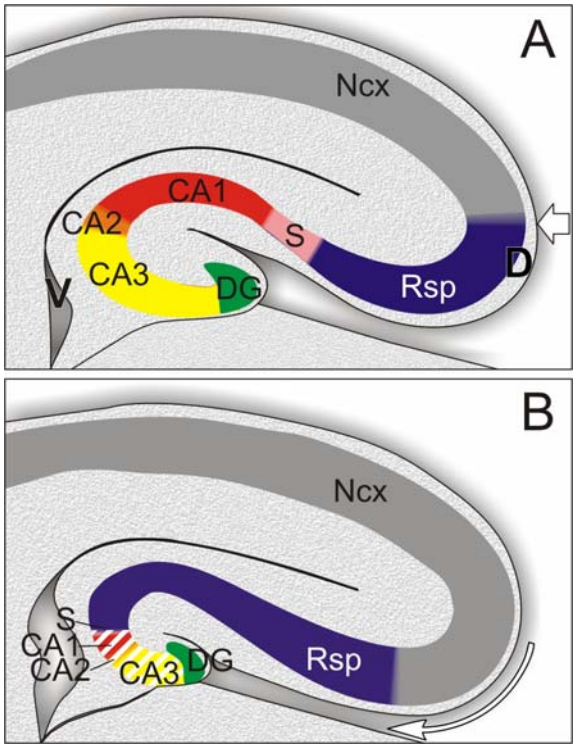

Fig. 38. Schematic presentation of detected defects in molecular patterning of medial pallium in the *Zbtb20* KO mice. Schema of WT (**A**) and *Zbtb20*-/- (**B**) cortex (coronal hemisections) is shown. *Zbtb20* normally shows a strongly regionalized expression confined to the hippocampal formation (DG, dentate gyrus; CA3, CA2, CA1 fields; S, subiculum) and the transitory (neocortical) retrosplenial cortex (Rsp) domain. The performed expression analysis indicates that in absence of *Zbtb20* molecularly defined expression borders (Rsp/S, S/CA1, CA1/CA2, CA2/CA3) progressively expand ventrally in expense of the squeezed CA3 domain. Analysis after Golgi staining revealed that the typical CA1 pyramidal neurons were replaced by neurons, resembling cells of the Rsp, suggesting that in the *Zbtb20*-/- mice, the CA1 area was transformed into Rsp. In (**B**) S and CA1-CA3 are represented cross-striped to indicate that the reduced S and CA1-CA3 domains most probably have changed their own original identity. Additionally, the neocortical domains seemed to expand into Rsp domain as seen by cresyl violet staining. Arrow in (**A**) points at the Ncx/Rsp border. Arrow in (**B**) indicates medial expansion of Ncx in the mutant. Further functional (neurophysiological) analysis is necessary to clarify these issues. D, dorsal, V, ventral.

Table 9. Summary of detected alterations of the expression patterns for genes enriched in distinct subregions of neocortex and hippocampus in the E16.5 control and *Zbtb20*-/- mutant cortex (next page).
Distinct levels of gene expression are designated: (++++) extremely strong expression, (+++) strong expression, (++) moderate expression, (+) low expression, (-) no expression. The filled arrows indicate a ventromedial displacement of the areal specific expression of the used marker into the neighboring (ventromedially located) area, in which the marker shows "ectopically" the expression trait of the original (dorsally located) area. This could lead either to an abnormal enhancement or diminishing of the normal expression level of the marker in the ventromedial area. The empty arrowheads are used to indicate similar ventromedial displacement of the patterning from regions that are normally either negative or slightly positive for the studied marker. This kind of mispatterning mostly results in an obvious dilution or neglecting of the expression signal in the neighboring areas.

		Cortex		Archicortex				
Marker	Genotype	Ncx	Rsp	S	CA1	CA2	CA3	DG
Id2	WT	++++	++++	++	+++	++	+	++
	Zbtb20-/-	++++	++++	++++	++++	+++	++	++
Math2	WT	++++	++++	++	+++	+++	++	-
	Zbtb20-/-	++++	++++	+++	++++	+++	+++	-
Foxg1	WT	++	++++	++	+++	++	++	++
	Zbtb20-/-	++	++++	++++	++++	+++	+++	++
Nef3	WT	++	++	+	+/-	-	-	+/-
	Zbtb20-/-	+++	+++	+++	++	+	-	+/-
Odz3	WT	+++	+++	+/-	-	-	-	+/-
	Zbtb20-/-	+++	+++	+++	+/-	-	-	+/-
SCIP	WT	++++	++++	++	+++	-	-	-
	Zbtb20-/-	++++	++++	++++	++	-	-	-
Steel	WT	+++	+++	-	++	+/-	-	+++
	Zbtb20-/-	+++	+++	+++	-	+	++	+
Nrp2	WT	-	-	-	++	++	+++	+++
	Zbtb20-/-	-	-	-	-	+/-	+++	++
Neurod1	WT	-	-	-	++	++	+++	+++
	Zbtb20-/-	-	-	-	-	+/-	+++	+++
Nk3	WT	+	+	-	++	-	-	+/-
	Zbtb20-/-	+	+	+/-	-	-	-	+/-
EphB1	WT	+++	+++	++++	-	-	++++	++
	Zbtb20-/-	+++	+++	+++	++++	+	++	++
Nurr1	WT	-	-	++++	+	-	-	-
	Zbtb20-/-	-	-	-	+/-	-	-	-
Er81	WT	++	+	++	+	-	-	-
	Zbtb20-/-	++	+	+	-	-	-	-
calretinin	WT	++	++	-	-	+/-	++	++
	Zbtb20-/-	++	++	++	-	+/-	++	++
KA1	WT	-	-	+/-	-	+++	+++	+
	Zbtb20-/-	-	-	-	-	-	++	+

3.2.2.4. *Zbtb20* in growth and differentiation of DG

Several marker genes in the performed pattern analysis showed disturbed expression not only in Rsp, S and hippocampus proper, but also in DG of the mutant (see summary Table 9). The presence of the anlage of DG was evident by the expression of *Id2, Neurod1, Foxg1, EphB1, Prox1, Id3* and *Sox2*. However, all of these markers indicated a decrease of the DG size in the mutant, affecting mainly the dentate enclosed (or suprapyramidal) blade. The production of the granule cell layer of DG starts at E10 in the mouse (Angevine, 1965) while the bulk of granule neurons is formed within three weeks after birth in rat (Bayer and Altman, 1975). Giving rise to projections into the CA3 area (Blackstad et al., 1970; Gaarskjaer, 1978; Schlessinger et al., 1978) the DG has an important role in the circuitry of the hippocampal formation. In addition, DG and the subventricular zone of Ncx are the two locations where cell proliferation and neurogenesis persists throughout life (Altman, 1969; Altman and Das, 1965a, b; Bayer, 1980; Cameron and McKay, 1998; Kempermann et al., 1997a, b).

How could *Zbtb20* influence the growth of hippocampal formation, including hippocampus proper and DG? As already noticed, in *Zbtb20* KO mice, a substantial decrease of the *Wnt3a* expression in the hem was detected, suggesting a deficiency of Wnt signaling, which seems to affect the growth of MP, without perturbing the early arealization of Ncx. Interestingly, a similar phenotype was reported for the *D6-Dkk1* transgenic mice (Solberg et al., 2008). Here, *Dickkopf1* (*Dkk1*), coding for a negative regulator of canonical Wnt signaling, was placed under the forebrain-specific promoter D6, causing reduced canonical Wnt activity in the germinal zones of the prospective Hi and DG after E11. In consequence, *Dkk1* mutants displayed a strong reduction of CA1-CA3 and DG while the patterning of Ncx regions was normal. Remarkably, transcript profiling experiments using liver tissue of *Zbtb20-/-* mice discovered a profound increase of the Wnt inhibitory factor 1 (*Wif1*), a secreted protein, which binds to Wnt proteins and inhibits their activities (Hsieh et al., 1999), in the mutant (Sutherland et al., 2009). These data suggest that *Zbtb20* could normally negatively regulate the expression of *Wif1*. As *Zbtb20* and *Wif1* are co-expressed in the embryonic hippocampus (Hu et al., 2008), the *Wif1* is likely to be de-repressed in the *Zbtb20-/-* in this structure. Together with the finding of this study, these results suggest that despite the late initiation of the expression of *Zbtb20* in the Hi anlage (at E12.5), Zbtb20 still might indirectly modulate the intensity of the Wnt3a signaling pathway in MP.

In absence of *Zbtb20*, the differentiation of granule cells in DG was severely affected, evident by the pronounced inhibition of the expression of three differentiation markers for

these cells: *Steel* (encoding c-kit ligand), *Prox1* (a homeobox protein gene), and bHLH TF gene *Neurod1* (Oliver et al., 1993; Tole et al., 2000; von Bohlen Und Halbach, 2007). Similarly, in the *Zbtb20* mutant, the VZ/SVZ of both, MP and Ncx, displayed enhanced expression of *Sox2,* a TF with a role for stem-cell maintenance (Wegner and Stolt, 2005) as well as for TF gene *Emx2,* known to promote symmetric (proliferative) versus asymmetric (neurogenic) division of the progenitors (Heins et al., 2001). To sum up, these findings suggest that *Zbtb20* might exert a more general role for neuronal differentiation. *Zbtb20* is a good candidate to play also a role for cortical neuronal differentiation. In this line, it is of interest to note that *Zbtb20* was recently identified as a novel candidate gene for treatment response to risperidone, a drug applied in the treatment of schizophrenia, a severe psychiatric disorder (Ikeda et al., 2009). As schizophrenia is widely believed to result from defective neurodevelopment (Weinberger, 1995), and risperidone exerts neurogenic action particularly in hippocampus and prefrontal cortex (Newton and Duman, 2007), *Zbtb20* as a putative schizophrenia correlated gene, may have still unknown role in cortical neurogenesis. This assumption, of course, requires further investigation.

3.2.2.6. Possible mechanisms of *Zbtb20* dependent areal patterning of MP

Several available evidence implicate that an interplay between *Zbtb20* and Wnt signaling pathway could be involved in defects of Hi proper, subiculum and DG detected in *Zbtb20* loss-of-function (this study), as well as in *Zbtb20* gain-of-function mice (Nielsen et al., 2007). Thus, both *Zbtb20-/-* mice (this study) and *D6-Dkk1* transgenic mice, overexpressing the Wnt pathway inhibitor Dkk1, showed similar defects: reduction of CA1-CA3 fields, DG, but leaving unaffected patterning of Ncx (Solberg et al., 2008). In contrast, in *D6-CLEF* mice, in which active canonical Wnt signaling was ectopically maintained in the entire developing cortex, cells with hippocampal identity were found spread into Ncx (Machon et al., 2007).

At a first glance, it is reasonable to assume that a regression of Hi subdomains into more ventromedial regions, seen in *D6-Dkk1* transgenic mice (Solberg et al., 2008) and in *Zbtb20* KO mutants (this work) may result from a weakened Wnt signaling. In opposite, spreading of Hi cell islands into Ncx, seen in *D6-CLEF* transgenes, could be a consequence of enforced Wnt activity (Machon et al., 2007). It is important to note, however, that the exact timing of Wnt activity has a crucial role for the patterning. Therefore, manipulation of gene activity at different developmental points could involve rather different mechanisms. For instance, because overexpression of *Zbtb20, Dkk1 or CLEF* in these studies was driven by the D6

promoter/enhancer (Machon et al., 2002), the transgenic activation was taking place very early (from E10.5 onwards). Under this condition, the area disturbances of Hi could be indeed a direct consequence of altered Wnt signaling, affecting the progenitor specification. However, a different mechanism appears to be involved in the defects in areal identity of the hippocampal formation in *Zbtb20-/-* mice reported here. As already noticed, the endogeneous expression of *Zbtb20* in the hem is observed not earlier that E12.5, a stage at which the general intrinsic patterning of the cortical primordium is already done. The so far available data allow to assume that late de-repression of *Wif1* (as discussed above) leads to diminished *Wnt* signaling in *Zbtb20* KO mice, affecting only the growth, but not the progenitor specification. Apart from this, decreased *Wnt3a* expression in the *Zbtb20* KO hem seems to contribute to the aggravation of the Wnt signaling defect, suggesting that TF Zbtb20 might positively regulate *Wnt3a* gene transcription.

Taken together with available literature data, the results presented in this study strongly suggest that the expression of *Zbtb20* in neurons of the Rsp and hippocampal formation seems to be necessary for a correct postmitotic acquisition of areal identity of archicortex as entity, as well as for determination of subregional identity of hippocampus proper.

3.2.3. Role of *Zbtb20* for the normal antero-posterior axis specification of the skeleton

Despite the highly variable appearance of creatures as different as flies and mice, their basic body plan is strikingly similar. They all share versions of the same genes, namely *Hox* genes.

The *Hox* gene family encodes the most conserved group of homeodomain proteins, which control segmental patterning of the vertebrate body plan during development, thereby sculpting the head-to-tail organization (Wellik, 2007). According to the '*Hox* code' model the character of an individual body segment is specified by the combination of functionally active *Hox* genes. Flies, for instance, have eight *Hox* genes while mice and other mammals have thirty-nine. Altered combination of *Hox* genes results in changing segmental identities, the so-called homeotic transformations. Posterior transformation can occur, for example, when expression boundaries of *Hox* genes are shifted in anterior position.

Frequently, *Zbtb20-/-* mice displayed a posterior transformation of lumbar vertebra 6 into sacral vertebra one. These possibly homeotic-like transformations in the mutant axial skeleton (L6→S1) were observed with a twofold higher frequency than in wild type. These differences, however, fail to achieve statistical significance. Certainly, a higher sample number may be better suited for obtaining more reliable evidence about a possible

relationship between lacking *Zbtb20* function and aberrant vertebral identity. However, this relationship cannot be ruled out. Probably, loss of *Zbtb20* leads to a perturbed vertebral identity with low penetrance.

Hox genes are expressed from E7.5 to E12.5 in particular in the neural tube and also in somites and sclerotomes while *Zbtb20* is expressed at E9.5 in the somites, from E10.5 onwards in the neural tube and the developing skeleton. A function of *Zbtb20* in *Hox* gene regulation is principally conceivable, as its expression overlaps spatially and temporally with the expression of *Hox* genes. An indirect role of *Zbtb20* in the regulation of *Hox* function is likely, for example, through the Wnt signaling pathway. Wnt signaling on *Hox* expression and AP vertebral patterning occurs through regulation of *Cdx1* expression (Ikeya and Takada, 2001; Lohnes, 2003). *Wnt3a* not only regulates somite formation but also somite specification along the anteroposterior axis (Ikeya and Takada, 2001; Takada et al., 1994).
Intriguingly, similar to the alteration of L6 into S1 in the *Zbtb20*-/-mice reported here (this study), the *Wnt3avt*/*vt* mutants (*vt*, vestigial tail, a *Wnt3a* hypomorph) display severe vertebrae transformations along the AP axis of the skeleton (Ikeya and Takada, 2001). As homeotic transformation strictly depends on *Hox* gene expression, it will be interesting to study whether TF Zbtb20 might be involved in *Hox* gene expression.

Notably, the closest homolog of Zbtb20, the TF PLZF (also named Znf145), a powerful regulator of limb and skeleton formation, exerts such a function. Mice deficient for *Plzf* display transformations throughout the axial skeleton and in the limbs at high frequency. For example, these animals have additional digits. These abnormalities occur as a result of misexpression of several *Bmp* and *Hox* genes in *Plzf*-/- (Barna et al., 2000). Interestingly, *Plzf* was an upregulated gene in ossification of the posterior longitudinal ligament of the spine (OPLL), which is an ectopic bone formation disease in human. In this context, *Plzf* is assumed to participate in this congenital disorder, as an upstream regulator of *Runx2*. Over-expression and silencing of the *Plzf* gene lead to enhanced levels or abolishment of *Runx2* and other bone marker genes, respectively. Therefore, *Plzf* is implicated to play an important role in early osteoblastic differentiation (Inoue et al., 2006).

A function for *Zbtb20* similar to *Plzf* is at least conceivable. A moderated skeletal patterning phenotype, like it was observed in *Zbtb20*-/- mice may result from a compensating function by *Plzf* for *Zbtb20* loss. No skeletal phenotype is reported from mice lacking Bcl6, another TF closely related to Zbtb20.

In further experiments the defects in *Zbtb20*-/- mutants should be determined in terms of the expression patterns of selected *Hox* genes.

3.2.4. *Zbtb20* is necessary for the integrity of vertebrae and for normal ossification

Since *Zbtb20*'s expression was detected to start from E10.5 in the nascent elements of the skeleton, it was asked if bone formation is *Zbtb20*-dependent. This appeared to be the case, for a marked delay of the ossification in the *Zbtb20-/-* mutant mice was observed, affecting virtually all parts of the axial and appendicular skeleton.

Bone development as well as bone remodeling throughout life are controlled by a bunch of molecules, including bone morphogenetic proteins (Bmps), Wnts, fibroblast growth factors (Fgfs), hedgehog proteins, insulin-like growth factors, and retinoids. These locally produced factors are essential for normal bone formation, which induce together with systemic factors such as growth hormone, thyroid hormone, oestrogen, androgen, vitamin D and glucocorticoids the growth of bone (Kronenberg, 2003).

During development, bone formation occurs by either endochondral or intramembranous ossification (Ducy, 2000; Ducy et al., 2000). The bones of the vertebral column, ribs, pelvis, and limbs are formed by the first mode, which is a multistep pathway, whereas the cranial vault, portions of the upper facial skeleton (vomer, palatine, mandibular, and premaxilla) are generated by the latter mode, which is a straightforward process. In brief, endochondral ossification encompasses the formation of cartilage tissue from aggregated mesenchymal cells, which is subsequently replaced by bone (Gilbert, 2006), involving the function of molecules such as Sonic hedgehog, Pax1, Bmps, N cadherin and N-CAM, Sox9 and Runx2. During endochondral ossification, precursor cells condense to become chondrocytes, the primary cell type of cartilage. Cells at the border of condensations form a perichondrium. Chondrocytes express a characteristic program driven by Sox9 and other TFs. While the chondrocytes proliferate and matrix is produced the cartilage enlarges. In this template for the future bone chondrocytes undergo hypertrophy and apoptosis to be later replaced by osteogenic cells. During intramembranous ossification, mesenchymal cells directly undergo osteogenesis without the cartilaginous template.

The current analysis of mice lacking functional *Zbtb20* provides a framework for hypotheses on the role of *Zbtb20* in skeletal development. The major defect seen in *Zbtb20*-/- mice was delayed endochondral ossification. Calcification of the hyaline ribs may be triggered by the same mechanism underlying ossification of endochondral bone. This thesis is supported by the fact that in transgenic overexpression of *Runx2* in wild type mice hypertrophy of normal chondrocytes is accelerated and even hypertrophy and subsequent

bone formation is induced in cartilage that normally never undergoes hypertrophy, such as the cartilage of tracheal rings. Furthermore, accelerated bone formation, which is seen in mice with a disrupted parathyroid hormone-related peptide (PTHrP) gene is accompanied with a perichondral ossification of the hyaline ribs (Karaplis et al., 1994). Moreover, the loss of *Zbtb20* led to slightly hypoplastic vertebrae, displaying defects at their arches, suggesting that the cartilageous mold of these vertebrae is not generated properly. Therefore, *Zbtb20* appears to be needed not only for normal ossification but also for the normal proliferation of chondrocytes along the vertebral column.

In the current study, due to limited time, it has not been possible yet to unravel any possibly disturbed genetic pathways within bone and cartilage in absence of *Zbtb20*. It is conceivable that altered Wnt signaling is responsible for the ossification/hypoplasia phenotype, given that *Wnt3a* or even other *Wnts* expression levels are reduced in the mutant. Whether this assumption is true remains to be determined. *Wnt3avt*/*vt* display vertebral defects in their caudal region, including abnormal centers of ossification, malformations, and fusions, while in *Wnt3aneo*/*vt* compound heterozygotes, these defects are even more severe. (Greco et al., 1996). Contradictory data has been delivered concerning the capacity of *Wnt3a* to promote mineralization in cell cultures (Liu et al., 2008). However, the skeletal phenotype observed in *Zbtb20*-/- might be at least in part result from attenuated *Wnt3a* expression, resulting in hampered Wnt signaling. Indeed, canonical Wnt signaling promotes osteogenesis by a direct stimulation of *Runx2* gene expression (Gaur et al., 2005). Studies in mutants deficient for components of the canonical Wnt signaling pathway suggest that Wnt signaling is necessary for both chondrogenesis as well as for the generation and differentiation of osteoblasts (Liu et al., 2008). The transcription factor Runx2 (formerly Cbfa1) is necessary for the development of both intramembranous and endochondral bone. As master regulatory factor in bone formation, *Runx2* is crucial e.g. for generation of hypertrophic chondrocytes and the differentiation of osteoblasts while integrating signaling responses (Ducy et al., 2000; Gilbert, 2006). Mice lacking *Runx2* develop to term with a normally patterned skeleton that is made exclusively of cartilage.

Apart from *Runx2*, other mouse mutants (e.g. either lacking one or both alleles of *Dmp1*, *Sox9, Connexin43* or *Sp3*) exhibiting altered ossification have been reported to date (Bi et al., 2001; Göllner et al., 2001; Lecanda et al., 2000; Otto et al., 1997; Ye et al., 2005). Mice deficient for Lrp5, a Wnt coreceptor, exhibit a delayed ossification phenotype similar to that observed in *Zbtb20*-/- mice, but milder. Interestingly, *Runx2* expression is not altered in *Lrp5*-/- (Kato et al., 2002). The defect in endochondral ossification may also be explained by

a dysregulation of *Bmp4* in *Zbtb20*-/- mutant, as *Bmp4* is implicated to have a role in endochondral bone formation (Li et al., 2005).

To what extent metabolic dysfunction (described in chapter 3.2.1.) can contribute to the delayed bone formation detected in *Zbtb20*-/- in the current study, however, remains an open question. In animals and humans calcium homeostasis is crucial for normal bone formation (DeLuca, 1988). Blood calcium levels in *Zbtb20*-/- however, were normal in comparison with the control. To date, no direct evidence has been supplied that hypoglycemia can lead to altered ossification.

Future experiments should reveal if a number of markers, first of all *Wnt, Bmp*, and *Runx2* expression in skeleton is affected by *Zbtb20* disruption. Furthermore answers should be addressed if and where Zbtb20 has a role in the function of differentiated osteoblasts, i.e. bone matrix deposition. This possibility should be investigated on the cellular level.

IV. Summary

The mammalian cortex is organized into functional areas that have distinct architecture, axonal connections, and function. Accumulating evidence indicates that combinatorial expression of sets of transcriptional factors (TFs) in gradients along anterior-to-posterior and medial-to-lateral axis in cortical germinative zones exerts a tight genetic regulation of cortical arealization, however, the controlled pathways by such TFs are still unknown. Studies on areal specification in the developing cerebral cortex have focused until now mainly on the neocortex (Ncx), a mammal-specific region produced by progenitors of the dorsal and lateral telencephalon. Only few recent data suggest genetic mechanisms controlling the regionalization of the archicortex, produced by the progenitors in the medial wall of telencephalon.

So far, the role of TF Emx2 in cortical arealization is most convincingly demonstrated. The first part of this work is dedicated to the goal to identify candidate genes acting in *Emx2*-dependent pathway in cortical neurogenesis. The performed comparative expression analysis for 10 genes, selected from previously performed microarray screen, in wild type and *Emx2-/-* backgrounds revealed an altered expression in *Emx2*-deficiency, placing at least six genes as putative players, acting downstream of *Emx2* in cortical arealization.

In the second, main part of this work, findings from performed functional analysis of the generated knockout mutant mice for TF Zbtb20 are presented, implicating that this factor exerts a genetic control for arealization of archicortex. Homozygous *Zbtb20* KO animals were viable at birth, but displayed dwarfism and died during the first month of postnatal life. The expression of *Zbtb20* in cortical germinal neuroepithelium begins at E12.5 and later on becomes restricted exclusively to postmitotic neurons of hippocampus (Hi) proper, dentate gyrus (DG), and two transitory zones, subiculum (S) and retrosplenial cortex (Rsp). Focusing on the cortical phenotype, the analysis revealed an alteration of cortical patterning at the border between neocortex and archicortex, a decrease of the size of archicortical derivatives (S, Hi proper, DG), and a dramatic change of the molecular patterning of the hippocampal fields S, CA1, CA2, CA3. Here, it is demonstrated that in absence of *Zbtb20* the restricted expression of distinct marker genes was compromised at four borders: Rsp/S, S/CA1, CA1/CA2, and CA2/CA3, leading to an ectopic expansion of dorsally located fields into their neighboring, more ventral fields, at the expense of the CA3 area. This pattern defect resulted

in a replacement of the densely packed large pyramidal neurons in hippocampus proper by ectopically spread neurons from adjacent subicular domain, with a wrongly acquired specification of the retrosplenial (neocortical) domain. Because *Zbtb20* expression can be identified only after the accomplishment of early progenitor specification, the intrinsic area specification of cortical progenitors appeared unaltered.

Together, these findings demonstrate that Zbtb20 might function as an area-specific TF that regulates postmitotic acquisition of area identities within the archicortex. Furthermore, results yielded in this work and literature data suggest that detected growth defect of Hi and DG in *Zbtb20* deficiency most probably involves modulation of the Wnt signaling pathway after midgestation stage.

A second phenotype described in this study is the observed marked delay of the ossification in the *Zbtb20-/-* mutant mice, affecting virtually all parts of the axial and appendicular skeleton. Noteworthy, although showing possibly a background dependent low penetrance of the phenotype, *Zbtb20*-/- mice displayed bone and vertebrae malformations, resembling to mice with *Wnt3a* deficiency. The suggested genetic interplay between *Zbtb20* and Wnt signaling for the growth of archicortex and possibly also for the skeletal ossification requires further experimentation.

In conclusion, the presented results in this work place Zbtb20 as the first known so far TF with a role in postmitotic acquisition of areal identity of the archicortex and its subfields.

V. Materials and methods

5.1. Organisms

5.1.1. Mice

Emx2 (Pellegrini et al., 1996) and *Zbtb20* (this work) mutant mice were used.

Homozygous mice were generated from intercrossings of heterozygous animals, which allowed a direct comparison of gene expression patterns between +/+, +/-, and -/- littermates of each mutant studied. *Emx2* mutant mice were maintained on a C57/BL6 background.

Zbtb20 gene deficient/mutant mice were produced by using 'MPI-II' ES cells of 129/Sv origin. Germline screenings were performed by mating ES cell generated chimeras with CD1 outbred strain. 129/Sv and C57/BL6-inbred strains were used during the matings for backcrossings and colony maintenance. For overnight matings, the morning when a vaginal plug was observed considered as E0.5. For timed-matings, the time of vaginal plug observation was accepted as E0. For analyses, mice were either sacrificed by cervical dislocations or by inhalation of CO_2.

5.1.2. Bacteria

Several strains of *E. coli* were used. For molecular cloning DH5α was utilized. XL1-Blue MRA (Stratagene) was used as host for phages. In recombineering experiments recombinogenic bacterial strain DY380 was used.

5.2. Materials

5.2.1. General Information

In the following percentage detail for solid matter is to be comprehended as mass percentage (g/ 100 ml), and in case of liquids as percent by volume. Solutions were usually prepared with water, the solvent is specified otherwise. The water was demineralized in an ion exchanger (MilliQ synthesis, Millipore) in advance and autoclaved.

5.2.2. Chemicals and enzymes

The companies Difco, Fluka, Gibco, Merck, Roth und Sigma were suppliers for chemicals. Chemicals of purity level "p.a." (per analysi) were used. DNA-Primers were ordered from IBA-GmbH, Göttingen, or Operon, Cologne.

If not specified differently, all enzymes were bought from NEB, Boehringer-Mannheim, Promega or GeneCraft.

5.2.3. Liquid and solid media

STI medium

Peptones	1.5%
Yeast extract	0.3%
NaCl	0.6%
Glucose	0.1%
pH 7.5	

STI^{Amp}-Medium: STI-Medium containing Ampicillin, 50 µg/ ml
STI^{Cam}-Medium: STI-Medium containing Chloramphenicol, 25 µg/ ml
STI^{Tet}-Medium: STI-Medium containing Tetracylin, 12.5 µg/ ml

NZY medium

Casein, enzymatically digested	1%
Yeast extract	0.5%
NaCl	0.5%
$MgCl_2$	0.094%
pH 7 +/- 0.2	

STI solid medium for bacteria: STI medium containing bacto agar, 1.5%

5.2.4. Standard solutions

Phosphate-buffered Saline (PBS)

NaCl	137 mM
KCl	2.7 mM
Na_2HPO_4	7.6 mM
NaH_2PO_4	0.7 mM
KH_2PO_4	1.4 mM
pH 7.2	

Paraformaldehyde (PFA)

Paraformaldehyde	40 g
PBS	1l
at 65 °C dissolved, pH 7.8	

SSC (20x)

NaCl	3 M
Sodium citrate	0.3 M
pH 4.5 or pH 7.0	

MOPS-buffer

3-(N-Morpholino)-propansulfonic acid	200 mM
Sodium acetate	50 mM
EDTA	10 mM
pH 7.0	

Tris EDTA (TE)

Tris-Cl	10 mM
EDTA	1 mM
pH 7.5 or 8.0	

$T_{1/10}E$:

Tris-Cl	10 mM
EDTA	0.1 mM
pH 8.0	

TBE (1x)

Tris-Borate	89 mM
Boric acid	89 mM
EDTA	2 mM
pH 8.0	

5.2.5. Vectors

Table 10. List of plasmids.

Name	Description	Reference/supplier
pBluescript II KS+	Cloning Vector, Amp^r	Stratagene
pBC KS+	Cloning Vector, Cam^r	Stratagene
pGEM-T-Easy	Cloning Vector, Amp^r	Promega
PL235	HSV-*TK* gene, MC1 promoter, pBS backbone, Amp^r	Pentao Liu
pKC414	*LacZ*pA-pGK*Neo*pA-cassette, pBS backbone, Amp^r	Kamal Chowdhury
pERλ2	16 kb cont. *Zbtb20* exon 6, pBC KS+, Amp^r	This study
RtV	Homology arms, PL235 backbone, Amp^r	This study
MTV	*LacZ*pA-pGK*Neo*pA-cassette and homology arms, Amp^r	This study
GRV	16 kb cont. *Zbtb20* exon 6, PL235 backbone, Amp	This study
pER4	KO construct for targeted disruption of *Zbtb20*, Amp^r	This study
pER5	RNA-ISH probe for *Zbtb20* exon 6, Amp^r	This study

5.2.6. Oligonucleotides

Table 11. List of oligonucleotides.

Purpose/Name	Direction Tag	Sequence (5' --> 3')	T_A (°C)
Genotyping of *Emx2*_KO mice			
GAB 42		GAACGACACAAGTCCCGAGAGTTTC	65
GAB 45		CTCATATTGCCCTAACAAAGCTGAGC	65
GAB 66		CACGAGACTAGTGAGACGTGCTAC	65
Genotyping of *Zbtb20*_KO mice			
ER_Zbtb_F	Forward	TCACAGCCAAACAGAACTACG	57
ER_Neo_F	Forward	TCTTCTGAGGGGATCAATTCTC	57
ER_Zbtb_R	Reverse	CAAGCTTTGGACCCACACTA	57
*Zbtb20*_KO-construct			
ERzA	Forward *NotI*	CAGTTTTCGCGGCCGCCTATGGGCTTTCTTACAGCGAG	60
ERzB	Reverse *HindIII*	CTGCCAAGCTTAGGCAAAGTCCAGGCTTTTGTG	60
ERzC	Forward *SpeI*	CTACTAGTTTTCTTGTGGATCCATATGAATGC	60
ERzD	Reverse *KpnI*	GAGGTACCGCGCTCGGTCATCCCCTTG	60
ERzE	Forward *XhoI*	TCAACTCGAGAATCAACAGAGCAAGATGATGC	60
ERzF	Reverse *HindIII*	GAGCAAGCTTTGGACCCACAC	60
ERzG	Forward *HindIII*	GAGGAAGCTTCCTTGTAATAAGAATGCCATGC	60
ERzH	Reverse *SpeI*	CCACTAGTACTACTCGGCCTAATAAATGCAC	60
ES-cell screening			
ERz5´extF1(5'probe)	Forward	TCAACATGGCTGAAGTGGAA	55
ERz5´extR1(5'probe)	Reverse	TGCACAGGTGTCCTGGTAAA	55
ERz3´F1 (3'probe)	Forward	AGAAGAAAAGGGCAGCAGGT	55
ERz3´R1 (3'probe)	Reverse	CAACGGATGCATGTGTTTTC	55
Zbtb20-exon 6-probe			
ERzEx6_F	Forward	ATCAGTTGCAAGGGGATGAC	56
ERzEx6_R	Reverse	GGCTGTGAAAGTCTTGTTGC	56

5.2.7. Antibodies

Table 12. List of antibodies.

Name	Origin	Host	Supplier	Dilution
Calretinin (prim. AB)	Human	Rabbit	Dako	1:300
Alexa 488	Rabbit	Goat	Molecular Probe	1:500

5.2.8. Anti-sense probes for ISH

Table 13. Plasmids used for synthesis of the digoxigenin labeled RNA.

Gene symbol and clone Nr.	Size of insert (bp)	Restriction Enzyme	Poly-merase	Reference/ Source
Bmp4	~1000	*EcoRI*	Sp6	Labstock
Ebf3 clone 87	877	*EcoRI*	T3	Image clone 4316932, RZPD, Berlin
Emx2	1400	*EcoRI*	T7	Labstock
Emx1	333	*EcoRI*	Sp6	Labstock
EphB1	800	*EcoRI*	T3	Elizabeth Grove
EST unknown/Clone 19	1081	*EcoRI*	T3	Image clone 1247849, RZPD
Er81	500	*ApaI*	Sp6	Labstock (Victor Tarabykin)
Flrt3 clone 105	726	*EcoRI*	T3	Image clone 3972772, RZPD
Foxg1	unknown	*SfiI*	T7	Labstock Nr. 102703
Grp clone 95	830	*EcoRI*	T3	Image clone 440937, RZPD
Hes5	1300	*HindIII*	T3	Labstock
Id2	766 cDNA	*SalI*	T3	Labstock Nr. 103086
Id3	~1000	*SacII*	T7	Labstock
IGluR7	563	*BglII*	T7	Elizabeth Grove
KA1	3312	*KpnI*	T3	Labstock Nr. 103298
Lhx2	> 1000	*NotI*	T7	Labstock
Mash1	1000	*XhoI*	Sp6	Labstock
Math2	> 700	*EcoRI*	Sp6	Labstock
Nef3 clone 93	~600	*XhoI*	T3	Image clone 385063, RZPD
Neurod1	1074	*HindIII*	T7	Labstock
NK3	2200	*PvuII*	T7	Elizabeth Grove
Nrp2 clone31	675	*EcoRI*	T3	Image clone 3416226, RZPD
Nr4a2 clone 73	417	*EcoRI*	T3	Image clone 1762441, RZPD
Nurr1	~1000	*NcoI*	Sp6	Labstock
Odz3 clone 84	784	*EcoRI*	T3	Image clone 3513892, RZPD
Odz3	1096	*EcoRI*	T7	Dennis D. M. O'Leary
Pax6	1090	*BamHI*	T3	Labstock
Prox1	300	*SacI*	T3	Labstock (Guillermo Oliver)
Svopl clone 97	1845	*EcoRI*	T3	Image clone 851221, RZPD
SCIP	2800	*BamHI*	T7	Elizabeth Grove
Sox2	750	*AccI or SalI*	T3	Labstock
Steel	2170	*XhoI*	T3	Labstock
Wnt3a	150	*EcoRI*	Sp6	Labstock
Zbtb20 clone 26	739	*EcoRI*	T3	Image clone 2236194, RZPD
Zbtb20 (exon 6)	999	*SpeI*	T3	Eva Rosenthal

5.3. Methods

5.3.1. General comments

Unless otherwise specified, experiments were done at room temperature (RT). For centrifugation of volumes up to 2 ml, Eppendorf centrifuges were used and spun at 13,000 rpm. Larger volumes (up to 50 ml) were spun in HS4 rotors in RC50 centrifuge (Sorvall) at up to 7,000 rpm.

5.3.2. Isolation, analysis and manipulation of nucleic acids

5.3.2.1. Analytic isolation of plasmid DNA from *E. coli* cells

Plasmid DNAs (5-15 µg) were isolated from 1.5 ml bacterial cultures by using a commercial Miniprep kit (Qiagen) or by the alkaline lysis method (Sambrook and Russell, 2001).

5.3.2.2. Preparative isolation of plasmid DNA from *E. coli* cells

Plasmid maxiprep DNAs were prepared from 200-500 ml of bacterial cultures by using the commercial Qiagen Maxi columns, as described in the "Plasmid Purification Handbook". Routinely 100-500 µg of plasmid DNA were obtained, dissolved in 200-500 µl of $T_{1/10}E$ (10mM Tris, 0.1 mM EDTA, pH 8.0) and frozen at -20 °C.

5.3.2.3. Determination of concentration of nucleic acids

The concentrations of DNAs and RNAs were determined by using the Nanodrop ND 1000 spectrophotometer (Peclab). 1 µl of the nucleic acid was used for the OD determination. 1 OD_{260} of DNA and RNA represents 50 µg and 40 µg/ml of nucleic acid, respectively. Concentrations of further diluted samples were checked on agarose gels by comparing with standards under UV light.

5.3.2.4. Agarose gel electrophoresis

Agarose gel electrophoresis was performed as described in detail in (Sambrook and Russell, 2001).

Briefly, depending on the sizes of the fragments analyzed, 0.5 – 2.0% agarose gels containing 0.1 µg/ ml Ethidium bromide (Roth) were prepared and run in 1xTBE buffer. Loading buffer (one tenth of the volume) was added to the samples prior to electrophoresis. Analytical gels were photographed under UV light of 258 nm wavelength. For preparative gels (to isolate DNA fragments for cloning), UV light of 366 nm was used.

Loading buffer	
Glycerin	30%
EDTA, pH 8.0	50mM
Bromphenolblue	0.25%
Xylencyanol	0.25%

1xTBE Electrophoresis buffer	
Tris-Cl	89 mM
Boric acid	89 mM
EDTA, pH 8.0	2 mM

5.3.2.5. Ethanol precipitation of DNA

To precipitate DNA, $^{1}/_{25}$ volume of 7.5 M Ammonium acetate and 2.5 volumes of ethanol was added, mixed and stored at -20 °C for at least 2 hours. DNA was pelleted by spinning at 10,000-15,000x g, washed with 75% ethanol and dried. The pellet was dissolved in appropriate volume of $T_{1/10}E$.

5.3.2.6. Phenol-Chloroform extraction

For removal of protein residues from DNA solutions, they were extracted first with equal volume of TE saturated PCI, pH 7.5 – 8.0 (Phenol:Chloroform:Isoamyl alcohol (25:24:1) and then with CI (Chloroform:Isoamyl alcohol (24:1). After vortexing and centrifugation the upper DNA layer was removed and precipitated with ethanol as described above.

5.3.2.7. Isolation of DNA from agarose gels

DNA bands were cut under long wavelength UV light (366 nm) and the DNA was isolated by using the commercial "Qiaquick Gel Extraction Kit" from Qiagen and eluted with 30-50 µl of $T_{1/10}E$ buffer.

5.3.2.8. Isolation of genomic DNA from mouse tail biopsy

Tail DNAs were isolated by digesting the tissue at 55 °C by shaking in 500 µl Proteinase K-lysis buffer overnight. DNAs were precipitated by adding 500 µl of Isopropanol. After mixing by hand, the DNAs were isolated by spinning at 13000x g for 5 minutes, washing with75 % ethanol and drying the pellets at 37 °C. The pellets were subsequently dissolved in 150-200 µl $T_{1/10}E$ at 65 °C for 1 hour and then at 37 °C overnight by gentle shaking.

Lysis buffer	
Tris-Cl pH 8	100 mM
EDTA	5 mM
SDS	0.2%
NaCl	200 mM
Proteinase K	0.5 mg/ ml

Proteinase K-lysis buffer	
Lysis buffer	19 ml
Proteinase K (10 mg/ ml)	1 ml

5.3.2.9. Preparation of genomic DNA from ES cell clones

After electroporation of the knockout construct into the ES-cells (MPI-II), they underwent a positive and negative selection respectively for about 10 days with geneticin (G418) and gancyclovir. Individual ES-cells that survived the selection were picked and separately

grown. While preparing the cryo-stocks of each clone, some cells from each were grown in parallel in 24-well plates without the feeder layers. The screening for the homologous recombination was done by using these ES cell cultures. Genomic DNAs from these ES cell clones were extracted by proteolytic digestion with Proteinase K (0.5 mg/ml) in lysis buffer at 55°C for overnight and then precipitating the genomic DNA with the addition of 0.7x volume Isopropanol onto the lysed samples. After mixing by hand, they were centrifuged for 20 minutes**,** and then the pellets were washed with 70% ethanol and finally dissolved in 100 µl of $T_{1/10}E$. DNAs (10-15 µl of each) were digested with 60-120 units of *KpnI* or *XhoI* in 50 µl final volume overnight at 37 °C and then electrophoresed in agarose gels for southern blotting.

5.3.2.10. Genotyping of mice mutants

For the genotyping of *Emx2*-/- (Pellegrini et al., 1996) or *Zbtb20-/-* mutants tail biopsy DNA was used in a standard master mix (below).

For genotyping *Emx2* mutants the primers GAB 42 (5´-GAA CGA CAC AAG TCC CGA GAG TTC-3´), GAB 45 (5´- CTC ATA TTG CCC TAA CAA AGC TGA GC-3´), GAB 66 (5´-CAC GAG ACT AGT GAG ACG TGC TAC-3´), 1.5 µl DNA and DNA-Polymerase (BioTherm, GeneCraft) 0,6 U/ reaction were used in a 25 µl reaction. The sizes of the wild type and recombined PCR products were of 350 and 450 bp, respectively.

PCR-program *Emx2*	
1. 94 °C	4 min
2. 94 °C	40 sec
3. 65 °C	40 sec
4. 72 °C	40 sec
5. 72 °C	10 min
(Steps 2-4: 30 Cycles)	

PCR reaction	
Buffer (GeneCraft)	1x
$MgCl_2$ (GeneCraft	2 mM
dNTP-Mix (GeneCraft	0.2 mM
Primer 1	0.25 µM
Primer 2	0.25 µM
Primer 3	0.25 µM
DNA	
DNA-Polymerase	

For genotyping *Zbtb20* mutants the primers ER_Zbtb_F (5'-TCA CAG CCA AAC AGA ACT ACG-3´), ER_Neo_F (5'-TCT TCT GAG GGG ATC AAT TCT C-3´), ER_Zbtb_R (5'-CAA GCT TTG GAC CCA CAC TA-3´), 1 µl genomic DNA and GoTaq DNA-Polymerase (Promega) 5 U/ reaction were used in a 20 µl reaction. The sizes of the wild type and recombined PCR products were of 313 and 518 bp respectively.

PCR-program *Zbtb20*
1. 94 °C 2 min
2. 94 °C 30 sec
3. 57 °C 30 sec
4. 72 °C 30 sec
5. 72 °C 5 min
(Steps 2-4: 30 Cycles)

5.3.2.11. Synthesis of radioactively labeled DNA probes

Approximately 50 - 100 ng of DNA fragment was labeled with 50 µCi ^{32}P-dCTP (Amersham) using the "Rediprime II Random Prime Labelling System" (Amersham). The labeling was terminated after 15 minutes at 37 °C by adding 5 µl of 0.2 M EDTA. The non-incorporated nucleotides were removed by spinning the sample through commercial sephadex G-50 minicolumns from Amersham. Radioactivity was measured in Beckman scintillation counter LS1700. Usually a specific activity of 5x 10^8 cpm/ min/ µg was obtained.

5.3.2.12. Southern blot analysis

This method is described in detail in (Sambrook and Russell, 2001). In brief, 10-15 µg of genomic DNA was digested in a total volume of 40 µl with the appropriate enzyme (10 U/ µg DNA) and 2 µl RNase A (1 mg/ ml) at 37 °C overnight, gently shaking. The reaction was electrophorized in a 0.5-0.8% Agarose gels at < 1 V/ cm O/N up to 24 h. The gel aligned with a ruler was briefly photographed under UV light. Dispensable parts of the gel were removed and one edge was cut (for orientation during the blotting procedure) before starting the blotting procedure. The gel was shaken gently in 0.25 M HCl for 15 min, washed briefly in dH_2O, shaken for 40 min in Blot I, washed as before and shaken for 40 min in BlotII. The gel was then treated with 20xSSC, pH 7 for 20 min. In the meantime, a nylon membrane (GeneScreen Hybridization Transfer Membrane, PerkinElmer) was soaked in dH_20 and shaken >10 min in 20xSSC pH 7. The DNA was blotted onto the membrane for 1-2 d and the transferred DNA was UV crosslinked (0.5 J/ cm^2, 312 nm, Fluo link) to the membrane. Radioactively labeled DNA probes were prepared as described earlier. The membrane was put in a hybridization bottle and washed with prewarmed (65 °C) 2xSSC/ 0.5% for 30 min at 65 °C. Prehybridization was performed for 2h at 65 °C with 7 ml prehybridization buffer before the membrane was hybridized O/N at 65 °C with 50 ng radioactively labeled probe. All 65 °C hybridization steps were carried out by gently rotating the bottle. Next day, the membrane was washed twice with prewarmed (65 °C) 2xSSC/ 0.5% SDS for 30 min before being washed with prewarmed (65 °C) 0.1xSSC/ 0.5% SDS for 30 min at 65 °C. The

membrane was allowed to air-dry on a Whatman 3MM paper. Next, the membrane was glued at the corners onto a Whatman 3MM paper and wrapped in Saran wrap. The covered membrane was exposed to an X-ray film (Biomax MR film, Kodak) in a cassette. The exposure time at -70 °C varied according to the strength of the radiolabeled probe (1 to 4 d).

10% SDS
Sodium dodecylsulfate 10% w/v
pH 7.2

Blot I		Blot II	
NaCl	1.5 M	NaCl	1.5 M
NaOH	0.5 M	Tris	1 M
		pH 7.2	

Hybridization buffer

NaCl	750 mM
$NaH_2PO_4xH_2O$	50 mM
EDTA (pH 7.4)	5 mM
SDS	0.5%
Ficoll	0.02%
Polyvinylpyrrolidon	0.02%
BSA	0.02%
Salmon sperm-DNA	50 µg/ml

5.3.2.13. Colony blot

Colony blotting was performed as described in detail (Fritsch et al., 1989). In brief: Bacterial colonies were allowed to grow ca. 2 mm ∅, transferred to nylon membranes and grown for additional 4-5 h. The colonies on the membranes were then disrupted in 10% SDS, denatured (Blot I), neutralized (Blot II) and UV crosslinked.

Hybridization and autoradiography: The membranes were washed at 65 °C for 30 min with 2x SSC/ 0.5 % SDS and prehybridized in the hybridization buffer for 2 h and subsequently hybridized overnight with radioactively labeled *Neo* probe. Washing and autoradiography were done as described earlier for southern/northern blotting.

5.3.3. Cloning DNA fragments

5.3.3.1. Restriction enzyme digestion of DNA

Vector DNA was digested with appropriate restriction enzyme (3-5 Units/ µg Plasmid-DNA) at 37 °C for 1 hour in the buffer supplied with the enzyme. Fragments for cloning were isolated from plasmids after digestion and agarose gel electrophoresis. Linearized plasmid

DNA to be used as cloning vectors (as well as template for preparing digoxigenin labeled probes) were prepared in a similar fashion and isolated from agarose gels.

5.3.3.2. Dephosporylation of linearized vector DNA

When vectors were prepared after digestion with only one restriction enzyme, the cleaved ends were dephosphorylated with calf intestine alkaline phosphatase (CIP) (Roche) according to the manufacturer's protocol. The reaction was stopped by adjusting to 10 mM EDTA, PCI extracted and ethanol precipitated as described earlier. When the vectors were cut with 2 restriction enzymes, they were not dephosphorylated.

5.3.3.3. Preparation of PCR fragments for cloning

Some fragments were PCR amplified from the mouse genomic DNA for subsequent cloning into "pGEM-T Easy" vector (Promega). The generated PCR products were purified using the "QIAquick PCR Purification Kit" (Qiagen) ethanol precipitates and dissolved in 20 - 50 µl of $T_{1/10}E$. Since the PCR products contained 3´A overhangs, they were cloned into T-easy vectors as described by the manufacturer.

Sometimes the PCR primers contained specific restriction sites. In such cases, the PCR fragments were digested with the corresponding enzyme before cloning into appropriate vector.

5.3.3.4. Blunt end cloning

To clone fragments into "blunt end" vectors (for example after cutting with *EcoRV*), 5´overhangs of fragments were filled in with dNTP and Klenow DNA Polymerase(Roche) in a buffer containing 50 µM dNTP; 10 mM $MgCl_2$; 5 Units/ µl Klenow enzyme for 15 minutes. 3´overhangs were removed by digesting with T4-DNA polymerase (15 min at RT; 100 µM dNTP; T4-DNA-Polymerase buffer, Roche). Treated DNAs were purified by PCI extraction and ethanol precipitation.

5.3.3.5. Ligation

The concentration of vectors and inserts were estimated in an agarose gel. The ratio of insert to vector was kept at about 3:1 in the ligation mixture. The ligation was performed at RT overnight.

Ligation (NEB)		Ligation (into pGEM-T Easy Vector)	
Insert	3 (150 ng)	PCR fragment	7 µl
Vector	1µl (50 ng)	T4-ligation buffer (10x)	1 µl
T4-ligation buffer (10x)	2 µl	pGEM-T Easy Vector	1 µl
T4-ligase (2.000 U/µl)	1 µl	T4-ligase	1 µl

5.3.3.6. Preparation of electro-competent bacteria

Single colony of *E. coli* DH5α was inoculated into 5 ml STI (Merck) medium and grown overnight at 37 °C by shaking. This culture was added to 2 l of STI medium and grown until OD_{600} of 0.5-0.6. The culture was then cooled down on ice-water for 15 min and pelleted at 4 °C, 4000x g for 20 min. The pellet was washed 3 times with ice cold sterile water by mixing the pellet and spinning at 4000x g. Finally the pellet was washed once with 10% glycerol and subsequently suspended again in 10% glycerol and frozen as 50 µl aliquots at -80°C.

5.3.3.7. Transformation of *E. coli* by electroporation

Electro competent *E. coli* were thawed on ice and mixed with 5 µl of a ligation reaction or ~1-10 ng plasmid DNA. This suspension was pipetted into an *E. coli* Pulser Cuvette (BioRad). The electroporation was performed using the Gene Pulser (BioRad, capacity: 25 µF, voltage: 1.8 kV, resistance: 200 Ω). An efficient transformation required a pulse length of 3.8 - 4.6 msec. After the electroporation the cells were directly mixed with 1 ml of prewarmed STI medium and incubated for an half an hour shaking at 200 rpm at 37°C. 100 µl and 20 µl of this culture were plated on prewarmed selective STI-agar plates containing either Ampicillin, Tetracyclin or Chloramphenicol, depending on the resistance gene included in the plasmid DNA. The plates were incubated at 37 °C O/N.

5.3.4. Screening of mouse genomic λ-phage library for the isolation of *Zbtb20* exon 6 clones

In order to obtain the desired genomic sequence containing the exon 6 of the *Zbtb20* locus, a λ-phage library (Lambda FIX II library by Stratagene containing genomic DNA of mouse 129/SvJ strain) was screened using a PCR amplification approach. This method is described at the internet site: http://www.methods.info/Methods/Library_screening/library_pcr.pdf. A brief description is presented below. Two individual but distinct λ clones were isolated (λ1 and λ2), both containing the locus of interest. For the generation of the knockout construct, λ2 was chosen, because it contained intronic DNA stretches 5' and 3' flanking exon 6 of adequate

length, 5.4 kb and 9.5 kb respectively. These are the homology regions – they should be long enough (approx. 10 kb total length) to ensure either efficient recombination in ES-cells (Thomas and Capecchi, 1987). The insert of λ2 containing the genomic region of interest was subcloned into a pBC KS vector. The cloning product (pERλ2, Cam^r) (Fig. 16A a) was used to create the targeting vector (see chapter 5.3.8.).

5.3.4.1. Preparation of the host bacteria

E. coli strain XL1-Blue MRA(Stratagene) was grown overnight in 50 ml NZY + 0.2% Maltose medium. Bacteria were pelleted (3000 rpm, 10 min, 4 °C and suspended in 25 ml of ice-cold 10 mM $MgSO_4$ and stored at 4 °C. The OD of the suspension corresponds to OD_{600} = 2.0. The treated bacteria remain competent for infection with lambda phage for ca. 2 weeks.

5.3.4.2. Determination of phage titer

Dilutions of 10^5 - $1:10^9$ fold were prepared from the lambda library in SM buffer for titration. From the number of plaques the amount of infective phages/ ml could be calculated.

SM Buffer	
NaCl	0.1 M
$MgSO_4$	8 mM
Tris-Cl, pH 7.5	0.05 M
Gelatine	0.01%

5.3.4.3. Plating the library

1 µl of the phage dilution was mixed with 200 µl of bacteria, kept for 15 min at RT, mixed with 2.5 - 3 ml of warm (48 °C) top agarose and plated onto 10 cm ∅ petridishes containing NZY+1.5% bactoagar. After solidification of the top agarose, the plates were inverted and incubated at 37°C for 6-8 h until plaques were visible. Phage titer was determined after counting the plaques.

Top agarose: NZY containig 0.2% Maltose and 0.7% Agarose

5.3.4.4. Identification of the appropriate lambda library fraction for screening

Since the library contained 4 different fractions, first the appropriate fraction was identified by PCR screening for the presence of the desired genomic *Zbtb20* fragment. PCR primers

representing the exon 6 of the gene were used for this purpose under the PCR condition as described below:

PCR program "Exon 6"		PCR reaction	(20 µl)
1. 94 °C	2 min	$MgCl_2$	1.5 mM
2. 56 °C	30 sec	dNTP-Mix	0.2 mM
3. 72 °C	90 sec	Forward primer	0.25 pM
4. 94 °C	30 sec	Reverse primer	0.25 pM
5. 72 °C	5 min	DNA	1 µl
(Steps 2-4: 30 cycles)		DNA-Polymerase	0.5 U

Forward -Primer (ERzEx3_F): 5´-ATCAGTTGCAAGGGGATGAC-3´
Reverse -Primer (ERzEx3_R): 5´-GGCTGTGAAAGTCTTGTTGC-3´

5.3.4.5. Screening of the positive library fraction and isolation of the lambda genomic clone for the *Zbtb20* gene as single plaque

The positive fraction was diluted in steps of 2 (2^{-1}-2^{-5}fold). 1 µl of each dilution was screened by the PCR described above. The dilution showing barely visible PCR band was determined and 1 µl of the next lower dilution was mixed with 1 ml of SM and 1 ml of competent XL1-Blue MRA cells. After 15 min, 18 ml of NZY + 0.2% Maltose medium was added to it, mixed and distributed into 8x8 wells of a 96 well microtiter plate as 100 µl aliquots. The plate was sealed with parafilm and shaken at 200-300 rpm overnight in 37 °C room. Next day, 20 µl aliquots from each row and columns were pooled, diluted 1:1 with water and analyzed by PCR (16 reactions). The positives pools were then screened individually and thus the individual positive well was identified. The phages from this well were rescreened several more times as above until almost all wells were positive.

5.3.4.5. Isolation of single *Zbtb20* positive plaques

Phages from the above mentioned positive well were diluted, mixed with competent bacteria and plated. Single plaques were picked, suspended in SM buffer and 1 µl aliquot was analyzed by PCR. After identification of such single positive plaques, the remaining amount of the phage suspension was used to generate a high titer stock and lambda DNA as described in (Sambrook and Russell, 2001)

5.3.5. RNA-in situ-Hybridization

All solutions (except Tris buffer) were treated with 0.1% DEPC at 37 °C and autoclaved next day. Tris buffers were autoclaved.

5.3.5.1. Synthesis of DIG labeled probes

Appropriate linearized plasmid DNAs (Table 13) were used for the synthesis of digoxigenin labeled cRNA probes by in vitro transcription method (Roche). The reaction mix (20 µl) contained 1 µg of the template DNA and T3/T7 RNA polymerase at 37 °C for 2 h or SP6 RNA polymerase at 40 °C for 2 h.

In vitro-Transcription mix (20 µl)	
Transcription buffer (Roche)	1x
DIG RNA Labeling Mix (Roche)	1 mM (each) ATP, CTP, GTP and 0.65 UTP/ DIG-11-UTP)
RNase-Inhibitor (RNasin, Promega)	20 units
RNA-Polymerase (Sp6, T3, T7; Promega)	20 units

After 2 h, the template DNA was digested with 2 µl (1 U/ µl) DNase (RQ1-DNase, Promega) for 10 min at 37 °C, 2 µl 0.2 M EDTA was added and the cRNA was precipitated by adding 2.5 µl 4 M LiCl and 75 µl Ethanol for 2 h at -80 °C. The RNA was recovered by centrifugation, dissolved in 100 µl DEPC treated water and aliquot was checked for its integrity in agarose gels (1%).

5.3.5.2. RNA-in situ-Hybridization (Moorman et al., 2001)

RNA in situ hybridizations was performed on 16-20 µm cryosections. All incubations are at room temperature (RT) unless mentioned otherwise.

After thawing the sections, they were fixed in 4% PFA for 15 minutes and then washed twice with 1X PBS for 5 minutes each. The proteolytic digestions were done with Proteinase K (10 µg/ml) at 37°C for 3 minutes. This permeabilization of sections was stopped with 0.2% Glycine (in PBS) and then they are washed twice with 1X PBS for 5 minutes each. Afterwards, they were post-fixed with 0.2% Glutaraldehyde/4% PFA (in PBS) for 20 minutes. They were again washed twice with 1x PBS for 5 minutes each, and then prehybridization solution was put onto them. After 2 hours of incubation at 70°C, the prehybridization solutions were replaced with hybridization solutions (prehybridization solution together with the denatured DIG-labeled RNA probes). Hybridizations were done overnight at 70°C.

Next day, the hybridization solutions were discarded, and sections were washed three times with 2x SSC (pH 4.5) /50% Formamide solutions at 65°C for 30 minutes each. Afterwards, they were washed twice with KTBT solution for 10 minutes each, and then

blocking solution was put onto them. After 2 hours of incubation, the blocking solutions were replaced with the antibody solutions (1:2000 anti-DIG antibody in blocking solution) for an overnight incubation at +4°C.

On the third day, the antibody solutions were discarded, and the sections were washed with KTBT solution for three times of 5 minutes each and a further 3 times of 30 minutes each. Afterwards, they are washed three times with NTMT solution for 5 minutes each. The color development reactions were started by adding the NBT-BCIP solution (from Roche) in NTMT (1:50) onto the sections. After obtaining satisfactory staining, the color development reactions were stopped by four times washing with PBT for 5 minutes each. Then the slides were mounted with Mowiol, and the pictures were taken under a light microscope with a digital camera (SZX-12 Olympus).

For all the ISH analyses done, proper controls with "sense" probes were done. No signals for any of these "sense" groups were observed.

5.3.5.3. Solutions used in ISH

All solutions used in the first day of ISH were prepared by DEPC (Sigma) treated solutions in order to prevent the RNase contamination. * indicates that the final concentrations of the ingredients are given.

Prehybridization solution*

50%	Formamide
5X	SSC
1% (w/v)	Blocking powder
1 mg/ml	Yeast tRNA
0.1% (w/v)	CHAPS
0.1% (v/v)	Tween-20
5mM	EDTA (pH 8.0)
0.1 mg/ml	Heparin

KTBT solution*

50 mM	Tris-Cl pH 7.5
150 mM	NaCl
10 mM	KCl
1% (v/v)	Tween-20

Blocking reagent*

80%	KTBT
20%	Sheep serum

NTMT solution*

100 mM	Tris-Cl pH 9.5
100 mM	NaCl
50 mM	MgCl2
0.1%	Tween-20
240 mg/ l	Tetramisol Hydrochlorid

Mowiol

9.6 g	Mowiol 4-88
24 g	Glycerol
24 ml	water (Millipore)
48 ml	Tris-Cl pH 8.5 200 mM

PBT*

1X	PBS
0.1%	Tween 20

5.3.6. Histological methods

5.3.6.1. Cryosections

Whole embryos or embryonic/postnatal brains were fixed in cold PFA (4 % in PBS) for appropriate time (see below). The tissues were then washed in cold PBS (2x30 min), stored in Sucrose (25% in PBS) for cryoprotection until sinking. Then they were frozen in tissue freezing medium (Leica) on dry ice. Cryosectioning was done with Cryostat S3000 (Leica) and transferred onto Super frost plus slides (Menzel-Gläser). After drying on a heating plate at 28 °C, the slides were stored at –20 °C.

Embryo E10.5	1 h fix	Brain E14.5	2 h fix
Embryo E12.5	3 h fix	Brain E16.5	2 – 2.5 h fix
		Brain E18.5	3 h fix
		Brain adolescent/adult	O/N fix

5.3.6.2. Paraffin sections

Briefly, dissected postnatal or embryonic mouse brains were fixed overnight in 4% PFA. In the following, each incubation step lasted one day or 1 h for postnatal or embryonic brains respectively. The brains were washed in 0.86% NaCl. Dehydration of brains was done through increasing Ethanol solutions (50%, 70%, 80%, 90%, 96%, and 100%). After incubation in Isopropanol, they were transferred into Toluol. All the incubations before Toluol were done at 4 °C, and Toluol at room temperature. Afterwards, brains were transferred into melted Paraplast (Tycon Healthcare) at 60°C. This step was repeated. The brains were then embedded into paraffin blocks for coronal sectioning with Microtome (Leica Instruments). 16 µm thick sections were prepared and transferred onto Super frost plus slides (Menzel-Gläser), which were air-dried O/N at 37 °C. Until usage, the slides were stored at 4 °C.

5.3.6.3. Gelatine albumin sections

LacZ stained embryos were PFA fixed, washed. To embed them in a gelatine/albumin mix first a form was built. Two L-shaped metal blocks were assembled on a glass plate to give rise to an inner cubic space of 1.5 cm side length. Excess liquid was removed from the embryos. In a small weighing boat 2 ml of the gelatine/albumin mix and 160 µl of 25% Glutaraldehyde were rapidly mixed and quickly poured into the space. After a short moment the embryo was placed onto the solidifying, still liquid surface. Fresh embedding mixture was prepared as

before and quickly poured onto the embryo to cover it bubble-free between the two phases. The embryo containing block was allowed to harden for a while before disassembly of the blocks. The sample was wrapped in Saran wrap to prevent it from drying out. After 15 min the sample could be cut or alternatively stored for 1-2 d at 4 °C until use. 3-300 µm sections prepared with Vibratome were transferred onto Super frost plus slides (Menzel-Gläser). The sections were mounted in Mowiol.

Gelatine/albumin mix	
Gelatine	0.98 g
PBS	200 ml
Albumin Bovine	60 g
Saccharose	40 g
(aliquots were stored at –20 °C)	

Embedding mixture (per layer)	
Gelatine/albumin mix	2 ml
Glutaraldehyde 25%	160 µl

5.3.6.4. Cresyl violet (Nissl) staining

By this method by Franz Nissl (1894) basophil components as RNA and DNA are stained in blue or violet. Therefore, only cell bodies, containing nuclei and ribosomes will be marked. The Nissl stain was carried out on Paraffin sections. For dewaxing, the sections were kept 3 times for 3 min each in Histoclear XEM200 (Vogel GmbH, Giessen) and subsequent incubations in decreasing Ethanol solutions (100%, 96%, 90%, 80%, 70%, 50%) for 3 min each. After storage in dH_2O for 2 min the sections were stained in Cresyl violet (0.5%) for 4 min. After a short dip in dH_2O they were placed in fresh dH_2O for 2 min. After 3 min incubation steps in Ethanol (50%, 70%, 80%), the sections were briefly dipped in 90% Ethanol/Acetic Acid (250:1), followed by increasing Ethanol solutions (90%, 96% and 100%) for 3 min each. After two incubations 3 min each in Histoclear, the samples were kept in Histoclear until mounted in Eukitt (O. Kindler GmbH).

5.3.6.5. Golgi staining

Modified Golgi-Cox impregnation of neurons was performed using specifications described in the FD Rapid GolgiStain Kit (FD Neurotechnologies). In brief, hemispheres from P20 mouse brains were immersed in impregnation solution for 3 weeks, transferred to “Solution C“ for 4 days, transferred in precooled (-80 °C) 2-Methylbutane (Sigma) and cut at 100 µm on the cryostat. Sections were mounted on superfrost plus slides (Menzel-Gläser) and dried for 2 weeks in prior to staining with silver nitrate solution “Solution D and E”. The sections were dehydrated and mounted with Eukitt (Kindler).

5.3.6.6. Skeletal preparations and staining

Skeletal preparations were made by an alcian blue/ alizarin red procedure (Kessel and Gruss, 1991), staining cartilage in blue and ossified tissue containing calcium in red. Pre- or postnatal mice were eviscerated, fixed in 100% ethanol for four days, kept in aceton for three days and rinsed with water. They were stained for three days in staining solution. After 3 washing steps, the specimens were kept in 20% glycerol/ 1% KOH at 37 °C for not longer than 16 h, and then at RT until tissue had completely cleared. For storage specimens were transferred into 50%, 80% and finally 100% glycerol.

Staining solution	
0.3% Alcian Blue 8GX (Sigma) in 70% ethanol	1 volume
0.1% Alizarin Red S (Sigma) in 95% ethanol	1 volume
100% Acetic acid	1 volume
Ethanol	17 volumes

5.3.7. Histochemical methods

5.3.7.1. β-Galactosidase enzyme histochemistry

LacZ reporter gene activity was analyzed in transgenic mice (Gossler and Zachgo, 1993). Adult brains (see below) or whole embryos were isolated and washed in PBS. Fixation was performed according to the stage or age of the tissue at 4 °C (see below). Adult mouse brains were prefixed for 1 h at 4 °C before being sliced into 1 mm coronal or sagittal sections with a brain slicer (MPI workshop). Brain sections were fixed for 1 h more. Embryos E13.5 and older were cut in half after half of the incubation time. Samples were washed twice for 20 min each in PBS (RT) and transferred into the staining solution where they were kept O/N at 30 °C, protected from light. After complete staining, the reaction was stopped by two washes in PBS at 20 min each. Tissues were cleared by subsequent incubations in increasing concentrations of glycerin solution (15%, 30%, 50% and 80% in PBS) at 4 °C O/N each. Tissues were stored in 80 or 100% glycerol in PBS.

E8.5	20 min FixA	E12.5	50 min FixB
E9.5-10.5	30 min FixA	E13.5	2x 30 min FixB
E11.5	40 min FixB	brain	2x 1 h

Fixing solution A	
Formaldehyde	1%
Glutaraldehyde	0.2%
Nonidet P-40	0.02%
in 1xPBS	

Fixing solution B	
Formaldehyde	1%
Glutaraldehyde	0.2%
Nonidet P-40	0.1%
Na deoxycholat	0.001%
in 1xPBS	

X-gal-staining solution	
X-gal	0.1 %
$K_3Fe(CN)_6$	5 mM
$K_4Fe(CN)_6$	5 mM
$MgCl_2$	1 mM
in 1xPBS	

5.3.7.2. Immunohistochemistry

Cryosections were washed 3 times for 5 min in PBT (PBS/0.1% Triton 100) and then they were blocked for 1 h in blocking solution (10% FCS in PBT). Diluted primary antibodies were incubated on the slides O/N at 4 °C in blocking solution. After 3 washes for 5 min in PBT the sections were incubated with the secondary antibodies in blocking solution for 1 h at RT. After washing the sections in PBT as before, they were mounted with Vectashield mounting-medium (Vector) containing DAPI as nuclear counterstain. The mounted sections were stored at 4 °C, protected from light.

5.3.8. Generation of the *Zbtb20* knockout construct via recombineering

To generate *Zbtb20* deficient mice, a knockout (KO) targeting vector was designed. This vector was created using a method referred to as recombineering (recombination mediated genetic engineering) or recombinogenic engineering (Liu et al., 2003; Muyrers et al., 2001; Warming et al., 2005). Recombineering is a method based on homologous recombination in *E. coli* using recombination proteins provided from a defective prophage in the bacterial genome. This defective prophage expresses the recombination genes *exo*, *bet* and *gam* from the λ*P*L promoter, which is under the control of the temperature-sensitive repressor *cI*857. *exo* encodes a 5'-3' exonuclease (Exo) that creates single-stranded overhangs on introduced linear DNA, *bet* encodes a pairing protein (Beta) which protects these overhangs and promotes the subsequent recombination process and *gam* encodes for the Gam protein that prevents degradation of linear DNA by inhibiting *E. coli* RecBCD protein. Bacteria containing the prophage do not express recombination proteins, when kept at 32 °C. But after a short heat-shock at 42 °C (induction), these recombination proteins are produced. Now, linear DNA containing 300-500 bp homology at 5' and 3' ends of the target DNA (already present in the bacteria) can be electroporated in the cells. Subsequently, homologous recombination occurs between this linear DNA and the target molecule.

5.3.8.1. The cloning strategy

The generation of the *Zbtb20* targeting construct required two sequential recombineering steps, referred to as “retrieving” and “first targeting” utilizing two vectors, the “retrieval plasmid” and the “mini-targeting vector”, respectively. For the construction of these vectors, primers were designed. The sequences of these primers are listed in Table 11.

In the first step, called “retrieving”, the 16 kb genomic fragment of including the target region (exon 6 of *Zbtb20* gene) was subcloned via recombineering from the pERλ2 plasmid into the “retrieval vector” (PL253) which produced the “gap repaired vector” (GRV) (see also Fig. 16). Ultimately, in this step, the *MC1-TK* cassette serving for negative selection in ES-cells was cloned at the 3' end of the genomic fragment.

In the next step “first targeting” was made using the mini-targeting vector: A *LacZ*polyA-*pGKNeo*polyA-cassette including polylinker was inserted 12 bp downstream of exon 6 start codon, hence placing the *LacZ* gene in frame with the translation start of exon 6. The *LacZ* gene facilitates β-galactosidase expression and serves as a reporter gene while the *Neo* gene makes ES-cells resistant to geneticin (G418).

5.3.8.2. Generation of the “retrieval vector”

For the retrieval vector (RtV), the region 5'-homology-exon 6-3'-homology was subcloned (retrieved) into the pBluescript-derived PL253, the first step in the construction of the gene targeting vector. PL253 contained a MC1-driven Thymidine Kinase (*TK*) cassette for negative selection in ES-cells. First, two ~400 bp DNA stretches located at the utmost border of 5' and 3' homology arms of pERλ2 were PCR amplified. At the ends of these fragments, “AB” (394 bp) and “GH” (348 bp), additional RE-sites, *NotI*/*HindIII* and *HindIII*/*SpeI*, were introduced. Ultimately, these fragments marked the endpoints of the region to be subsequently subcloned into PL253, thereby determining the length of the 5' and 3' homology.

For removing the template, the PCR fragments AB and GH were purified in a 1.5% agarose gel and extracted using Qiaquick extraction Kit protocol. The purified PCR fragments “AB” and “GH” were double-digested with enzymes *NotI*/*HindIII* and *HindIII*/*SpeI*, respectively. Vector PL253 was cleaved with *NotI* and *SpeI*. Thereupon, the purified components, fragments AB, GH and PL253 were ligated to generate RtV, which was subsequently *HindIII*-linearized, resulting in a double-strand break, the prerequisite for gap repair.

5.3.8.3. Generation of the “mini-targeting vector” (MTV)

Using pERλ2 as template, two 200-300 bp DNA stretches were PCR amplified from left and right homology region, flanking exon 6. The four primers were designed to include additional RE-sites to produce fragments “CD” (288 bp) and “EF” (228 bp) with introduced *SpeI*, *KpnI* or *XhoI* sites, respectively. After gel purification, CD and EF were respectively double

digested with *SpeI* and *KpnI* or *XhoI* and *HindIII*. In parallel, the vector KC414, which included a *LacZ*/*Neo*-cassette, was *KpnI*/*XhoI* cut. Thereby, a 5 kb fragment containing the cassette, was released and isolated. For the generation of the vector-backbone of the MTV, a pBSII SK+ was *SpeI*/*HindIII* digested and the linearized plasmid isolated. The four cleaved and purified components: fragments CD and EF, the 5kb *LacZ*/*Neo*-cassette, as well as the linear pBSII SK+ were combined in a single ligation reaction to produce the MTV. The *LacZ*/*Neo* cassette plus fragments CD and EF were excised by *NotI* and *SalI* digestion, releasing the targeting cassette.

5.3.8.4. Transformation of pERλ2 into the recombinogenic *E. coli* stain DY380 (Tet)

For each transformation the electrocompetent recombinogenic bacterial cells were prepared freshly. DY380 cells were grown O/N in 5 ml STI^{Tet} at 32 °C shaking. The O/N culture was diluted 1:50 in 25 ml STI^{Tet} and the bacteria were grown for further 3-5 h, till they had reached an OD_{600} of 0.6. Then the cells were cooled down in an ice/waterbath for a few minutes and spun down in 50 ml Falcon™ tubes at 5,000 rpm and 0 °C for 5 minutes. Cells were washed by resuspending the cell pellet in 1 ml of ice-cold 10% glycerol while the tube was moved gently through an ice-slurry. After transfer into a 1.5 ml tube, and centrifugation for 20 sec at 13,000 and 0 °C, the supernatant was removed. This washing-step was once repeated and the cell pellet was resuspended in the residual amount of 10% glycerol (~50 µl). The cells were mixed with 1 ng pERλ2 and incubated on ice for 5 min. The electroporation was carried out at 200 Ω, 1.8 kV, 25 µF. After the transformation the bacteria were transferred into 1 ml STI medium and incubated at 32 °C in a shaking heat block for 1 h. Finally the bacteria were plated on STI^{Cam} selective medium and incubated at 32 °C for 18-24 hours. Several colonies were analyzed by restriction digestion.

5.3.8.5. Retrieving

DY380 bacteria containing the target plasmid pERλ2 were cultured as described above, except that $STI^{Tet/Cam}$ medium was used. When the culture reached an OD_{600} of 0.6 on next day, 10 ml were transferred into a 50 ml Falcon™ tube and incubated shaking at 42 °C for 15 minutes. This heat shock enabled the bacteria to produce a sufficient amount of recombination proteins for the subsequent homologous recombination. The rest of the bacteria served as a control and was put back at 32 °C. Both heat shock-induced and the uninduced cultures were cooled down by gently shaking them in an ice/waterbath for a few minutes, washed and

transformed as described above using 40 ng of the *HindIII*-linearized retrieval vector RtV. After 1 h incubation at 32 °C in 1 ml STI medium, bacteria were selected on STI^{Amp} plates, which were incubated at 32 °C for 18 to 24 hours. Clones harboring the recombinant gap-repaired vector (GRV) were identified by a specific 527 bp *NotI*/*SpeI* band.

5.3.8.6. Targeting

DY380 bacteria containing the gap-repaired vector (GRV) were cultured as described above, except that $STI^{Tet/Amp}$ was used. The cells were made electrocompetent and were heat-shock induced as described in the "Retrieving" paragraph. 200 ng of the targeting cassette (*LacZ*/*Neo*) were electroporated into the cells. After recovery, the bacteria were plated on STI^{Amp} plates. Colonies positive for the resulting KO-construct (pER4) were identified using the "colony blot" protocol and a *Neo* specific probe. For generation of the probe a 1.4 kb *SpeI*/*XhoI* fragment from *lacz*polyA-pGK*Neo*polyA-cassette (KC414 vector) was isolated.

5.3.9. Gene targeting in mouse ES cells and production of chimeras

The *Zbtb20* KO targeting vector (pER4) was subsequently linearized with *NotI* (digestion O/N), and a phenol/chloroform extraction and ethanol precipitation was carried out. 40 µg of the vector was electroporated into the MPI-II ES cells. ES cells were subjected to positive/negative selection with G418 and gancyclovir (Ganc) respectively. Exposure to G418 and ganciclovir (Ganc) only allowed the survival of ES cells harboring the *Neo* cassette but not those containing the *TK* cassette. These were theoretically the candidates, which had undergone a targeted homologous recombination. Electroporation, selection and culture of the ES cells was carried out at the departmental cell culture facility by Sharif Mashur. The $G418^r$ $Ganc^r$ selected ES cell colonies were picked for southern analysis to confirm targeted insertion of the KO construct. Positive ES cells were used to generate chimeras. The ES cells were aggregated with diploid CD1 morula-stage embryos and cultured to the blastocyst-stage. The aggregated blastocyst was transferred into the oviduct of pseudopregnant female recipient mice. Aggregation and oviduct transfer was performed at the departmental animal house facility by Ulrich Franke. Chimeric mice, which gave germline transmission, were used for subsequent matings.

References

Alcamo, E.A., Chirivella, L., Dautzenberg, M., Dobreva, G., Farinas, I., Grosschedl, R., and McConnell, S.K. (2008). Satb2 regulates callosal projection neuron identity in the developing cerebral cortex. Neuron *57*, 364-377.

Altman, J. (1969). Autoradiographic and histological studies of postnatal neurogenesis. IV. Cell proliferation and migration in the anterior forebrain, with special reference to persisting neurogenesis in the olfactory bulb. J Comp Neurol *137*, 433-457.

Altman, J., and Bayer, S.A. (1990a). Migration and distribution of two populations of hippocampal granule cell precursors during the perinatal and postnatal periods. J Comp Neurol *301*, 365-381.

Altman, J., and Bayer, S.A. (1990b). Mosaic organization of the hippocampal neuroepithelium and the multiple germinal sources of dentate granule cells. J Comp Neurol *301*, 325-342.

Altman, J., and Bayer, S.A. (1990c). Prolonged sojourn of developing pyramidal cells in the intermediate zone of the hippocampus and their settling in the stratum pyramidale. J Comp Neurol *301*, 343-364.

Altman, J., and Das, G.D. (1965a). Autoradiographic and histological evidence of postnatal hippocampal neurogenesis in rats. J Comp Neurol *124*, 319-335.

Altman, J., and Das, G.D. (1965b). Post-natal origin of microneurones in the rat brain. Nature *207*, 953-956.

Andersen, P. (2007). The hippocampus book (Oxford, Oxford University Press).

Angevine, J.B., Jr. (1965). Time of neuron origin in the hippocampal region. An autoradiographic study in the mouse. Exp Neurol Suppl, Suppl 2:1-70.

Arlotta, P., Molyneaux, B.J., Chen, J., Inoue, J., Kominami, R., and Macklis, J.D. (2005). Neuronal subtype-specific genes that control corticospinal motor neuron development in vivo. Neuron *45*, 207-221.

Assimacopoulos, S., Grove, E.A., and Ragsdale, C.W. (2003). Identification of a Pax6-dependent epidermal growth factor family signaling source at the lateral edge of the embryonic cerebral cortex. J Neurosci *23*, 6399-6403.

Bakker, J., De Mees, C., Douhard, Q., Balthazart, J., Gabant, P., Szpirer, J., and Szpirer, C. (2006). Alpha-fetoprotein protects the developing female mouse brain from masculinization and defeminization by estrogens. Nat Neurosci *9*, 220-226.

Bani-Yaghoub, M., Tremblay, R.G., Lei, J.X., Zhang, D., Zurakowski, B., Sandhu, J.K., Smith, B., Ribecco-Lutkiewicz, M., Kennedy, J., Walker, P.R., *et al.* (2006). Role of Sox2 in the development of the mouse neocortex. Dev Biol *295*, 52-66.

Bannerman, D.M., Rawlins, J.N., McHugh, S.B., Deacon, R.M., Yee, B.K., Bast, T., Zhang, W.N., Pothuizen, H.H., and Feldon, J. (2004). Regional dissociations within the hippocampus--memory and anxiety. Neurosci Biobehav Rev *28*, 273-283.

Barna, M., Hawe, N., Niswander, L., and Pandolfi, P.P. (2000). Plzf regulates limb and axial skeletal patterning. Nat Genet *25*, 166-172.

Barnicot, N.A. (1941). Studies on the factors involved in bone absorption I. The effect of subcutaneous transplantation of bones of the Grey-Lethal house mouse into normal hosts and of normal bones into Grey-Lethal hosts. American Journal of Anatomy *68*, 497-531.

Bateson, W. (1894). Materials for the study of variation treated with special regard to discontinuity in the origin of species (London, Macmillan).

Baumgartner, S., Martin, D., Hagios, C., and Chiquet-Ehrismann, R. (1994). Tenm, a Drosophila gene related to tenascin, is a new pair-rule gene. Embo J *13*, 3728-3740.

Bayer, S.A. (1980). Development of the hippocampal region in the rat. I. Neurogenesis examined with 3H-thymidine autoradiography. J Comp Neurol *190*, 87-114.

Bayer, S.A., and Altman, J. (1975). The effects of X-irradiation on the postnatally-forming granule cell populations in the olfactory bulb, hippocampus, and cerebellum of the rat. Exp Neurol *48*, 167-174.

Ben-Zur, T., Feige, E., Motro, B., and Wides, R. (2000). The mammalian Odz gene family: homologs of a Drosophila pair-rule gene with expression implying distinct yet overlapping developmental roles. Dev Biol *217*, 107-120.

Bi, W., Huang, W., Whitworth, D.J., Deng, J.M., Zhang, Z., Behringer, R.R., and de Crombrugghe, B. (2001). Haploinsufficiency of Sox9 results in defective cartilage primordia and premature skeletal mineralization. Proc Natl Acad Sci U S A *98*, 6698-6703.

Bishop, K.M., Goudreau, G., and O'Leary, D.D. (2000). Regulation of area identity in the mammalian neocortex by Emx2 and Pax6. Science *288*, 344-349.

Blackstad, T.W., Brink, K., Hem, J., and Jeune, B. (1970). Distribution of hippocampal mossy fibers in the rat. An experimental study with silver impregnation methods. J Comp Neurol *138*, 433-449.

Braak, H., and Braak, E. (1998). Evolution of neuronal changes in the course of Alzheimer's disease. J Neural Transm Suppl *53*, 127-140.

Britanova, O., Akopov, S., Lukyanov, S., Gruss, P., and Tarabykin, V. (2005). Novel transcription factor Satb2 interacts with matrix attachment region DNA elements in a tissue-specific manner and demonstrates cell-type-dependent expression in the developing mouse CNS. Eur J Neurosci *21*, 658-668.

Britanova, O., de Juan Romero, C., Cheung, A., Kwan, K.Y., Schwark, M., Gyorgy, A., Vogel, T., Akopov, S., Mitkovski, M., Agoston, D., *et al.* (2008). Satb2 is a postmitotic determinant for upper-layer neuron specification in the neocortex. Neuron *57*, 378-392.

Britz, O., Mattar, P., Nguyen, L., Langevin, L.M., Zimmer, C., Alam, S., Guillemot, F., and Schuurmans, C. (2006). A role for proneural genes in the maturation of cortical progenitor cells. Cereb Cortex *16 Suppl 1*, i138-151.

Brodmann, K. (1909). Vergleichende Lokalisationslehre der Großhirnrinde (Leipzig, Barth).

Brown, T.A., and McKnight, S.L. (1992). Specificities of protein-protein and protein-DNA interactions of GABP alpha and two newly defined ets-related proteins. Genes Dev *6*, 2502-2512.

Bulchand, S., Grove, E.A., Porter, F.D., and Tole, S. (2001). LIM-homeodomain gene Lhx2 regulates the formation of the cortical hem. Mech Dev *100*, 165-175.

Cameron, H.A., and McKay, R. (1998). Stem cells and neurogenesis in the adult brain. Curr Opin Neurobiol *8*, 677-680.

Campbell, K. (2003). Dorsal-ventral patterning in the mammalian telencephalon. Curr Opin Neurobiol *13*, 50-56.

Cecchi, C., and Boncinelli, E. (2000). Emx homeogenes and mouse brain development. Trends Neurosci *23*, 347-352.

Chen, H., Bagri, A., Zupicich, J.A., Zou, Y., Stoeckli, E., Pleasure, S.J., Lowenstein, D.H., Skarnes, W.C., Chedotal, A., and Tessier-Lavigne, M. (2000). Neuropilin-2 regulates the development of selective cranial and sensory nerves and hippocampal mossy fiber projections. Neuron *25*, 43-56.

Chen, H., Chedotal, A., He, Z., Goodman, C.S., and Tessier-Lavigne, M. (1997). Neuropilin-2, a novel member of the neuropilin family, is a high affinity receptor for the semaphorins Sema E and Sema IV but not Sema III. Neuron *19*, 547-559.

Ciani, L., and Salinas, P.C. (2005). WNTs in the vertebrate nervous system: from patterning to neuronal connectivity. Nat Rev Neurosci *6*, 351-362.

Cook, E.H. (1990). Autism: review of neurochemical investigation. Synapse *6*, 292-308.

Copeland, N.G., Jenkins, N.A., and Court, D.L. (2001). Recombineering: a powerful new tool for mouse functional genomics. Nat Rev Genet *2*, 769-779.

Costoya, J.A. (2007). Functional analysis of the role of POK transcriptional repressors. Brief Funct Genomic Proteomic *6*, 8-18.

Danglot, L., Triller, A., and Marty, S. (2006). The development of hippocampal interneurons in rodents. Hippocampus *16*, 1032-1060.

DeFelipe, J. (1997). Types of neurons, synaptic connections and chemical characteristics of cells immunoreactive for calbindin-D28K, parvalbumin and calretinin in the neocortex. J Chem Neuroanat *14*, 1-19.

DeLuca, H.F. (1988). The vitamin D story: a collaborative effort of basic science and clinical medicine. Faseb J *2*, 224-236.

Doetschman, T.C., Eistetter, H., Katz, M., Schmidt, W., and Kemler, R. (1985). The in vitro development of blastocyst-derived embryonic stem cell lines: formation of visceral yolk sac, blood islands and myocardium. J Embryol Exp Morphol *87*, 27-45.

Ducy, P. (2000). Cbfa1: a molecular switch in osteoblast biology. Dev Dyn *219*, 461-471.

Ducy, P., Schinke, T., and Karsenty, G. (2000). The osteoblast: a sophisticated fibroblast under central surveillance. Science *289*, 1501-1504.

Friedman, G.C., and O'Leary, D.D. (1996). Eph receptor tyrosine kinases and their ligands in neural development. Curr Opin Neurobiol *6*, 127-133.

Fritsch, E.F., Sambrook, J., and Maniatis, T. (1989). Molecular Cloning (Cold Spring Harbor Laboratory Press).

Frodl, T., Meisenzahl, E.M., Zetzsche, T., Born, C., Groll, C., Jager, M., Leinsinger, G., Bottlender, R., Hahn, K., and Moller, H.J. (2002). Hippocampal changes in patients with a first episode of major depression. Am J Psychiatry *159*, 1112-1118.

Furuta, Y., Piston, D.W., and Hogan, B.L. (1997). Bone morphogenetic proteins (BMPs) as regulators of dorsal forebrain development. Development *124*, 2203-2212.

Gaarskjaer, F.B. (1978). Organization of the mossy fiber system of the rat studied in extended hippocampi. II. Experimental analysis of fiber distribution with silver impregnation methods. J Comp Neurol *178*, 73-88.

Gabant, P., Forrester, L., Nichols, J., Van Reeth, T., De Mees, C., Pajack, B., Watt, A., Smitz, J., Alexandre, H., Szpirer, C.*, et al.* (2002). Alpha-fetoprotein, the major fetal serum protein, is not essential for embryonic development but is required for female fertility. Proc Natl Acad Sci U S A *99*, 12865-12870.

Galceran, J., Miyashita-Lin, E.M., Devaney, E., Rubenstein, J.L., and Grosschedl, R. (2000). Hippocampus development and generation of dentate gyrus granule cells is regulated by LEF1. Development *127*, 469-482.

Gaur, T., Lengner, C.J., Hovhannisyan, H., Bhat, R.A., Bodine, P.V., Komm, B.S., Javed, A., van Wijnen, A.J., Stein, J.L., Stein, G.S., *et al.* (2005). Canonical WNT signaling promotes osteogenesis by directly stimulating Runx2 gene expression. J Biol Chem *280*, 33132-33140.

Gilbert, S.F. (2006). Developmental Biology, 8 edn (Massachusetts, Sinauer Associates, Inc.).

Göllner, H., Dani, C., Phillips, B., Philipsen, S., and Suske, G. (2001). Impaired ossification in mice lacking the transcription factor Sp3. Mech Dev *106*, 77-83.

Gossler, A., and Zachgo, J. (1993). Gene and enhancer trap screen in ES cell chimeras, Gene Targeting: A Practical Approach (Oxford, Oxford University Press).

Götz, M., and Huttner, W.B. (2005). The cell biology of neurogenesis. Nat Rev Mol Cell Biol *6*, 777-788.

Götz, M., Stoykova, A., and Gruss, P. (1998). Pax6 controls radial glia differentiation in the cerebral cortex. Neuron *21*, 1031-1044.

Gould, E. (2007). How widespread is adult neurogenesis in mammals? Nat Rev Neurosci *8*, 481-488.

Graham, V., Khudyakov, J., Ellis, P., and Pevny, L. (2003). SOX2 functions to maintain neural progenitor identity. Neuron *39*, 749-765.

Greco, T.L., Takada, S., Newhouse, M.M., McMahon, J.A., McMahon, A.P., and Camper, S.A. (1996). Analysis of the vestigial tail mutation demonstrates that Wnt-3a gene dosage regulates mouse axial development. Genes Dev *10*, 313-324.

Grove, E.A., Tole, S., Limon, J., Yip, L., and Ragsdale, C.W. (1998). The hem of the embryonic cerebral cortex is defined by the expression of multiple Wnt genes and is compromised in Gli3-deficient mice. Development *125*, 2315-2325.

Gulisano, M., Broccoli, V., Pardini, C., and Boncinelli, E. (1996). Emx1 and Emx2 show different patterns of expression during proliferation and differentiation of the developing cerebral cortex in the mouse. Eur J Neurosci *8*, 1037-1050.

Haas, C.A., Dudeck, O., Kirsch, M., Huszka, C., Kann, G., Pollak, S., Zentner, J., and Frotscher, M. (2002). Role for reelin in the development of granule cell dispersion in temporal lobe epilepsy. J Neurosci *22*, 5797-5802.

Haines, B.P., Wheldon, L.M., Summerbell, D., Heath, J.K., and Rigby, P.W. (2006). Regulated expression of FLRT genes implies a functional role in the regulation of FGF signalling during mouse development. Developmental Biology *297*, 14-25.

Hanashima, C., Li, S.C., Shen, L., Lai, E., and Fishell, G. (2004). Foxg1 suppresses early cortical cell fate. Science *303*, 56-59.

Harboe, T.L., Tumer, Z., Hansen, C., Jensen, N.A., and Tommerup, N. (2000). Assignment of the human zinc finger gene, ZNF288, to chromosome 3 band q13.2 by radiation hybrid mapping and fluorescence in situ hybridisation. Cytogenet Cell Genet *89*, 156-157.

Hébert, J.M., and Fishell, G. (2008). The genetics of early telencephalon patterning: some assembly required. Nat Rev Neurosci *9*, 678-685.

Hébert, J.M., Mishina, Y., and McConnell, S.K. (2002). BMP signaling is required locally to pattern the dorsal telencephalic midline. Neuron *35*, 1029-1041.

Heins, N., Cremisi, F., Malatesta, P., Gangemi, R.M., Corte, G., Price, J., Goudreau, G., Gruss, P., and Gotz, M. (2001). Emx2 promotes symmetric cell divisions and a multipotential fate in precursors from the cerebral cortex. Mol Cell Neurosci *18*, 485-502.

Hevner, R.F. (2006). From radial glia to pyramidal-projection neuron: transcription factor cascades in cerebral cortex development. Mol Neurobiol *33*, 33-50.

Hirabayashi, Y., and Gotoh, Y. (2005). Stage-dependent fate determination of neural precursor cells in mouse forebrain. Neurosci Res *51*, 331-336.

Hirabayashi, Y., Itoh, Y., Tabata, H., Nakajima, K., Akiyama, T., Masuyama, N., and Gotoh, Y. (2004). The Wnt/beta-catenin pathway directs neuronal differentiation of cortical neural precursor cells. Development *131*, 2791-2801.

Hirsch, C., Campano, L.M., Wohrle, S., and Hecht, A. (2007). Canonical Wnt signaling transiently stimulates proliferation and enhances neurogenesis in neonatal neural progenitor cultures. Exp Cell Res *313*, 572-587.

Horowitz, M., and Fraser, R. (1994). Disordered gastric motor function in diabetes mellitus. Diabetologia *37*, 543-551.

Houser, C.R., Miyashiro, J.E., Swartz, B.E., Walsh, G.O., Rich, J.R., and Delgado-Escueta, A.V. (1990). Altered patterns of dynorphin immunoreactivity suggest mossy fiber reorganization in human hippocampal epilepsy. J Neurosci *10*, 267-282.

Hsieh, J.C., Kodjabachian, L., Rebbert, M.L., Rattner, A., Smallwood, P.M., Samos, C.H., Nusse, R., Dawid, I.B., and Nathans, J. (1999). A new secreted protein that binds to Wnt proteins and inhibits their activities. Nature *398*, 431-436.

Hu, Y.A., Gu, X., Liu, J., Yang, Y., Yan, Y., and Zhao, C. (2008). Expression pattern of Wnt inhibitor factor 1(Wif1) during the development in mouse CNS. Gene Expr Patterns *8*, 515-522.

Huttner, W.B., and Kosodo, Y. (2005). Symmetric versus asymmetric cell division during neurogenesis in the developing vertebrate central nervous system. Curr Opin Cell Biol *17*, 648-657.

Ikeda, M., Tomita, Y., Mouri, A., Koga, M., Okochi, T., Yoshimura, R., Yamanouchi, Y., Kinoshita, Y., Hashimoto, R., Williams, H.J., *et al.* (2009). Identification of Novel Candidate Genes for Treatment Response to Risperidone and Susceptibility for Schizophrenia: Integrated Analysis Among Pharmacogenomics, Mouse Expression, and Genetic Case-Control Association Approaches. Biol Psychiatry.

Ikeya, M., and Takada, S. (2001). Wnt-3a is required for somite specification along the anteroposterior axis of the mouse embryo and for regulation of cdx-1 expression. Mech Dev *103*, 27-33.

Inoue, I., Ikeda, R., and Tsukahara, S. (2006). Current topics in pharmacological research on bone metabolism: Promyelotic leukemia zinc finger (PLZF) and tumor necrosis factor-alpha-stimulated gene 6 (TSG-6) identified by gene expression analysis play roles in the pathogenesis of ossification of the posterior longitudinal ligament. J Pharmacol Sci *100*, 205-210.

Jacomy, H., Zhu, Q., Couillard-Despres, S., Beaulieu, J.M., and Julien, J.P. (1999). Disruption of type IV intermediate filament network in mice lacking the neurofilament medium and heavy subunits. J Neurochem *73*, 972-984.

Jen, Y., Manova, K., and Benezra, R. (1997). Each member of the Id gene family exhibits a unique expression pattern in mouse gastrulation and neurogenesis. Dev Dyn *208*, 92-106.

Jones, E.G. (2007). The Thalamus, 2nd edn (Cambridge, Cambridge University Press).

Joshi, P.S., Molyneaux, B.J., Feng, L., Xie, X., Macklis, J.D., and Gan, L. (2008). Bhlhb5 regulates the postmitotic acquisition of area identities in layers II-V of the developing neocortex. Neuron *60*, 258-272.

Julien, J.P., Meyer, D., Flavell, D., Hurst, J., and Grosveld, F. (1986). Cloning and developmental expression of the murine neurofilament gene family. Brain Res *387*, 243-250.

Kahle, W., and Frotscher, M. (2002). Color Atlas and Textbook of Human Anatomy, Vol 3, 5th edn (Thieme).

Kandel, E.R., Schwartz, J.H., and Jessell, T.M. (2000). Principles of Neural Science.

Karaplis, A.C., Luz, A., Glowacki, J., Bronson, R.T., Tybulewicz, V.L., Kronenberg, H.M., and Mulligan, R.C. (1994). Lethal skeletal dysplasia from targeted disruption of the parathyroid hormone-related peptide gene. Genes Dev *8*, 277-289.

Karaulanov, E.E., Bottcher, R.T., and Niehrs, C. (2006). A role for fibronectin-leucine-rich transmembrane cell-surface proteins in homotypic cell adhesion. EMBO Rep *7*, 283-290.

Kato, M., Patel, M.S., Levasseur, R., Lobov, I., Chang, B.H., Glass, D.A., 2nd, Hartmann, C., Li, L., Hwang, T.H., Brayton, C.F.*, et al.* (2002). Cbfa1-independent decrease in osteoblast proliferation, osteopenia, and persistent embryonic eye vascularization in mice deficient in Lrp5, a Wnt coreceptor. J Cell Biol *157*, 303-314.

Kelly, K.F., and Daniel, J.M. (2006). POZ for effect--POZ-ZF transcription factors in cancer and development. Trends Cell Biol *16*, 578-587.

Kempermann, G., Kuhn, H.G., and Gage, F.H. (1997a). Genetic influence on neurogenesis in the dentate gyrus of adult mice. Proc Natl Acad Sci U S A *94*, 10409-10414.

Kempermann, G., Kuhn, H.G., and Gage, F.H. (1997b). More hippocampal neurons in adult mice living in an enriched environment. Nature *386*, 493-495.

Kessel, M., and Gruss, P. (1991). Homeotic transformations of murine vertebrae and concomitant alteration of Hox codes induced by retinoic acid. Cell *67*, 89-104.

Kronenberg, H.M. (2003). Developmental regulation of the growth plate. Nature *423*, 332-336.

Lacy, S.E., Bonnemann, C.G., Buzney, E.A., and Kunkel, L.M. (1999). Identification of FLRT1, FLRT2, and FLRT3: a novel family of transmembrane leucine-rich repeat proteins. Genomics *62*, 417-426.

Lariviere, R.C., and Julien, J.P. (2004). Functions of intermediate filaments in neuronal development and disease. J Neurobiol *58*, 131-148.

Leamey, C.A., Merlin, S., Lattouf, P., Sawatari, A., Zhou, X., Demel, N., Glendining, K.A., Oohashi, T., Sur, M., and Fassler, R. (2007). Ten_m3 regulates eye-specific patterning in the mammalian visual pathway and is required for binocular vision. PLoS Biol *5*, e241.

Lecanda, F., Warlow, P.M., Sheikh, S., Furlan, F., Steinberg, T.H., and Civitelli, R. (2000). Connexin43 deficiency causes delayed ossification, craniofacial abnormalities, and osteoblast dysfunction. J Cell Biol *151*, 931-944.

Lee, E.C., Yu, D., Martinez de Velasco, J., Tessarollo, L., Swing, D.A., Court, D.L., Jenkins, N.A., and Copeland, N.G. (2001). A highly efficient Escherichia coli-based chromosome engineering system adapted for recombinogenic targeting and subcloning of BAC DNA. Genomics *73*, 56-65.

Lee, S.M., Tole, S., Grove, E., and McMahon, A.P. (2000). A local Wnt-3a signal is required for development of the mammalian hippocampus. Development *127*, 457-467.

Lein, E.S., Zhao, X., and Gage, F.H. (2004). Defining a molecular atlas of the hippocampus using DNA microarrays and high-throughput in situ hybridization. J Neurosci *24*, 3879-3889.

Levine, A., Bashan-Ahrend, A., Budai-Hadrian, O., Gartenberg, D., Menasherow, S., and Wides, R. (1994). Odd Oz: a novel Drosophila pair rule gene. Cell *77*, 587-598.

Li, G., Peng, H., Corsi, K., Usas, A., Olshanski, A., and Huard, J. (2005). Differential effect of BMP4 on NIH/3T3 and C2C12 cells: implications for endochondral bone formation. J Bone Miner Res *20*, 1611-1623.

Li, H., Bishop, K.M., and O'Leary, D.D. (2006). Potential target genes of EMX2 include Odz/Ten-M and other gene families with implications for cortical patterning. Mol Cell Neurosci *33*, 136-149.

Li, Z.L., Chisaka, O., Koseki, H., Akasaka, T., Ishibashi, M., and Shiota, K. (1997). Heat shock-induced homeotic transformations of the axial skeleton and associated shifts of Hox gene expression domains in mouse embryos. Reprod Toxicol *11*, 761-770.

Liu, F., Kohlmeier, S., and Wang, C.Y. (2008). Wnt signaling and skeletal development. Cell Signal *20*, 999-1009.

Liu, M., Pleasure, S.J., Collins, A.E., Noebels, J.L., Naya, F.J., Tsai, M.J., and Lowenstein, D.H. (2000a). Loss of BETA2/NeuroD leads to malformation of the dentate gyrus and epilepsy. Proc Natl Acad Sci U S A *97*, 865-870.

Liu, P., Jenkins, N.A., and Copeland, N.G. (2003). A highly efficient recombineering-based method for generating conditional knockout mutations. Genome Res *13*, 476-484.

Liu, Q., Dwyer, N.D., and O'Leary, D.D. (2000b). Differential expression of COUP-TFI, CHL1, and two novel genes in developing neocortex identified by differential display PCR. J Neurosci *20*, 7682-7690.

Logan, C.Y., and Nusse, R. (2004). The Wnt signaling pathway in development and disease. Annu Rev Cell Dev Biol *20*, 781-810.

Lohnes, D. (2003). The Cdx1 homeodomain protein: an integrator of posterior signaling in the mouse. Bioessays *25*, 971-980.

Lorente de Nó, R. (1934). Studies on the structure of the cerebral cortex. II. Continuation of the study of the ammonic system. J Psychol Neurol *46*, 113-177.

Lurton, D., Sundstrom, L., Brana, C., Bloch, B., and Rougier, A. (1997). Possible mechanisms inducing granule cell dispersion in humans with temporal lobe epilepsy. Epilepsy Res *26*, 351-361.

Machon, O., Backman, M., Machonova, O., Kozmik, Z., Vacik, T., Andersen, L., and Krauss, S. (2007). A dynamic gradient of Wnt signaling controls initiation of neurogenesis in the mammalian cortex and cellular specification in the hippocampus. Dev Biol *311*, 223-237.

Machon, O., van den Bout, C.J., Backman, M., Kemler, R., and Krauss, S. (2003). Role of beta-catenin in the developing cortical and hippocampal neuroepithelium. Neuroscience *122*, 129-143.

Machon, O., van den Bout, C.J., Backman, M., Rosok, O., Caubit, X., Fromm, S.H., Geronimo, B., and Krauss, S. (2002). Forebrain-specific promoter/enhancer D6 derived from the mouse Dach1 gene controls expression in neural stem cells. Neuroscience *112*, 951-966.

Mallamaci, A., Iannone, R., Briata, P., Pintonello, L., Mercurio, S., Boncinelli, E., and Corte, G. (1998). EMX2 protein in the developing mouse brain and olfactory area. Mech Dev *77*, 165-172.

Mallamaci, A., Mercurio, S., Muzio, L., Cecchi, C., Pardini, C.L., Gruss, P., and Boncinelli, E. (2000a). The lack of Emx2 causes impairment of Reelin signaling and defects of neuronal migration in the developing cerebral cortex. J Neurosci *20*, 1109-1118.

Mallamaci, A., Muzio, L., Chan, C.H., Parnavelas, J., and Boncinelli, E. (2000b). Area identity shifts in the early cerebral cortex of Emx2-/- mutant mice. Nat Neurosci *3*, 679-686.

Mallamaci, A., and Stoykova, A. (2006). Gene networks controlling early cerebral cortex arealization. Eur J Neurosci *23*, 847-856.

Mangale, V.S., Hirokawa, K.E., Satyaki, P.R., Gokulchandran, N., Chikbire, S., Subramanian, L., Shetty, A.S., Martynoga, B., Paul, J., Mai, M.V., *et al.* (2008). Lhx2 selector activity specifies cortical identity and suppresses hippocampal organizer fate. Science *319*, 304-309.

Mansouri, A. (2001). Determination of gene function by homologous recombination using embryonic stem cells and knockout mice. Methods Mol Biol *175*, 397-413.

Maretto, S., Muller, P.S., Aricescu, A.R., Cho, K.W., Bikoff, E.K., and Robertson, E.J. (2008). Ventral closure, headfold fusion and definitive endoderm migration defects in mouse embryos lacking the fibronectin leucine-rich transmembrane protein FLRT3. Dev Biol *318*, 184-193.

McConnell, J. (1990). Cell cycle control in early mouse development. J Reprod Fertil Suppl *42*, 205-213.

Menegola, E., Broccia, M.L., and Giavini, E. (2001). Atlas of rat fetal skeleton double stained for bone and cartilage. Teratology *64*, 125-133.

Miller, J.R., Hocking, A.M., Brown, J.D., and Moon, R.T. (1999). Mechanism and function of signal transduction by the Wnt/beta-catenin and Wnt/Ca2+ pathways. Oncogene *18*, 7860-7872.

Mitchelmore, C., Kjaerulff, K.M., Pedersen, H.C., Nielsen, J.V., Rasmussen, T.E., Fisker, M.F., Finsen, B., Pedersen, K.M., and Jensen, N.A. (2002). Characterization of two novel nuclear BTB/POZ domain zinc finger isoforms. Association with differentiation of hippocampal neurons, cerebellar granule cells, and macroglia. J Biol Chem *277*, 7598-7609.

Miyata, T., Maeda, T., and Lee, J.E. (1999). NeuroD is required for differentiation of the granule cells in the cerebellum and hippocampus. Genes Dev *13*, 1647-1652.

Molyneaux, B.J., Arlotta, P., Menezes, J.R., and Macklis, J.D. (2007). Neuronal subtype specification in the cerebral cortex. Nat Rev Neurosci *8*, 427-437.

Monuki, E.S., Porter, F.D., and Walsh, C.A. (2001). Patterning of the dorsal telencephalon and cerebral cortex by a roof plate-Lhx2 pathway. Neuron *32*, 591-604.

Moon, R.T., Kohn, A.D., De Ferrari, G.V., and Kaykas, A. (2004). WNT and beta-catenin signalling: diseases and therapies. Nat Rev Genet *5*, 691-701.

Moorman, A.F., Houweling, A.C., de Boer, P.A., and Christoffels, V.M. (2001). Sensitive nonradioactive detection of mRNA in tissue sections: novel application of the whole-mount in situ hybridization protocol. J Histochem Cytochem *49*, 1-8.

Motro, B., Wojtowicz, J.M., Bernstein, A., and van der Kooy, D. (1996). Steel mutant mice are deficient in hippocampal learning but not long-term potentiation. Proc Natl Acad Sci U S A *93*, 1808-1813.

Mühlfriedel, S., Kirsch, F., Gruss, P., Chowdhury, K., and Stoykova, A. (2007). Novel genes differentially expressed in cortical regions during late neurogenesis. Eur J Neurosci *26*, 33-50.

Muyrers, J.P., Zhang, Y., and Stewart, A.F. (2001). Techniques: Recombinogenic engineering--new options for cloning and manipulating DNA. Trends Biochem Sci *26*, 325-331.

Muzio, L., DiBenedetto, B., Stoykova, A., Boncinelli, E., Gruss, P., and Mallamaci, A. (2002). Emx2 and Pax6 control regionalization of the pre-neuronogenic cortical primordium. Cereb Cortex *12*, 129-139.

Muzio, L., and Mallamaci, A. (2003). Emx1, emx2 and pax6 in specification, regionalization and arealization of the cerebral cortex. Cereb Cortex *13*, 641-647.

Muzio, L., and Mallamaci, A. (2005). Foxg1 confines Cajal-Retzius neuronogenesis and hippocampal morphogenesis to the dorsomedial pallium. J Neurosci *25*, 4435-4441.

Nakahira, E., and Yuasa, S. (2005). Neuronal generation, migration, and differentiation in the mouse hippocampal primoridium as revealed by enhanced green fluorescent protein gene transfer by means of in utero electroporation. J Comp Neurol *483*, 329-340.

Newton, S.S., and Duman, R.S. (2007). Neurogenic actions of atypical antipsychotic drugs and therapeutic implications. CNS Drugs *21*, 715-725.

Nicholls, J.G., Martin, A.R., Wallace, B.G., and Fuchs, P.A. (2001). From neuron to brain, 4 edn (Sinauer Associates).

Nielsen, J.V., Nielsen, F.H., Ismail, R., Noraberg, J., and Jensen, N.A. (2007). Hippocampus-like corticoneurogenesis induced by two isoforms of the BTB-zinc finger gene Zbtb20 in mice. Development *134*, 1133-1140.

Nieto, M., Schuurmans, C., Britz, O., and Guillemot, F. (2001). Neural bHLH genes control the neuronal versus glial fate decision in cortical progenitors. Neuron *29*, 401-413.

O'Leary, D.D. (1989). Do cortical areas emerge from a protocortex? Trends Neurosci *12*, 400-406.

O'Leary, D.D., Chou, S.J., and Sahara, S. (2007). Area patterning of the mammalian cortex. Neuron *56*, 252-269.

O'Leary, D.D., and Nakagawa, Y. (2002). Patterning centers, regulatory genes and extrinsic mechanisms controlling arealization of the neocortex. Curr Opin Neurobiol *12*, 14-25.

O'Mara, S.M., Commins, S., Anderson, M., and Gigg, J. (2001). The subiculum: a review of form, physiology and function. Prog Neurobiol *64*, 129-155.

Oliver, G., Sosa-Pineda, B., Geisendorf, S., Spana, E.P., Doe, C.Q., and Gruss, P. (1993). Prox 1, a prospero-related homeobox gene expressed during mouse development. Mech Dev *44*, 3-16.

Oohashi, T., Zhou, X.H., Feng, K., Richter, B., Morgelin, M., Perez, M.T., Su, W.D., Chiquet-Ehrismann, R., Rauch, U., and Fassler, R. (1999). Mouse ten-m/Odz is a new family of dimeric type II transmembrane proteins expressed in many tissues. J Cell Biol *145*, 563-577.

Otto, F., Thornell, A.P., Crompton, T., Denzel, A., Gilmour, K.C., Rosewell, I.R., Stamp, G.W., Beddington, R.S., Mundlos, S., Olsen, B.R., *et al.* (1997). Cbfa1, a candidate gene for cleidocranial dysplasia syndrome, is essential for osteoblast differentiation and bone development. Cell *89*, 765-771.

Patton, J.T., and Kaufman, M.H. (1995). The timing of ossification of the limb bones, and growth rates of various long bones of the fore and hind limbs of the prenatal and early postnatal laboratory mouse. J Anat *186 (Pt 1)*, 175-185.

Paxinos, G. (2004). The rat nervous system, 3 edn (Amsterdam [u.a.], Elsevier Acad. Press).

Pellegrini, M., Mansouri, A., Simeone, A., Boncinelli, E., and Gruss, P. (1996). Dentate gyrus formation requires Emx2. Development *122*, 3893-3898.

Pellet-Many, C., Frankel, P., Jia, H., and Zachary, I. (2008). Neuropilins: structure, function and role in disease. Biochem J *411*, 211-226.

Pleasure, S.J., Collins, A.E., and Lowenstein, D.H. (2000). Unique expression patterns of cell fate molecules delineate sequential stages of dentate gyrus development. J Neurosci *20*, 6095-6105.

Plessen, K.J., Bansal, R., Zhu, H., Whiteman, R., Amat, J., Quackenbush, G.A., Martin, L., Durkin, K., Blair, C., Royal, J.*, et al.* (2006). Hippocampus and amygdala morphology in attention-deficit/hyperactivity disorder. Arch Gen Psychiatry *63*, 795-807.

Pomeranz, H.D., Sherman, D.L., Smalheiser, N.R., Tennyson, V.M., and Gershon, M.D. (1991). Expression of a neurally related laminin binding protein by neural crest-derived cells that colonize the gut: relationship to the formation of enteric ganglia. J Comp Neurol *313*, 625-642.

Ragsdale, C.W., and Grove, E.A. (2001). Patterning the mammalian cerebral cortex. Curr Opin Neurobiol *11*, 50-58.

Rakic, P. (1988). Specification of cerebral cortical areas. Science *241*, 170-176.

Rash, B.G., and Grove, E.A. (2006). Area and layer patterning in the developing cerebral cortex. Curr Opin Neurobiol *16*, 25-34.

Raz, N., Torres, I.J., Briggs, S.D., Spencer, W.D., Thornton, A.E., Loken, W.J., Gunning, F.M., McQuain, J.D., Driesen, N.R., and Acker, J.D. (1995). Selective neuroanatomic abnormalities in Down's syndrome and their cognitive correlates: evidence from MRI morphometry. Neurology *45*, 356-366.

Ross, M.E., Swanson, K., and Dobyns, W.B. (2001). Lissencephaly with cerebellar hypoplasia (LCH): a heterogeneous group of cortical malformations. Neuropediatrics *32*, 256-263.

Rubenstein, J.L., Anderson, S., Shi, L., Miyashita-Lin, E., Bulfone, A., and Hevner, R. (1999). Genetic control of cortical regionalization and connectivity. Cereb Cortex *9*, 524-532.

Sambrook, J., and Russell, D.W. (2001). Molecular Cloning, 3 edn (New York, Cold Spring Harbor Laboratory Press).

Sato, N., Hatakeyama, S., Shimizu, N., Hikima, A., Aoki, J., and Endo, K. (2001). MR evaluation of the hippocampus in patients with congenital malformations of the brain. AJNR Am J Neuroradiol *22*, 389-393.

Schlessinger, A.R., Cowan, W.M., and Swanson, L.W. (1978). The time of origin of neurons in Ammon's horn and the associated retrohippocampal fields. Anat Embryol (Berl) *154*, 153-173.

Schvarcz, E., Palmer, M., Aman, J., Lindkvist, B., and Beckman, K.W. (1993). Hypoglycaemia increases the gastric emptying rate in patients with type 1 diabetes mellitus. Diabet Med *10*, 660-663.

Schwab, M.H., Druffel-Augustin, S., Gass, P., Jung, M., Klugmann, M., Bartholomae, A., Rossner, M.J., and Nave, K.A. (1998). Neuronal basic helix-loop-helix proteins (NEX, neuroD, NDRF): spatiotemporal expression and targeted disruption of the NEX gene in transgenic mice. J Neurosci *18*, 1408-1418.

Sessa, A., Mao, C.A., Hadjantonakis, A.K., Klein, W.H., and Broccoli, V. (2008). Tbr2 directs conversion of radial glia into basal precursors and guides neuronal amplification by indirect neurogenesis in the developing neocortex. Neuron *60*, 56-69.

Shigemoto, R., Yokota, Y., Tsuchida, K., and Nakanishi, S. (1990). Cloning and expression of a rat neuromedin K receptor cDNA. J Biol Chem *265*, 623-628.

Shimogori, T., Banuchi, V., Ng, H.Y., Strauss, J.B., and Grove, E.A. (2004). Embryonic signaling centers expressing BMP, WNT and FGF proteins interact to pattern the cerebral cortex. Development *131*, 5639-5647.

Shinozaki, K., Yoshida, M., Nakamura, M., Aizawa, S., and Suda, Y. (2004). Emx1 and Emx2 cooperate in initial phase of archipallium development. Mech Dev *121*, 475-489.

Simeone, A., Gulisano, M., Acampora, D., Stornaiuolo, A., Rambaldi, M., and Boncinelli, E. (1992). Two vertebrate homeobox genes related to the Drosophila empty spiracles gene are expressed in the embryonic cerebral cortex. Embo J *11*, 2541-2550.

Solberg, N., Machon, O., and Krauss, S. (2008). Effect of canonical Wnt inhibition in the neurogenic cortex, hippocampus, and premigratory dentate gyrus progenitor pool. Dev Dyn *237*, 1799-1811.

Staff, N.P., Jung, H., Thiagarajan, T., Yao, M., and Spruston, N. (2000). Resting and Active Properties of Pyramidal Neurons in Subiculum
and CA1 of Rat Hippocampus. Journal of Neurophysiology *64*, 2398-2408.

Stoykova, A., Fritsch, R., Walther, C., and Gruss, P. (1996). Forebrain patterning defects in Small eye mutant mice. Development *122*, 3453-3465.

Stoykova, A., Treichel, D., Hallonet, M., and Gruss, P. (2000). Pax6 modulates the dorsoventral patterning of the mammalian telencephalon. The Journal of Neuroscience *20*, 8042–8050.

Sur, M., and Rubenstein, J.L. (2005). Patterning and plasticity of the cerebral cortex. Science *310*, 805-810.

Sutherland, A.P., Zhang, H., Zhang, Y., Michaud, M., Xie, Z., Patti, M.E., Grusby, M.J., and Zhang, W.J. (2009). Zinc finger protein Zbtb20 is essential for postnatal survival and glucose homeostasis. Mol Cell Biol *29*, 2804-2815.

Suzuki, N., Rohdewohld, H., Neuman, T., Gruss, P., and Scholer, H.R. (1990). Oct-6: a POU transcription factor expressed in embryonal stem cells and in the developing brain. Embo J *9*, 3723-3732.

Suzuki, S.C., Inoue, T., Kimura, Y., Tanaka, T., and Takeichi, M. (1997). Neuronal circuits are subdivided by differential expression of type-II classic cadherins in postnatal mouse brains. Mol Cell Neurosci *9*, 433-447.

Sweet, H.O., and Green, M.C. (1981). Progressive ankylosis, a new skeletal mutation in the mouse. J Hered *72*, 87-93.

Takada, S., Stark, K.L., Shea, M.J., Vassileva, G., McMahon, J.A., and McMahon, A.P. (1994). Wnt-3a regulates somite and tailbud formation in the mouse embryo. Genes Dev *8*, 174-189.

Tao, W., and Lai, E. (1992). Telencephalon-restricted expression of BF-1, a new member of the HNF-3/fork head gene family, in the developing rat brain. Neuron *8*, 957-966.

Tecott, L.H. (2003). The genes and brains of mice and men. Am J Psychiatry *160*, 646-656.

Teillet, M.A., Kalcheim, C., and Le Douarin, N.M. (1987). Formation of the dorsal root ganglia in the avian embryo: segmental origin and migratory behavior of neural crest progenitor cells. Dev Biol *120*, 329-347.

Thomas, K.R., and Capecchi, M.R. (1987). Site-directed mutagenesis by gene targeting in mouse embryo-derived stem cells. Cell *51*, 503-512.

Tole, S., Christian, C., and Grove, E.A. (1997). Early specification and autonomous development of cortical fields in the mouse hippocampus. Development *124*, 4959-4970.

Tole, S., Goudreau, G., Assimacopoulos, S., and Grove, E.A. (2000). Emx2 is required for growth of the hippocampus but not for hippocampal field specification. J Neurosci *20*, 2618-2625.

Tole, S., and Grove, E.A. (2001). Detailed field pattern is intrinsic to the embryonic mouse hippocampus early in neurogenesis. J Neurosci *21*, 1580-1589.

Torii, M., Matsuzaki, F., Osumi, N., Kaibuchi, K., Nakamura, S., Casarosa, S., Guillemot, F., and Nakafuku, M. (1999). Transcription factors Mash-1 and Prox-1 delineate early steps in differentiation of neural stem cells in the developing central nervous system. Development *126*, 443-456.

Travis, A., Hagman, J., Hwang, L., and Grosschedl, R. (1993). Purification of early-B-cell factor and characterization of its DNA-binding specificity. Mol Cell Biol *13*, 3392-3400.

Tzeng, S.F., and de Vellis, J. (1998). Id1, Id2, and Id3 gene expression in neural cells during development. Glia *24*, 372-381.

Vann, S.D., Aggleton, J.P., and Maguire, E.A. (2009). What does the retrosplenial cortex do? Nat Rev Neurosci *10*, 792-802.

von Bohlen Und Halbach, O. (2007). Immunohistological markers for staging neurogenesis in adult hippocampus. Cell Tissue Res *329*, 409-420.

Walther, C., and Gruss, P. (1991). Pax-6, a murine paired box gene, is expressed in the developing CNS. Development *113*, 1435-1449.

Wang, S.S., Lewcock, J.W., Feinstein, P., Mombaerts, P., and Reed, R.R. (2004). Genetic disruptions of O/E2 and O/E3 genes reveal involvement in olfactory receptor neuron projection. Development *131*, 1377-1388.

Warming, S., Costantino, N., Court, D.L., Jenkins, N.A., and Copeland, N.G. (2005). Simple and highly efficient BAC recombineering using galK selection. Nucleic Acids Res *33*, e36.

Wegner, M., and Stolt, C.C. (2005). From stem cells to neurons and glia: a Soxist's view of neural development. Trends Neurosci *28*, 583-588.

Weinberger, D.R. (1995). From neuropathology to neurodevelopment. Lancet *346*, 552-557.

Weinberger, D.R. (1999). Cell biology of the hippocampal formation in schizophrenia. Biol Psychiatry *45*, 395-402.

Wellik, D.M. (2007). Hox patterning of the vertebrate axial skeleton. Dev Dyn *236*, 2454-2463.

Wirtschafter, Z. (1960). The genesis of the mouse skeleton - A laboratory atlas (Springfield, Illinois. USA, Charles C Thomas).

Witter, M.P., and Wouterlood, F.G. (2002). The parahippocampal region: organization and role in cognitive function (Oxford University Press).

Wood, S.A., Allen, N.D., Rossant, J., Auerbach, A., and Nagy, A. (1993). Non-injection methods for the production of embryonic stem cell-embryo chimaeras. Nature *365*, 87-89.

Woodhams, P.L. (1993). Laminar and region-specific cell surface markers in the entorhinal cortex and hippocampus. Hippocampus *3 Spec No*, 183-189.

Xie, Z., Zhang, H., Tsai, W., Zhang, Y., Du, Y., Zhong, J., Szpirer, C., Zhu, M., Cao, X., Barton, M.C.*, et al.* (2008). Zinc finger protein ZBTB20 is a key repressor of alpha-fetoprotein gene transcription in liver. Proc Natl Acad Sci U S A *105*, 10859-10864.

Xuan, S., Baptista, C.A., Balas, G., Tao, W., Soares, V.C., and Lai, E. (1995). Winged helix transcription factor BF-1 is essential for the development of the cerebral hemispheres. Neuron *14*, 1141-1152.

Ye, L., Mishina, Y., Chen, D., Huang, H., Dallas, S.L., Dallas, M.R., Sivakumar, P., Kunieda, T., Tsutsui, T.W., Boskey, A.*, et al.* (2005). Dmp1-deficient mice display severe defects in cartilage formation responsible for a chondrodysplasia-like phenotype. J Biol Chem *280*, 6197-6203.

Yoneshima, H., Yamasaki, S., Voelker, C.C., Molnar, Z., Christophe, E., Audinat, E., Takemoto, M., Nishiwaki, M., Tsuji, S., Fujita, I.*, et al.* (2006). Er81 is expressed in a subpopulation of layer 5 neurons in rodent and primate neocortices. Neuroscience *137*, 401-412.

Young, T.R., and Leamey, C.A. (2009). Teneurins: important regulators of neural circuitry. Int J Biochem Cell Biol *41*, 990-993.

Zembrzycki, A., Griesel, G., Stoykova, A., and Mansouri, A. (2007). Genetic interplay between the transcription factors Sp8 and Emx2 in the patterning of the forebrain. Neural Dev *2*, 8.

Zetterstrom, R.H., Williams, R., Perlmann, T., and Olson, L. (1996). Cellular expression of the immediate early transcription factors Nurr1 and NGFI-B suggests a gene regulatory role in several brain regions including the nigrostriatal dopamine system. Brain Res Mol Brain Res *41*, 111-120.

Zhang, W., Mi, J., Li, N., Sui, L., Wan, T., Zhang, J., Chen, T., and Cao, X. (2001). Identification and characterization of DPZF, a novel human BTB/POZ zinc finger protein sharing homology to BCL-6. Biochem Biophys Res Commun *282*, 1067-1073.

Zhao, L.Y., Niu, Y., Santiago, A., Liu, J., Albert, S.H., Robertson, K.D., and Liao, D. (2006). An EBF3-mediated transcriptional program that induces cell cycle arrest and apoptosis. Cancer Research *66*, 9445-9452.

Zhou, C., Tsai, S.Y., and Tsai, M.J. (2001). COUP-TFI: an intrinsic factor for early regionalization of the neocortex. Genes Dev *15*, 2054-2059.

Abbreviations

Short name	Full name
AB	antibody
A/P	Anteriorposterior
Amy	Amygdala
bHLH	Basic helix-loop-helix
bp	Base pair(s)
BG	Basal ganglia
BPs	Basal progenitors
BCIP	5-bromo-4-chloro-3-idolyl-phosphate
°C	Degree Celsius
Cb	Cerebellum
CA	Cornu Ammonis
CC	Corpus callosum
cDNA	Complementary DNA
CGE	Caudal ganglionic eminence
Cgl	Cingulate cortex
CIP	Calf intestinal alkaline phosphatase
CNS	Central nervous system
CP	Cortical plate
CR	Cajal-Retzius
cRNA	Complementary RNA
D/V	Dorsoventral
DEPC	Diethylpyrocarbonate
DG	Dentate gyrus
DIG	Digoxygenin
DNA	Desoxyribonucleic acid
dNTP	Desoxyribonucleoside-triphosphate
DP	Dorsal pallium
E	Embryonal day
EDTA	Ethylenediaminetetraacetic acid
ES-cell	Embryonic stem cell
EST	Expressed sequence tag
Fi	Fimbria
et al.	Et alteri
gcl	Granule cell layer
Hi	Hippocampus
IHC	Immunohistochemistry
INs	Interneurons
IPs	Intermediate progenitors
ISH	In situ hybridization
IZ	Intermediate zone
kb	Kilo bases
kDa	Kilo-Dalton
KO	Knockout
LacZ	Beta-galactosidase
L1-6	Layer1-6
LP	Lateral pallium
LGE	Lateral ganglionic eminence
LOF	Loss-of-function
LP	Lateral pallium
M	Motor cortex
Mes	Mesencephalon
MGE	Medial ganglionic eminence
MP	Medial pallium
mRNA	Messenger RNA
MZ	Marginal zone

Ncx	Neocortex
NE	Neuroepithelial cells
OB	Olfactory bulb
Occ	Occipital cortex
OD	Optic density
O/N	Overnight
ORF	Open reading frame
P	Postnatal day
PBS	Phosphate buffered saline
PBT	PBS with Tween-20
PCR	Polymerase chain reaction
pcl	Pyramidal cell layer
PFA	Paraformaldehyde
pH	Potentia Hydrogenii
PP	Preplate
RG	Radial glia
RNA	Ribonucleic acid
RMS	Rostral migratory stream
rpm	Rounds per minute
Rsp	Retrosplenial cortex
RT	Room temperature
S	Subiculum
Sey	Small eye, *Pax6* allele
SS	Somatosensory cortex
SSC	Sodium saline citrate
Str	Striatum
slm	*Stratum lacunosum-moleculare*
sm	*Stratum moleculare*
so	*Stratum oriens*
sp	*Stratum pyramidale*
sr	*Stratum radiatum*
SVZ	Subventricular zone
T_A	Annealing temperature
TBE	Tris-Boric acid-EDTA buffer
TCA	Thalamocortical axon
TE	Tris-EDTA buffer
TF	Transcription factor
TK	Tymidine Kinase
Tris	Tris(hydroxymethyl)aminomethan
Th	Thalamus
VP	Ventral pallium
U	Unit
UTR	Untranslated region
UV	Ultra violet
Vi	Visual cortex
VZ	Ventricular zone
WT	Wild type
X-gal	5-Bromo-4-chloro-3-indolyl-beta-D-galacosidase

List of figures

List of tables

Acknowledgements

Firstly, I would like to thank my supervisor Dr. Kamal Chowdhury for giving me the opportunity to work in his laboratory on this interesting topic in neuroscience and for teaching me sophisticated cloning strategies, the basis for the success of this study.

I am thankful to Prof. Dr. Anastassia Stoykova for provision of her outstanding knowledge, for invaluable discussion of my work and current flow of helpful suggestions in the process of writing.

I would like to acknowledge Prof. Dr. Hans-Henning Arnold and Prof. Dr. Martin Korte (both TU Braunschweig) for their contributions as members of my thesis committee.

Furthermore I appreciate all the support, critics and intellectual input I have received from Dr. Willem van den Akker, and his corrections of the manuscript.

Special thanks go to Dr. Anton Tonchev for discussion and advice concerning the Golgi staining technique.

Furthermore, I am grateful to the members of the Department Molecular Cell Biology for their continuous support.

My gratitude goes especially to Sabine Geisendorf, Martina Daniel and Andrea Conrad for technical assistance and for encouraging guidance to learn new methods; Sigurd Hille, Ralf Altschäffel, Sharif Mahsur, Dr. Bernd Föhring and the BTL staff for their technical support, Tamara Rabe, Dr. Mihaela Diaconu and Sandra Kappler for the nice working atmosphere in the “girls lab” and your helpfulness and support in many issues and for caring about my work; Dr. Yuh-Shin Chang, Dr. Ahmet Ucar, Dr. Tran Cong Tuoc, Prof. Dr. Michael Kessel, Dr. Patrick Collombat and Dr. Yvonne Uerlings for new insights, scientific and non-scientific discussions and current supply of protocols.

Last, but not least, to Christian, my family and all our friends: I thank you so much for believing in me and my work, for your understanding and support without any doubt.